# Copyright Warning & Restrictions

The copyright law of the United States (Title 17, United States Code) governs the making of photocopies or other reproductions of copyrighted material.

Under certain conditions specified in the law, libraries and archives are authorized to furnish a photocopy or other reproduction. One of these specified conditions is that the photocopy or reproduction is not to be "used for any purpose other than private study, scholarship, or research." If a, user makes a request for, or later uses, a photocopy or reproduction for purposes in excess of "fair use" that user may be liable for copyright infringement,

This institution reserves the right to refuse to accept a copying order if, in its judgment, fulfillment of the order would involve violation of copyright law.

Please Note: The author retains the copyright while the New Jersey Institute of Technology reserves the right to distribute this thesis or dissertation

Printing note: If you do not wish to print this page, then select "Pages from: first page # to: last page #" on the print dialog screen

NJIT New Jersey's Science & Technology University

The Van Houten library has removed some of the personal information and all signatures from the approval page and biographical sketches of theses and dissertations in order to protect the identity of NJIT graduates and faculty.

## ABSTRACT

## BIOMIMETIC AND VASCULARIZED 3-D LIVER CANCER MODEL

**by**
**Derek Yip**

Anti-angiogenic drugs have failed to show significant extended mortality, except when co-administered with chemotherapy drugs in clinical trials. This should be predicted by in vitro models, and yet 2D in vitro models of liver cancer co-administered with these two types of drugs show increased cell viability, contradicting clinical trials. In vitro models should mimic clinical trials in order to accurately predict drug outcomes. 2D in vitro models fail because they lack features of the cancer environment such as presence of stromal cells and a vasculature.

In order to achieve a biomimetic and vascularized in vitro model that would better recapitulate the cancer environment, a vascularized 3D in vitro liver cancer model is proposed in which: 1) heterospheroids, agglomerations of liver cancer HepG2 and stromal cells, are fabricated and encapsulated in collagen gel; 2) heparin crosslinked, wet-spun chitosan microfiber/electrospun chitosan mat tube are coated with endothelial cells; and 3) spheroids and endothelial coated electrospun chitosan mat tube are embedded together on Matrigel.

Using the hanging drop method, spheroids are formed and encapsulated in collagen before exposure to the anti-cancer drug doxorubicin. Cell viability, bile canaliculi, and cytochrome p450 activity are measured afterwards, showing greater maintenance of liver cell function for heterospheroids in collagen gel.

Blood vessel constructs are developed using chitosan microfibers/tubes. Chitosan is modified with heparin and is confirmed by Toluidine blue staining and FTIR (Fourier

Transform Infrared Spectroscopy). Fibronectin and VEGF are then adsorbed showing greater cell adhesion. Microfibers/electrospun mat tubes are incubated with endothelial cells and embedded on Matrigel resulting in vascular sprouting.

Triculture spheroids, heterospheroids which also contain endothelial cells, and cell coated chitosan electrospun mat tube are combined on Matrigel to form a vascularized model. Triculture spheroids on Matrigel are exposed to anti-cancer drugs, and vascular sprouts are measured showing expected decrease in length. Spheroids and cell coated tube together show anastomosis and migration, and fluorescent compounds injected into the model show their presence in nascent lumen.

Overall, a vascularized model is made which exhibits similar qualities to cancer in vivo and therefore can be used as a platform for anti-cancer drug testing.

# BIOMIMETIC AND VASCULARIZED 3-D LIVER CANCER MODEL

**by**
**Derek Yip**

**A Dissertation**
**Submitted to the Faculty of**
**New Jersey Institute of Technology and**
**Rutgers, The State University of New Jersey-Newark**
**in Partial Fulfillment of the Requirements for the Degree of**
**Doctor of Philosophy in Biomedical Engineering**

**Department of Biomedical Engineering**

**August 2016**

Copyright © 2016 by Derek Yip

ALL RIGHTS RESERVED

.

**APPROVAL PAGE**

**BIOMIMETIC AND VASCULARIZED 3-D LIVER CANCER MODEL**

**Derek Yip**

---

Dr. Cheul H. Cho, Dissertation Advisor — Date
Assistant Research Professor of Biomedical Engineering, NJIT

---

Dr. Bryan Pfister, Committee Member — Date
Associate Professor of Biomedical Engineering, NJIT

---

Dr. Eun J. Lee, Committee Member — Date
Assistant Professor of Biomedical Engineering, NJIT

---

Dr. George Collins, Committee Member — Date
Research Professor of Biomedical Engineering, NJIT

---

Dr. Pranela Rameshwar, Committee Member — Date
Professor of Medicine-Hematology/Oncology, Rutgers-New Jersey Medical School

---

Dr. Diego Fraidenraich, Committee Member — Date
Assistant Professor of Cell Biology and Molecular Medicine, Rutgers-New Jersey Medical School

## BIOGRAPHICAL SKETCH

**Author:** Derek Yip

**Degree:** Doctor of Philosophy

**Date:** August 2016

**Undergraduate and Graduate Education:**

- Doctor of Philosophy in Biomedical Engineering,
  New Jersey Institute of Technology, Newark, NJ, 2016
- Master of Science in Biomedical Engineering,
  New Jersey Institute of Technology, Newark, NJ, 2010
- Bachelor of Arts in Molecular Biology,
  UC Berkeley, Berkeley, CA, 2008

**Major:** Biomedical Engineering

**Presentations and Publications:**

Yip, D.; Cho, C.H. "A multicellular 3D heterospheroid model of liver tumor and stromal cells in collagen gel for anti-cancer drug testing." Biochemical and Biophysical Research Communications **433**(3): 327-332.

Hussain, A.; Collins, G.; Yip, D.; Cho, C.H. "Functional 3-D cardiac co-culture model using bioactive chitosan nanofiber scaffolds." Biotechnology and Bioengineering **110**(2): 637-647.

Shrirao, A.; Kung, F.; Yip, D.; Cho, C.H.; Townes-Anderson, E. "Vacuum-assisted fluid flow in microchannels to pattern substrates and cells." Biofabrication **6**(3): 035016.

Yip, D.; Beshai, M.; Abu-Hakmeh, A.; Cho, C.H."Vascularized Chitosan Wet Spun Fibers for Cancer Models." 9th Annual Graduate Student Association Research Day, Newark, NJ, November 2013.

Yip, D.; Cho, C.H. "A Multicellular 3D Heterospheroid Liver Tumor Models for Anti-Cancer Drug Testing." Society for Biomaterials, Boston, MA, April 2013.

Yip, D.; Cho, C. H. “Multicellular 3D Heterospheroid Tumor Model for Anti-Cancer Drug Testing.” 8th Annual Graduate Student Association Research Day, Newark, NJ, November 2012.

Yip, D.; Cho, C.H. “A Thermosensitive Chitosan/β-Glycerophosphate Hydrogel with Poly-L-Lysine for Liver Tissue Engineering.” 6th Annual Graduate Student Association Research Day, Newark, NJ, November 2010.

## ACKNOWLEDGMENT

Many thanks to Dr. Cheul Cho for helping me with paper and grant writing, dealing with my obfuscation, and giving me guidance during the course of this study.

Thanks to Committee Members: Dr. Bryan Pfister, Dr. Eun J. Lee, Dr. George Collins, Dr. Pranela Rameshwar, and Dr. Diego Fraidenraich, for reviewing my dissertation.

Thanks to Lab Neighbors: Anil Shrirao and Venkatakrishnan "Krish" Rengarajan for accepting my advice and my pacing around.

Thanks to Wai & Ada Yip for their moral and financial support, and for putting up with my years of searching for myself.

Thanks to Michael & Amy Ling for allowing me into their home, feeding me, and allowing me to take food.

Thanks to Desmond Ling & Daisy Ling for letting me into their home and dealing with my travel plans.

Thanks to Alvin Yip, for tech support and for keeping me real.

Thanks to Lab Mates Ali Hussain, Nolan Skop, and Noel Alfonso for giving guidance and accepting my guidance.

Thanks to Jennifer Min for keeping me sane in college.

## TABLE OF CONTENTS

**TABLE OF CONTENTS**
**(Continued)**

**Chapter** **Page**

**TABLE OF CONTENTS**
**(Continued)**

**Chapter** **Page**

**TABLE OF CONTENTS**
**(Continued)**

**Chapter** **Page**

**TABLE OF CONTENTS**
**(Continued)**

**Chapter** **Page**

**TABLE OF CONTENTS**
**(Continued)**

**Chapter** **Page**

## LIST OF FIGURES

## LIST OF FIGURES
## (Continued)

**Figure** **Page**

## LIST OF FIGURES
## (Continued)

**Figure** **Page**

## LIST OF DEFINITIONS

| | |
|---|---|
| C | Chitosan |
| CF | Chitosan Fibronectin |
| CH | Chitosan Heparin |
| CHF | Chitosan Heparin Fibronectin |
| CYPA1 | Assay to measure cytochrome p-450 activity |
| ECM | Extracellular Matrix |
| EDC | 1-ethyl-3-(3-dimethylaminopropyl) carbodiimide |
| EROD | Assay to measure drug metabolism activity |
| Fibroblast | 3T3-J2 fibroblast |
| HepG2 | Hepatocellular carcinoma |
| MVEC | Human microvacular endothelial cell |
| NHS | n-hydroxysulfosuccinimide |
| RAEC | Rat aortic endothelial cell |
| TCP | Tissue Culture Plate |
| VEGF | Vascular endothelial growth factor |

# CHAPTER 1

# INTRODUCTION

## 1.1 Background Information

Liver cancer is the fifth most common cancer and the third most prevalent cause of cancer related mortality for men worldwide.[1] Liver cancer is a result of cirrhosis of the liver due to alcoholism, hepatitis, and/or aflatoxin exposure. In an effort to treat this disease and other cancer types, anti-angiogenic drugs have been developed.

Judah Folkman's landmark paper on cancer and angiogenesis, posited that for a solid tumor to continue growing beyond the limits of diffusion, it must induce angiogenesis, the process by which new blood vessels are formed from pre-existing ones. [2] Thus, by preventing angiogenesis, it is believed that the solid tumors will either stop growing or even regress. This is known as the anti-angiogenic strategy and seems to have been realized as a cancer treatment with the advent of such anti-angiogenic drugs as bevacizumab, sunitinib, and sorafenib. However, many of these anti-angiogenic drugs have shown minimal/negligible results in promoting overall survival of patients.

Besides toxicity/limited efficacy, for which bevacizumab [Avastin] was discontinued as a treatment for breast cancer, many of these drugs have either been ineffectual or show minimal success. Bevacizumab, in phase III clinical trials, only showed overall survival in breast cancer patients of 3 months.[3] Sorafenib, which is considered a success, only shows significant progression free survival and a modest increase of overall survival of 3 months to a year. [4-6] Sunitinib showed time to tumor progression of 5.3 months, but also a high toxicity. [7, 8]

The reasons for the failure of the anti-angiogenic strategy is not exactly known, however, many theories for the intrinsic and extrinsic/acquired resistance to anti-angiogenic drugs exist. Intrinsic resistance, resistance to the anti-angiogenic drug before exposure, can be the result of metastatic potential without the need for angiogenesis, susceptibility to hypoxia, and redundancy of angiogenic mechanisms. Metastatic potential without the need for angiogenesis is exemplified by breast cancer which may be angiogenic independent compared to other cancers such as renal or liver cancer. [9] Susceptibility to hypoxia varies amongst cancer types and even a specific cancer itself as exemplified by the varied reactions of colon cancer cells lines to bevacizumab. [10] Redundancy of angiogenic mechanisms is due to the fact that angiogenesis is governed by many different growth factors such as PDGF, FGF, and VEGF. [11] Despite this, most anti-angiogenic drugs such as bevacizumab only target VEGF, thus, allowing for continued angiogenesis via other growth factors. Acquired resistance can occur following anti-angiogenic drug exposure, when hypoxia brought on by the anti-angiogenic drugs causes an upregulation in pro-angiogenic growth factors and causes activation of an invasive phenotype. [11-13]

Despite spending hundreds of millions of dollars and putting decades into the research and development of anti-angiogenic drugs, there is little to show for the effort. Part of the blame for the failure can be attributed to the failure of in vitro models to recapitulate the environment which they are modelling during the drug development process and, thus, accurately predict drug outcomes.

Drug development can be divided into pre-clinical testing and clinical testing. In pre-clinical testing, a drug is tested on an in vitro model and then followed by animal studies. This is then followed by ever increasing sized clinical trials. Each phase of

development, becomes exponentially more expensive and there is a very high attrition rate as it is estimated that 1 in 5,000 drug candidates is able to reach market.[14] Therefore, determining a drug's failure early in the drug development cycle would prevent a great waste of money and time given that a single drug's development costs $403 million (US 2000) [15]. Money saved by determining early failure could, thus, be diverted to better drug candidates. To this end, an appropriate in vitro model would provide a solution to the problem, unfortunately, most in vitro models fail to accurately model the condition they are testing.

Most in vitro models are two-dimensional monocultures and therefore fail to recapitulate the three dimensional nature and cellular heterogeneity of the human body. Animal models do recapitulate dimensionality and cellular heterogeneity of the human body, but may differ in their physiology/biochemistry. Numerous examples where animal models fail to mimic humans abound. Thalidomide was tested on rats and found to be safe, and, thus, was marketed to relieve morning sickness. However, thalidomide has no effect in rats, but is a potent teratogen in human beings, resulting in mothers giving birth to children with deformities, namely deformed or absent limbs. Another difficulty in using animals as models of disease is that certain diseases such as HIV can only infect primates, and rodent models of HIV are only accomplished via genetic modification and with limited success.[16] Therefore, an in vitro model which could incorporate human cells would better recapitulate human physiology/biochemistry and ultimately, better predict drug candidates.

A better model is herein proposed to model the aforementioned difficulties found with anti-angiogeneic drugs on hepatocellular cancer. *In order to address the problems*

*involved in in vitro testing, a new model must be constructed that incorporates various aspects of cancer.* Specifically, an in vitro model of the hepatocellular carcinoma is constructed which incorporates liver cancer and a vasculature together. Endothelial cell coated chitosan microfibers or electrospun tubes with HepG2/fibroblast spheroids encapsulated in Matrigel will serve as a platform to test anti-angiogenic and chemotherapy drugs.

## 1.2 Aims

*The goal of this study is to develop a biomimetic and vascularized liver cancer model as a platform for anti-cancer drug testing.* In order to achieve the objective, three aims are proposed:

- Aim 1: To develop biomimetic multicellular cancer spheroids for anti-cancer drug testing.
- Aim 2: To fabricate and characterize chitosan-heparin micro/nanofiber scaffolds seeded with endothelial cells to act as tissue engineered blood vessel as a substrate for angiogenesis.
- Aim 3: To construct a biomimetic and vascularized liver cancer model combining multicellular cancer spheroids and chitosan-heparin micro/nanofiber scaffold recapitulating tumor angiogenesis such that a vasculature is formed to allow passage of a drug into the spheroid.

# CHAPTER 2

# SPHEROIDS

Aim 1 is to develop biomimetic multicellular cancer spheroids for anti-cancer drug testing. We hypothesize that co-cultures of HepG2, liver carcinoma, cells and stromal fibroblasts fabricated via the hanging drop method into heterospheroids and embedded in ECM gel, results in a model which recapitulates drug resistance found in cancer in vivo.

## 2.1 Background

Spheroids are agglomerations of cells shaped like a sphere. In this study, spheroids are used to promote vascularization. Spheroids which grow to a radius greater than 100 μm will become hypoxic as diffusion is only capable of delivering nutrients and gases up to ~100 μm. As a result a hypoxic/necrotic core will start to form in the center of the spheroid. Such an arrangement in spheroids, in which there are regions of oxia and hypoxia, are similar to the environment found in cancer and, thus, make spheroids an ideal model system for cancer drug testing.[17] Furthermore, the three-dimensional arrangement of the spheroid maintains cell differentiation in regards to albumin production and cytochrome p450 activity when compared to monolayer cultures. [18, 19] [20, 21]

There are two types of spheroids, homospheroids and heterospheroids. Homospheroids are composed of only one cell type, whereas heterospheroids are composed of multiple cell types. The multiple cell types present in heterospheroids not only recapitulate in vivo conditions, in which multiple cell types are present, but aids in viability as the different cells may interact with each other to promote survival. For this

study, the liver model is composed of heterospheroids formed from two types of cells: parenchymal cells HepG2 and non-parenchymal cells 3T3-J2 fibroblasts. HepG2 cells are liver cancer derived cells and serve to model the liver cancer cells. Fibroblasts are connective tissue cells responsible for the secretion and remodeling of ECM via the synthesis of fibrillar collagen and matrix metalloproteases. Co-cultures of hepatocytes and fibroblasts are shown to improve liver function such as albumin secretion, urea secretion, and cytochrome p450 activity. [21-28] Cancer-associated fibroblasts aid the parenchymal cells by not only secreting and remodeling the ECM, but also by upregulating pro-survival signal transduction pathways. [29-32] These cancer fibroblasts differ from normal fibroblasts in that they have undergone the "angiogenic switch". The "angiogenic switch" refers to a phenotypic change in the fibroblast in which the fibroblast upon exposure to the tumor microenvironment becomes permanently "activated" producing higher than normal amounts of ECM and producing a-SMA. [29, 33, 34] Furthermore, these fibroblasts are known to remodel the environment to promote invasion/metastasis. [35, 36] Besides, aiding the liver cancer, fibroblasts will also serve to stabilize the structure of growing blood vessels, which is important in later sections. [29, 30, 37] Thus, by including fibroblasts into our spheroids, the spheroids will show greater resistance to the anti-cancer drugs as expected in vivo.

To culture this co-culture of HepG2 and fibroblast cell, the hanging drop method is used. In the hanging drop method, cells are trypsanized and the appropriate number of cells are pipetted onto a lid. The lid is then turned over to form the droplets, in which gravity pull the cells together to form agglomerations/spheroids.

Agglomerations/spheroids are harvested by turning over the dish and adding to liquid to cause droplets with the agglomerations/spheroids to pool together. The advantage of using the hanging drop method is that it doesn't require any specialized equipment, however, a disadvantage to this process is that it forces the formation of spheroids as a result of gravity, rather than as the result of cancer stem cells and their ability to form spheroids by themselves. However, this study is not interested in the subject of cancers stem cells and simply requires spheroids for their physical shape.

Once the spheroids are harvested, they will be encapsulated in collagen gel. ECM, such as collagen, not only plays an important part in promoting cell survival, but is used in this study as a barrier to drug diffusion. ECM is critical as a natural scaffold for cells to adhere to and to prevent anoikis, in which detached non-cancerous cells undergo apoptosis. Attachment of cells to ECM is known to promote cell viability, metabolism, and proliferation. Along this mode of thought, attachment of HepG2 to ECM components such as collagen or Matrigel, or ECM analogues such as chitosan or alginate is known to improve HepG2 adhesion, phenotype, and proliferation. [19, 38-41] Thus, to aid in HepG2 functionality, collagen gel is added to the model. Collagen is triple helix peptide chains containing the RGD peptide sequence, responsible for binding with integrins of the cell. In this study, heterospheroids are not embedded on collagen gel, but rather are embedded in the collagen gel. In vivo, the path for a drug to reach the tumor requires the molecule to traverse from the blood stream and through layers of cells including the tunica intima, tunica media, tunica adventitia, space of Disse, and normal hepatocytes to the tumor. The collagen gel is, thus, used to prevent the free diffusion of the drug to the spheroid. In other studies in which spheroids are embedded in gel, the spheroids show greater viability after

drug exposure compared to non-embedded counterparts. [42] Furthermore, the ECM of the tumor environment is known to have a higher stiffness than normal tissue due the greater expression of lysyl oxidase causing the crosslinking of collagen and has the ability to affect hepatocyte expression of cytochrome p450 metabolism and proliferation. [43, 44] To mimic this, a higher concentration of collagen gel is used to increase stiffness.

*To form a more biomimetic liver cancer model, co-cultures of HepG2 and 3T3-J2 fibroblasts are fabricated via the hanging drop method into heterospheroids and encapsulated in collagen gel, resulting in a model which recapitulates drug resistance found in cancer*. To measure this resistance, the heterospheroids are exposed to various drug conditions and measured for relative cell population and bile canaliculi. Measuring relative cell population via Alamar blue will show the effect of the cancer drugs on cell viability. The Alamar blue assay is a colormetric assay in which Alamar blue/resorufin is metabolized to ethoxyresorufin, and as a result changes color which can be used as a measure of cell population. To prevent, the fibroblast cell population from being included in this measurement of the effect of the drug on the HepG2 cancer, the fibroblasts are initially treated with mitomyocin C; a compound known to arrest cell growth. Measuring functioning of bile canaliculi via cholyl-lysyl-fluorescein (CLF) staining will show the ability of various 2D and 3D HepG2 cultures to maintain a functioning bile canaliculi, even after exposure to a choleostatic drug. Cholyl-lysyl fluorescein (CLF) is a fluorescent compound that resembles the bile salt cholyl glycine and so can be absorbed into the liver cell and become transported by a bile transporter such as MRP2 (multi-resistant protein 2) into the bile canaliculi and therefore can show the activity of the bile transporter and

visualize the bile canaliculi. Such a visual assay can, thus, be used to determine the effect of choleostatic drugs on liver cells, as choleostatic drugs impair the bile transporters.

## 2.2 Methods

### 2.2.1 Culture (HepG2/Fibroblast 3T3-J2)

Human hepatocellular liver carcinoma cell line (HepG2; gift from Dr. Charles Ross, Rutgers University) cells are cultured in DMEM High Glucose, 10% FBS (Biowest, Miami, FL), 2% penicillin and streptomycin (P/S, Gibco, Gaithersburgh, MD) and 2mM L-glutamine (Gibco) at 37$^{o}$C and 10% $CO_2$. The medium is changed every 2-3 days. Murine stromal cells (3T3-J2 fibroblasts, purchased from Howard Green, Harvard Medical School, Boston, MA) are maintained in DMEM plus 10% FBS and 1% P/S.

### 2.2.2 Hanging Drop Method-Homospheroids and Heterospheroids

The hanging drop technique is used to agglomerate cells into spheroids. For homospheroid formation, a density of 1,000 HepG2 cancer cells per 30 μL is obtained. For heterospheroid formation, a density of 1,000 HepG2 cells and 1,000 growth-arrested fibroblasts per 30 μL is obtained. Using a multi-channel pipette, 30 μL of cell suspension is pipetted onto the lid of a 100-mm Petri dish. Lid is flipped onto bottom dish to form droplets. The dish is filled with sterile deionized water to prevent the droplets from evaporating. Droplets are incubated for 2 days to form spheroids. Spheroids are then harvested for cell culture.

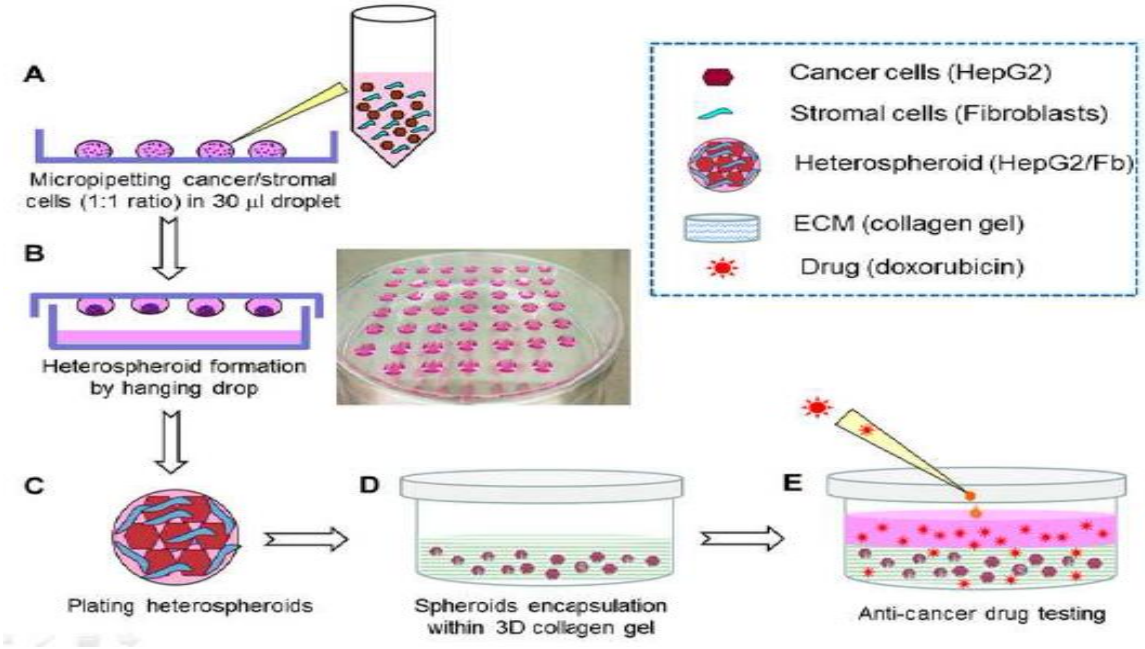


**Figure 2.1** Hanging Drop Method Fabrication (Homospheroid and Heterospheroid). Schematic of hanging drop fabrication shows steps in spheroid manufacture. A) shows liver cancer and stromal cells being pipetted onto a Petri dish lid. B) shows lid being flipped over to form hanging drops. C) shows heterospheroids being harvested. D) shows heterospheroids being encapsulated in collagen gel. E) shows anti-cancer drug being added to heterospheroid/collagen gel system.

### 2.2.3 Mitomycin C

Fibroblasts are seeded on a tissue culture plate and grown to confluence. Confluent fibroblasts are growth-arrested by treatment with 12 µg/ml of mitomycin C (Sigma) for 2.5 hr. After incubation, fibroblasts are washed and trypsanized prior to hanging drop method.

### 2.2.4 Collagen Hydrogel

For spheroid culture in collagen gel, approximately 50 spheroids are mixed with 0.3 mL collagen solution of 9 parts of type I rat tail collagen (1.2 mg/mL, BD Bioscience) and 1 part 10x DMEM. The mixed solution is added into 24-well and incubated for 1 hr at 37C to form a collagen gel and spheroid encapsulation within the gel. After gelation, 0.5 mL of

HepG2 culture medium is added and incubated at 37$^{o}$C and 10% $CO_2$ for anti-cancer drug testing.

### 2.2.5 Spheroid Diameter

To examine the spheroid growth over time, spheroids obtained from the hanging drop method are transferred in a Petri dish for suspension culture. Spheroid images in suspension culture are captured over 5 days and analyzed by Sigma Scan Pro image software (SPSS, Inc, Chicago, IL) to measure the diameter.

### 2.2.6 LIVE/DEAD Assay

For the Live/Dead Assay, 1 μM calcein AM and 1 μM ethidium homodimer (Invitrogen) are added to the model and then incubated at 37C for 10 min. Following incubation, culture/spheroids are visualized with fluorescent microscopy using a Nikon Eclipse TI-5 microscope.

### 2.2.7 Alamar Blue Assay

Cell population can be measured using the Alamar Blue assay, in which the dye resazurin is incubated with the spheroids, aliquots are taken after 1 hr, and then measured with a fluorometer. The absorbance values correlate with the cell population.

10 μM resazurin (Fisher) is added to 500 μL cell culture media in a 24-well plate and incubated at 37°C for 1 hr. The samples are collected every day and transferred to 96 well plates for the assay. After the sample collection, the cell culture plates are washed with PBS and fresh media with the anti-cancer drug is added to each well. Fluorescent

intensity of the samples are measured using a fluorescent microplate reader (Gemini XPS, Molecular Devices) at wavelengths 530 nm for excitation and 590 nm for emission.

Alamar blue assay is performed to create:

1) A standard assay (based on fibroblast cell population) in which fibroblasts of known quantity are inoculated into a 48 well plate and Alamar blue assay performed the next day.

2) To compare 2D monolayer (HepG2) exposed with and without anti-cancer drug. 50,000 HepG2 cells are inoculated into a 24 well plate and Alamar blue assay is performed on 0, 1, 2, 3, and 4 days. Culture is exposed to 10 μM doxorubicin, which is changed every day.

3) To compare 3D homospheroids embedded in collagen gel (1.2 mg/mL) exposed with and without anti-cancer drug on 0, 1, 2, 3, and 4 days. 3D homospheroids are encapsulated as described in section 2.2.4. Culture is exposed to 10 μM doxorubicin, which is changed every day.

4) To compare 3D heterospheroids embedded in collagen gel (1.2 mg/mL) and 10x DMEM exposed with and without anti-cancer drug on 0, 1, 2, 3, and 4 days. 3D homospheroids are encapsulated as described in section 2.2.4. Culture is exposed to 10 μM doxorubicin, which is changed every day.

### 2.2.8 Cell Tracker Assay

To examine initial cell distribution of HepG2 and fibroblasts within the heterospheroids, HepG2 are labeled with 1 μM 5-chloromethyl fluorescein diacetate (CMFDA, green cell tracker dye, Invitrogen) and fibroblasts are labeled with 1 μM CMTPX red cell tracker dye (Invitrogen) for 15 min prior to addition as droplets on lid to form hanging drops. The spheroids are observed by the fluorescent microscopy.

### 2.2.9 Cytochrome p450 Assay

Cytochrome P-450 A1 (CYPA1) enzymatic assay is performed by measuring the ethoxyresorufin-O-deethylase (EROD) activity. The EROD activity assay measures drug metabolism by measuring the ability of the HepG2 cells to convert ethoxyresorufin to resorufin. After 5 days of anti-cancer drug treatment, the cultures are induced to produce CYPA1 by 2 μM 3-methylcholanthren (3-MC, Sigma) for 48 hours. The cells are then washed well with PBS, followed by 1 hr incubation with 8 μM ethoxyresorufin (Sigma) in phenol red free culture medium at 37C. The sample medium is collected after incubation and the fluorescence intensity is measured at 530 nm excitation/580 nm emission wavelength by the fluorescence microplate reader. Resorufin (Sigma) standards at the range of 1-1,000 nM are used to determine the sample concentration.

### 2.2.10 CLF Staining

Bile canaliculi are tubes found between hepatocytes and the excretion of bile salts through bile transporters into these bile canaliculi can be impaired by exposure to choleostatic drugs. Cholyl-lysyl-fluorescein (CLF) is a fluorescent bile acid which localizes to the bile canaliculi, and therefore can be used as a measure of the effect of drugs on a culture of hepatocytes. Cultures are exposed to 10 μM CLF for 40 min and washed twice before visualization. For drug conditions, culture or spheroids are exposed to 20 μM cyclosporine for 2 hrs and washed twice before incubation with CLF.

## 2.3 Results

### 2.3.1 Spheroid Diameter

Spheroid diameters of homospheroids and heterospheroids are measured over 5 days using the image analysis software. Uniform s*pheroids* with *diameters* between 300-400 μm are obtained after 2 days of culture by the hanging drop method. After plating the spheroids in a Petri dish for suspension culture, the spheroid diameter initially decreases due to cellular reorganization. The spheroid diameter then increased continuously. The diameter increases by 35% for homospheroids and by 14% for heterospheroids at day 5. Homospheroids demonstrated higher spheroid growth rate compared to heterospheroids but there is no statistically significant differences over the 5 days of culture.

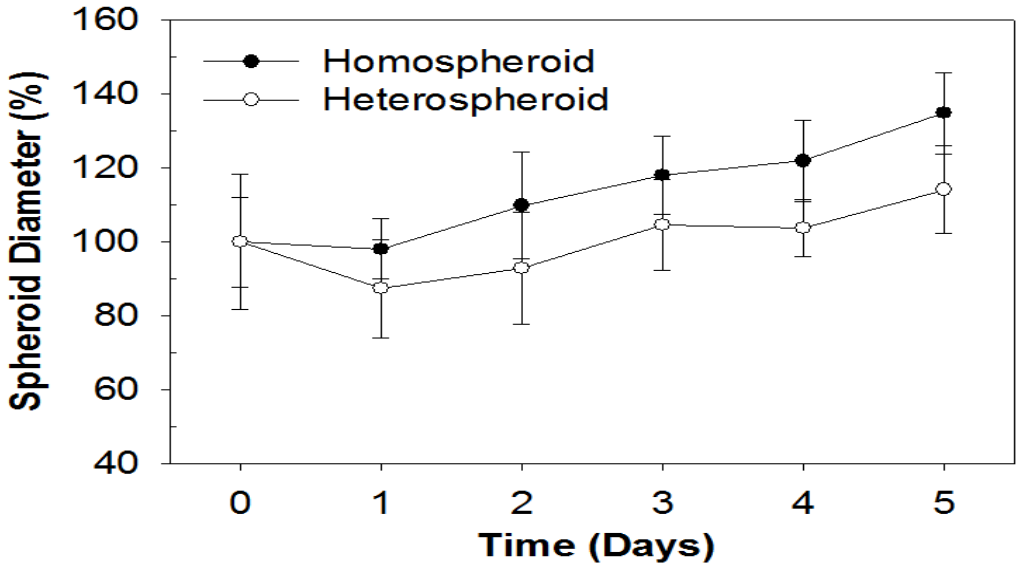


**Figure 2.2** Spheroid Diameter of Homospheroids versus Heterospheroids. Graph compares relative spheroid diameter growth of homospheroid and heterospheroid growth measured over 5 days. Homospheroids shows greater spheroid diameter growth than heterospheroids. Ability of fibroblasts to contract may explains why heterospheroids showed less spheroid diameter growth than homospheroids. Values represent averages ± SD (n=3).

### 2.3.2 LIVE/DEAD

Two types of spheroids are fabricated using the hanging drop technique: homospheroids and heterospheroids. Homospheroids are composed of one thousand HepG2 liver carcinoma cells each. Heterospheroids are composed of one thousand HepG2 liver carcinoma cells and one thousand stromal fibroblasts each. Live/Dead cell staining is performed with calcein-AM and ethidium homodimer to examine the viability of the cells within the spheroids formed by the hanging drop method. Figure 2.3 shows phase and fluorescent images of HepG2 homospheroids stained with the Live/Dead cell dyes. Highly compact cell aggregates are formed within the spheroids. Most of the cells are stained with green for live cells and only a few cells express red for dead cells, indicating good cell viability within spheroids.

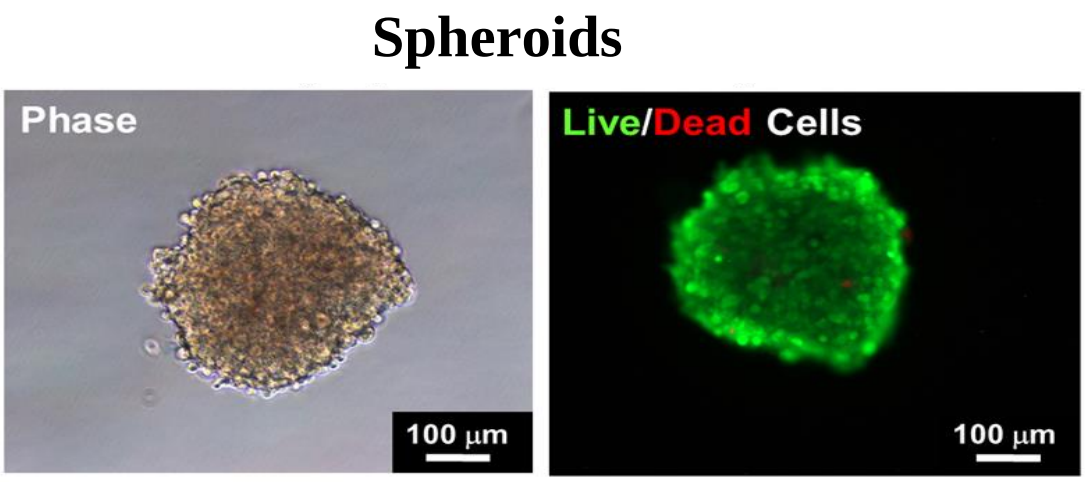


**Figure 2.3** LIVE/DEAD Assay of Spheroid. Live/Dead assay of spheroid shows overall green coloration of the spheroid, showing ability of the spheroid to maintain cell viability.

### 2.3.3 Alamar Blue Assay (Standard Curve, 2D Monolayer)

To examine cytotoxicity and proliferation of the spheroids for anti-cancer drug treatment, Alamar blue (resazurin) assay is performed by treating the cells with 10 μM doxorubicin. Figure 2.4 A) exhibits a standard curve of HepG2 cells at various cell densities determined by the Alamar blue assay. There is a linear relationship between the fluorescence intensity and HepG2 cell number. Before testing anti-cancer drug treatment in the 3D spheroid hydrogel culture system, HepG2 cancer cells are tested in a 2D monolayer culture system as a control to investigate the effect of doxorubicin. Over the 4 days of the monolayer culture, treatment with 10 μM doxorubicin results in 54% and 17% cell viability on days 2 and 4, respectively as shown in Figure 2.4B). In contrast, the HepG2 cells cultured without doxorubicin exhibit continuous increase in cell number during the culture period, demonstrating 334% cell growth (2.3-fold increase) after 4 days of culture. There are statistically significant differences between no drug and drug conditions on cell viability and proliferation on days 1-4.

A) **Alamar blue assay (standard curve)**

B) **2D monolayer culture**

C) **3D Spheroid culture**

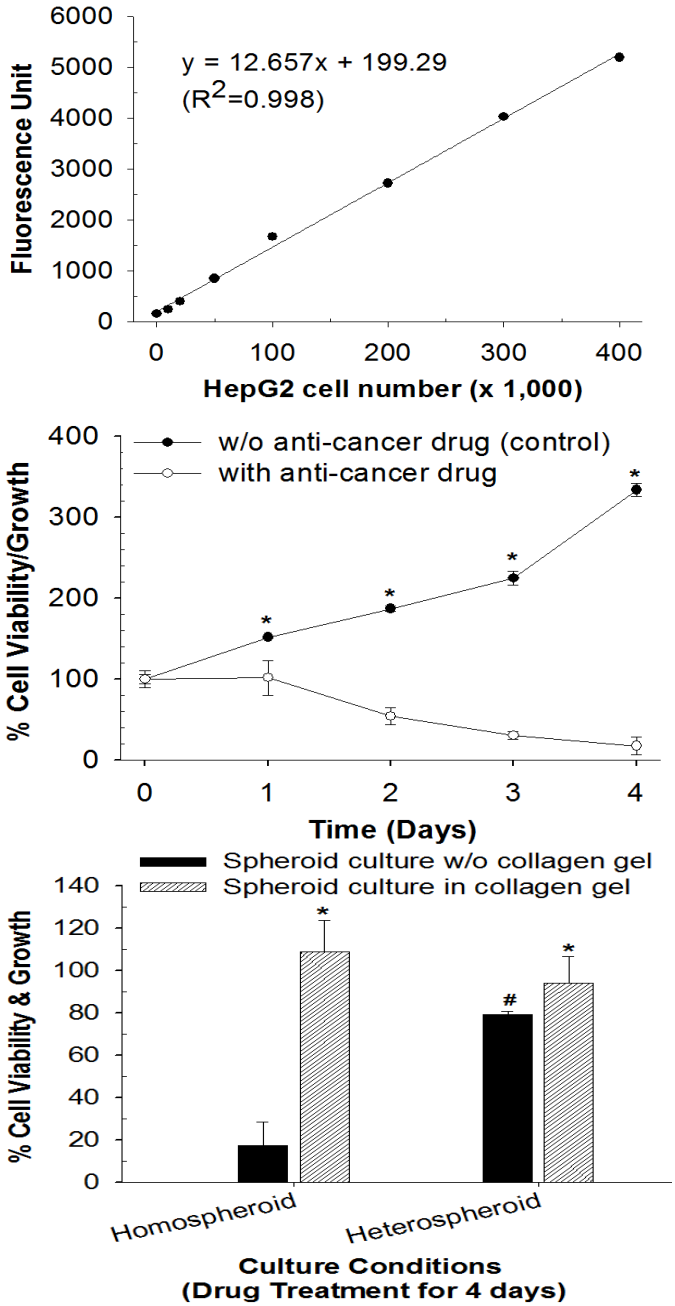


**Figure 2.4** Graphs of Standard Curve, 2D Monolayer Cultures, and 3D Spheroid Cultures. Graphs pertaining to cell viability as measured by the Alamar Blue assay are shown. A) is a standard showing fluorescence and comparable cell population. B) compares 2D cell culture growth with or without 10 μM doxorubicin, showing decreased viability upon drug exposure. C) compares cell growth of homospheroids versus heterospheroids and with versus without collagen gel, showing greater resistance in heterospheroids compared to homospheroids in non-gel conditions, and high and no significant difference between homospheroids and heterospheroids in collagen gel conditions. Values represent averages ± SD (n=3, $P<0.05$, *Spheroids in collagen gel vs. non-gel, # homospheroids non-gel vs. heterospheroid non-gel cultures.

### 2.3.4 Alamar Blue Assay (Homo/Heterospheroid w and w/o Collagen Gel)

Alamar blue assay in the 3D spheroid cultures reveals that 3D homo- and heterospheroid cultures in collagen gel show significantly higher drug resistance to 2D cell cultures after 4 days of doxorubicin drug treatment as shown in Figure 2.4C). Homospheroids in collagen gel culture system show more drug resistance than those not cultured in collagen gel. Similar results are observed in heterospheroid cultures. Among cell cultures without collagen gel, heterospheroid culture show significantly higher drug resistance than homospheroids and 2D monolayer cultures, but no significant difference in collagen gel cultures. Results of this study indicate that stromal fibroblasts and collagen hydrogel culture system provide more resistance to the anti-cancer drug.

### 2.3.5 Cell Tracker Assay

To monitor HepG2 and fibroblasts within the heterospheroids, cells are labeled with two different fluorescent cell tracker dyes prior to spheroid formation and observed by fluorescent microscopy after spheroid formation by the hanging drop method. As shown in Figure 2.5, two cell types form the heterospheroid that are spatially controlled by the hanging drop method, demonstrating homotypic and heterotypic cell-cell interactions between HepG2 and fibroblasts. Most of the growth-arrested stromal fibroblasts are observed in the center core of the spheroids, whereas HepG2 are observed both in the center core and at the spheroid periphery.

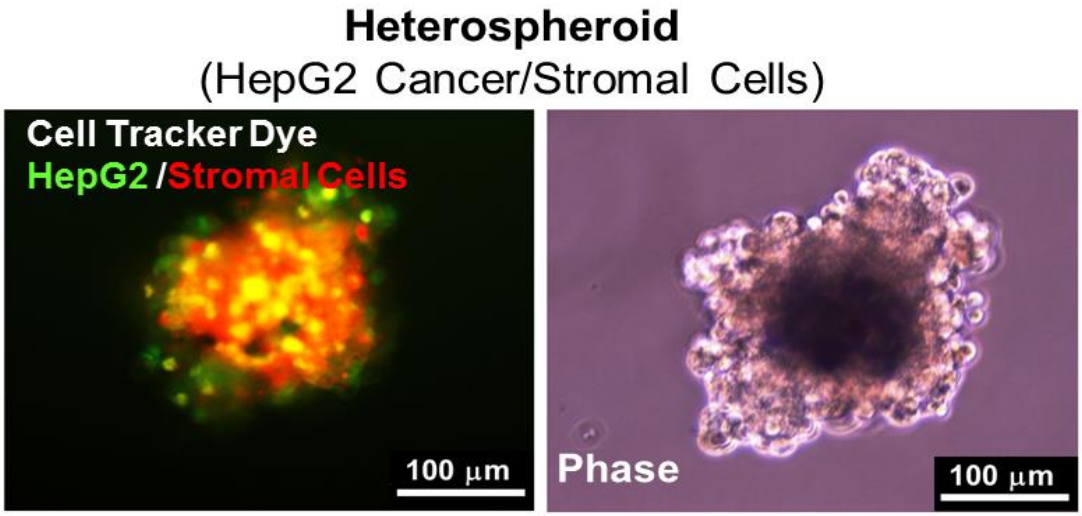


**Figure 2.5** Cell Tracker Dye of Heterospheroid. Cell tracker dye of Heterospheroid containing HepG2 cells (in green) and fibroblast cells (in red) shows the even distribution of Cell tracker green stained HepG2 and Cell tracker red stained stromal cells, as evident by yellow overlap.

### 2.3.6 Alamar Blue Assay (Heterospheroid Drug Exposure)

Cell viability and growth in the 3D heterospheroid hydrogel culture system with or without doxorubicin treatment for 4 days are shown in Figure 2.6. 10 μM doxorubicin treatment results in 116% and 89% cell viability on days 2 and 4, indicating high drug resistance compared to 2D monolayer culture, as shown in Fig. 2.4 B. For the heterospheroid hydrogel culture condition without doxorubicin, the cell number increased continuously throughout the culture period, showing 274% cell growth (1.7-fold increase) on day 4.

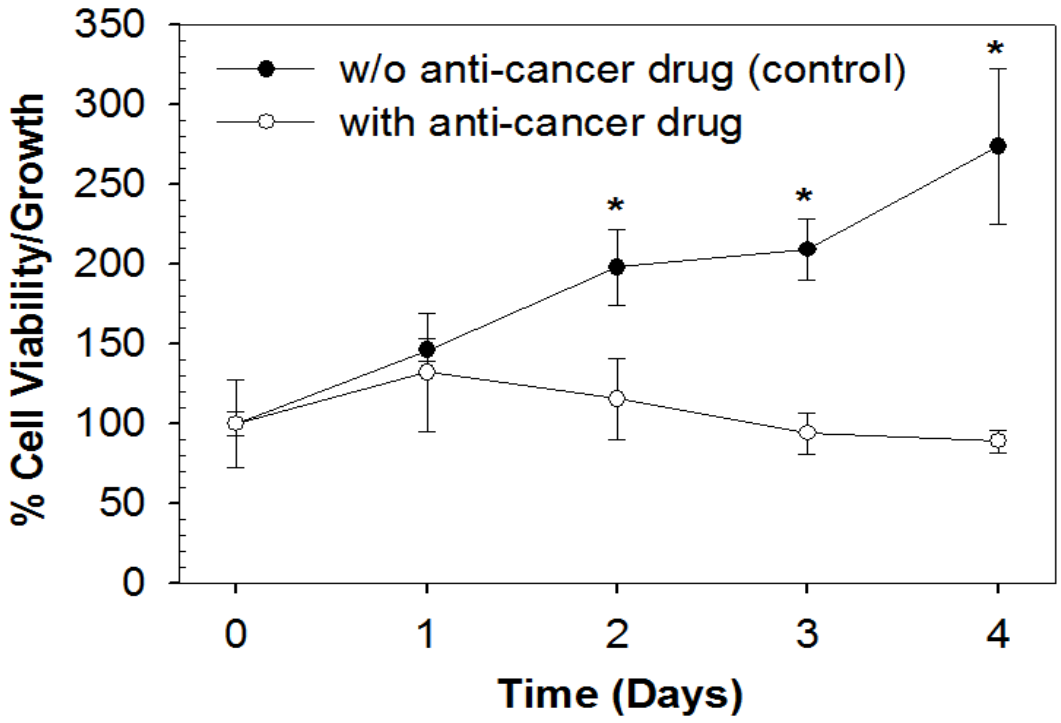


**Figure 2.6** Cell Viability of Heterospheroids in Collagen Gel Exposed to Drug. Heterospheroids in collagen gel are exposed to 10 μM doxorubicin and Alamar blue assay is used to measure cell populations on day 0 through day 4. Upon drug exposure heterospheroid viability drops. Values represent averages ± SD (n=3, *P<0.05).

### 2.3.7 Heterospheroid Drug Exposure (Phase Imaging)

Heterospheroid morphology cultured in collagen gel with and without 10 μM doxorubicin treatment at day 4 are shown in Figure 2.7. The doxorubicin treatment for 4 days suppressed the spheroid growth and results in deterioration of spheroid structure and cell membranes, whereas the heterospheroids without the drug treatment retains good spheroid morphology.

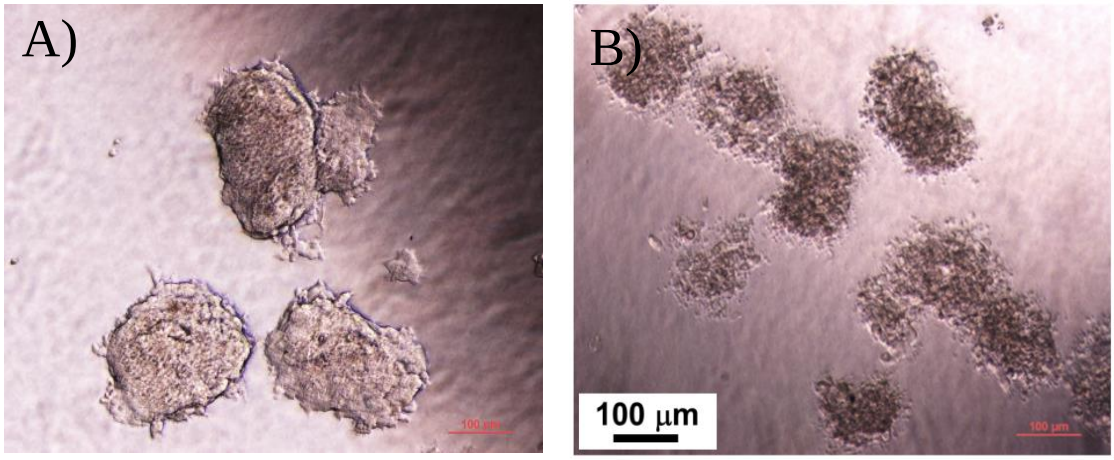


**Figure 2.7** Phase Images of Heterospheroids in Collagen Gel Exposed to Drug. Heterospheroids are exposed to 10 μM doxorubicin and 10x phase images of A) non-exposed conditions and B) exposed condition are imaged.

### 2.3.8 Heterospheroid Drug Exposure (Cytochrome p450 Assay)

Cytochrome P-450 A1 (CYPA1) enzymatic assay is performed to assess the drug metabolism function of HepG2 in 3D heterospheroid culture system with and without the doxorubicin treatment. The CYPA1 assay measures drug metabolism by measuring the ability of the HepG2 cells to convert ethoxyresofurin to resorufin. The assay reveals that heterospheroids in collagen gel show significantly higher drug metabolism function than those without gel, indicating more drug resistance as shown in Figure 2.8. The resorufin production rate of heterospheroid culture with 10 μM doxorubicin treatment is 0.047 ± 0.013 [nM/hr] for collagen gel culture and 0.015 ± 0.002 [nM/hr]. Similar results are observed in the heterospheroid culture without the doxorubicin treatment.

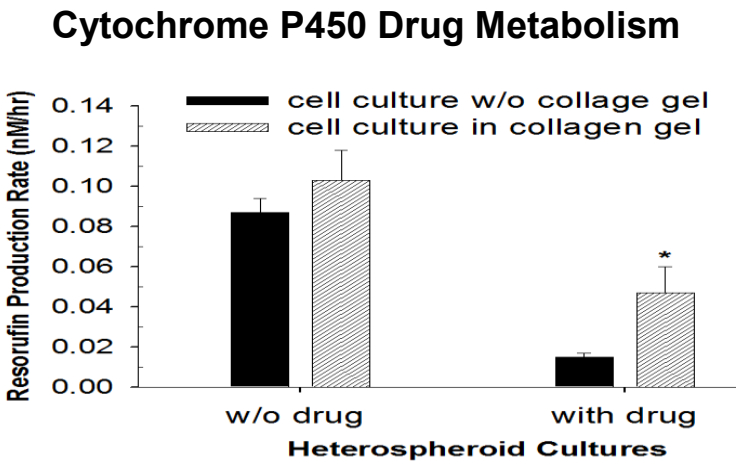


**Figure 2.8** Graph of Cytochrome p450 Metabolism of Heterospheroids in Collagen Gel Exposed to Drug. Graph compares cytochrome p450 drug metabolism of heterospheroids with or without drug and with or without collagen gel after 5 days. Graph shows that heterospheroid culture in collagen gel produces a greater cytochrome p450 metabolism compared to conditions without collagen gel. Values represent averages ± SD (n=3, *P<0.05, collagen gel vs. non-gel cultures).

### 2.3.9 CLF Staining

To investigate the uptake and inhibition of fluorescent probe substrate (CLF) into bile canaliculi, CLF staining is performed on 2D HepG2 culture, 3D homospheroids, and 3D heterospheroids, with or without exposure to 20μM cyclosporine A (transporter inhibitor). Green fluorescence is present along the edge of the cells, where bile transporters are located between adjacent hepatocytes. As shown in Figure 2.9B), the 2D HepG2 culture shows no green fluorescence, indicating no bile canaliculi formation. In contrast, 3D homospheroid showed strong expression of CLF staining, indicating good bile canaliculi formation. Similar results are observed in 3D heterospheroids, forming good bile canaliculi formation as shown by Figure 2.10D). Exposure of 3D heterospheroids to cyclosporine shows a decrease of green fluorescence, which indicates the efflux of the CLF substrate into bile canaliculi via MRP2 transporter is blocked by the Cyclosporin A inhibitor.

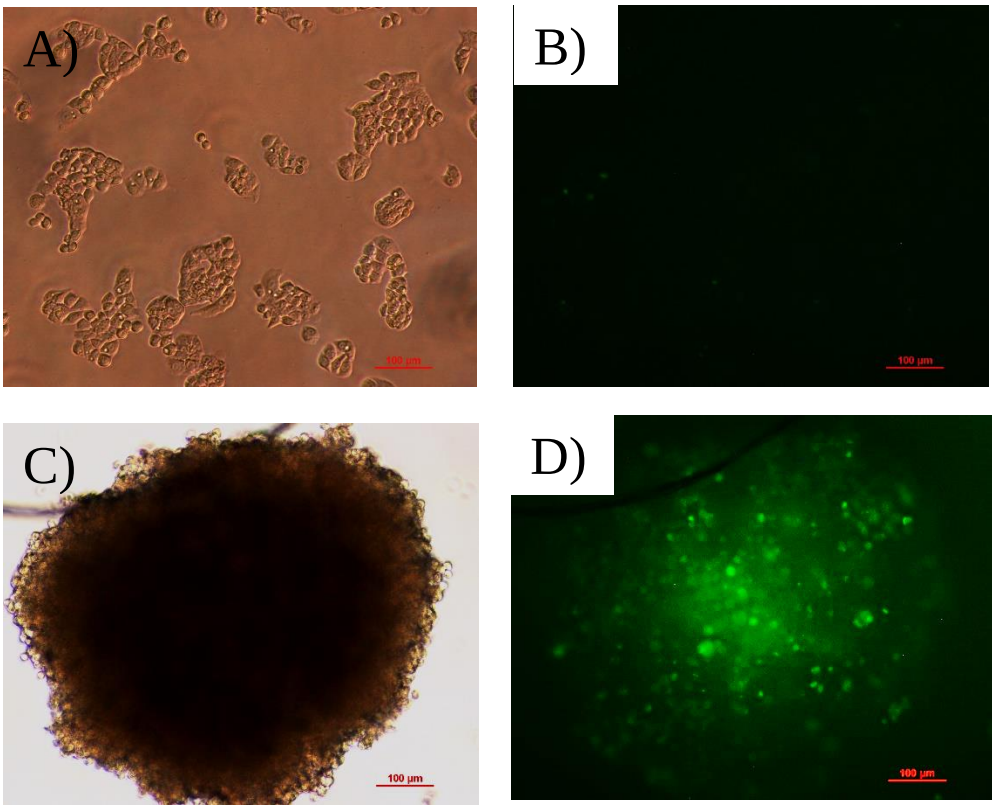


**Figure 2.9** CLF Staining of 2D Monolayer versus 3D Homospheroids. Bile canaliculi is imaged using CLF staining at 10x magnification to compare 2D and 3D cultures. A) is a 2D HepG2 culture and B) is the subsequent CLF stained image. C) is a 3D HepG2 homospheroid culture and D) is the subsequent CLF stained image. 3D spheroids more brightly express bile canaliculi compared to 2D cultures.

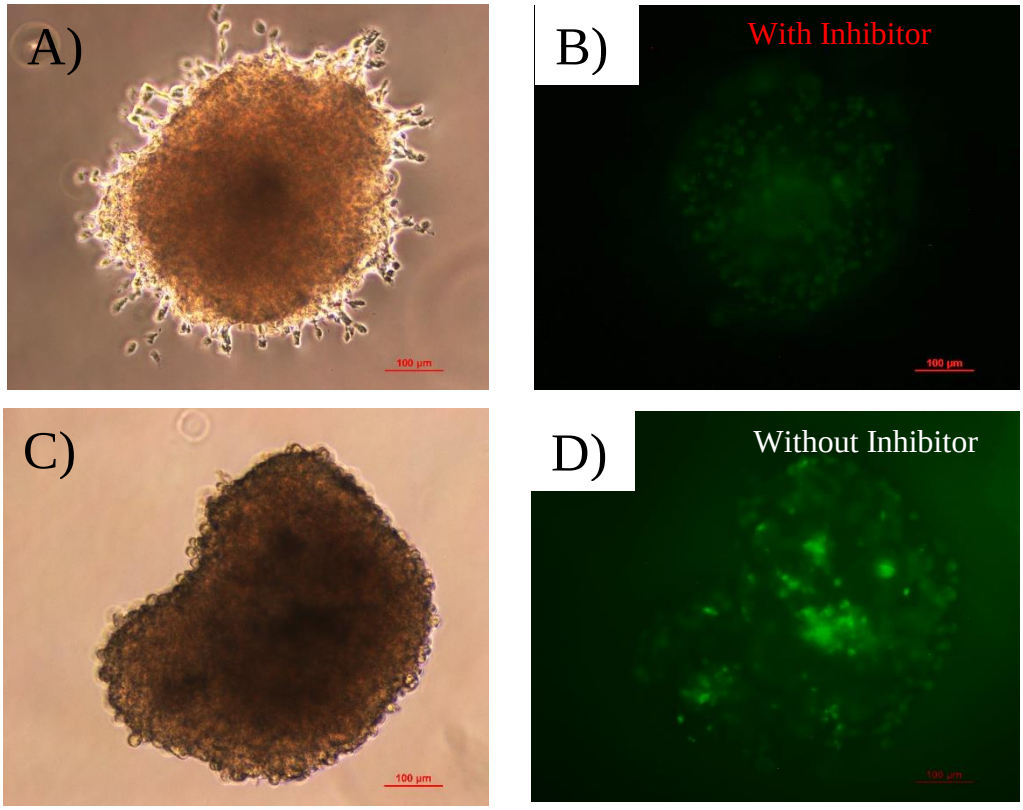


**Figure 2.10** CLF Staining of Heterospheroids Exposed to Cyclosporine A (Transporter Inhibitor). Bile canaliculi is imaged using CLF staining at 10x magnification to compare cyclosporine exposed and non-cyclopsorine exposed heterospheroids. Fluorescent images of 3D spheroids show A) phase image and subsequent B) CLF stained image after exposure to 20μM cyclosporine for 2 hrs. Fluorescent images of 3D spheroids show C) phase image and subsequent D) CLF stained image without exposure to cyclosporine. The cyclosporine condition shows a greater decrease of CLF staining, than in the control condition.

## 2.4 Discussion

### 2.4.1 Spheroid

A spheroid is an agglomeration of cells shaped like a sphere resulting in a construct which has three dimensions, much like cancer in the human body. Furthermore, due to its shape, spheroids prevent the diffusion of oxygen into the core of the spheroid resulting in hypoxia and necrosis similar to that of a tumor. Due to these reasons, spheroids are used in this study as an in vitro model of cancer.

Spheroids are developed using the hanging drop method, in which cells in media are hung as droplets which form spheroids due to gravity, and are assessed to determine if such a construct would be a viable system to maintain cells. A LIVE/DEAD cell assay is performed on a homospheroid, a spheroid composed, in this case, of only the hepatocellular cancer revealing living cells in green and dead cells in red. As can be seen by Figure 2.3, the entirety of the spheroid fluoresces green with little to any red, showing that the spheroid is a viable system to maintain cells.

Spheroid diameter is measured between homospheroids and heterospheroids, and shows no significant difference between their diameters. Spheroid diameters are often used as correlative with cell proliferation and growth. The fibroblasts within the heterospheroids are supposed to improve cell proliferation as it known that co-culture of fibroblasts and HepG2 cells improve this aspect of HepG2 cells, and yet the conclusion of this experiment does not support this claim. A theory for the disparity may be the remodeling capabilities of fibroblasts. Fibroblasts are responsible for remodeling ECM and as such have contractile capabilities. As such it can be assumed that the fibroblasts are able to contract the spheroid, effectively decreasing the diameter.

To determine the effectiveness of spheroids as a culture system to maintain cell viability similar to conditions in vivo after exposure to anti-cancer drugs, 3D homospheroids and 2D HepG2 cells are incubated with doxorubicin. When exposed to the drug doxorubicin, the 3D model shows increased resistance to the drug compared to 2D. Using the Alamar Blue assay, as shown in Figure 2.4, the relative percentages are calculated. The 3D model in Figure 2.4 C) shows a higher cell population than the 2D model in Figure 2.4 B) on day 4. Thus, the 3D model shows a greater degree of drug

resistance than the 2D model, and, thus, mimics in vivo conditions showing the validity of the 3D model as an in vitro model. As expected, 3D spheroids are able to maintain cell viability because of the multiple barriers within the culture, including the gel and the layers of cells, preventing the diffusion of the doxorubicin. Cell-cell contacts promote pro-viability signaling and a three-dimensional culture increases the number of cell-cell contacts as each cell is not only in contact with another cell on the same plane, but with those cells on planes above and below. The results of these cell contacts is improved function and viability of the cell culture, including improved albumin secretion and cytochrome p450 activity. [45-47] The three-dimensional culture also has the ability to promote cancer stem cells/tumor progenitor cells in HepG2 spheroids and spheroid forming cancer cells in general. [48-50]

Another aspect of dimensionality is drug exposure. In the human body, a drug is physically blocked from reaching the cancer by the tortuosity of the blood vessels leading to the cancer, limitations of diffusion through multiple layers of cells, and the over-accumulation of extracellular matrix. [51] The monolayer culture does not have any physical barrier to prevent exposure of the culture to the drug and so requires only a smaller dosage of a drug to render the same effect as that of the in vivo condition. To mimic the in vivo condition, cancer cells are often embedded in hydrogels much like our collagen gel, which provide an additional physical barrier. [41, 52]. By being more viable than 2D cultures, the 3D cultures system shows itself to be a more correct drug cancer model.

### 2.4.2 Co-culture

Two-dimensional cultures as in vitro cancer models are unreliable as they fail to mimic the complexity of the in vivo conditions that they are modelling, not only in terms of

dimensionality, but in regards to cell type. The human body consists of more than two hundred cell types. In terms of drug testing of in vitro cancer models, the lack of similarity can drastically affect the results of such testing and lead to erroneous conclusions.

To recreate this aspect of the tumor environment, heterospheroids are made in which spheroids contain one or more cell type, in this case hepatocellular cancer and fibroblasts. It should be noted here that ideally, the fibroblasts used would be of human origin and of a cancerous phenotype. However, due to the difficulty in obtaining fibroblasts with both characteristics, 3T3-J2 fibroblasts were used instead. 3T3-J2 fibroblasts are an embryonic mouse line and it is assumed due to the culturing of these fibroblasts on a stiff surface, i.e. the tissue culture plate, and its presence near cancer cells in the spheroid, that the fibroblasts transform into a cancerous phenotype. In the future, fibroblasts of a human origin and cancerous phenotype should be used. Cell Tracker imaging is performed on the cells of the heterospheroid in which hepatocellular cancer cells are labelled in green and fibroblast cells are labelled in red. As shown in Figure 2.5, the cells distributed randomly as evident by the uneven distribution of green/hepatocellular and red/fibroblasts cells as well as large swaths of yellow showing overlap of these two types of cells. When heterospheroids are grown on collagen gel and exposed to doxorubicin as shown in Figure 2.7, blebbing can be seen around the edges of the spheroid. In the future, TUNEL assay should be used to determine the presence of apoptosis in these images.

Growing spheroid diameter can be correlated to tumor volume, a measure of cancer growth in animal studies. To this end, the spheroid diameters of homospheroids and heterospheroids are compared. It should be expected that given that fibroblasts are known to improve HepG2 proliferation, that the spheroid diameter of heterospheroid should be

significantly larger than that of homospheroids. In reality, the opposite is true as shown in Figure 2.2 in which homospheroids show an average diameter larger than heterospheroids on days 1 through 5, although not significantly different. Although, fibroblasts are known to aid in proliferation, they also are known for their contractile ability, hence the fibroblasts may have caused compaction of the heterospheroid. Tumor volume is often used as a correlative of tumor growth in animal studies and so the spheroid cannot be compared to the animal studies in this regard.

Another experiment to determine the effectiveness of heterospheroids, co-cultures of HepG2 and fibroblasts, versus homospheroids, is to compare their viability after exposure to doxorubicin as shown by Figure 2.4C). When exposed to the drug doxorubicin, the heterospheroids without collagen gel show increased resistance to the drug compared to homospheroids without collagen gel after 4 days exposure to doxorubicin, showing relative percentage of 17.5 ± 11% compared to 79.1 ± 1.6 %. The reason for heterospheroid's resistance to the anti-cancer drugs can be explained by the inclusion of fibroblasts which are shown to promote resistance of cancer cells towards anti-cancer drugs. [20, 21, 31, 53, 54] Fibroblasts promote drug resistance in a variety of manners ranging from the secretion of ECM components, the release of exogenous growth factors, and the promotion of neoangiogenesis. [31, 55-57] However, when homospheroids and heterospheroids are incubated in collagen gel, the spheroids show no significant difference between the conditions, showing comparable viability of 108.7 ± 15.1% and 94.0 ± 12.9%, respectively. The collagen gel may be the primary reason for drug resistance as it prevents the diffusion of the drug to the spheroid and so mask any effects of fibroblast drug resistance. Collagen can act physically and biochemically to promote drug resistance/cell

viability. Physically, collagen can act as a barrier to prevent the diffusion of drugs and is used in this study to recapitulate the physical barrier a drug encounters on its path to the tumor. Most notably, the collagen acts like the space of Disse, which is a layer of collagen which separates the endothelial cells from the hepatocytes in the liver. Biochemically, collagen acts as an ECM substrate by which cells can adhere and can transduce signals through integrins to promote cell viability. This study does not delve into the etiology for drug resistance caused by collagen, though in the future the etiology of drug resistance/cell viability could be determined by encapsulating spheroids in alginate gel. Alginate gel can also act as a physical barrier, however, because it has no binding sites for cells, it does not act biochemically to promote cell viability. Thus, if spheroids in alginate gel show comparable viability to spheroids in collagen following exposure to an anti-cancer drug, then it can be concluded that the gels act primarily as a barrier to drug diffusion, rather than acting on signaling transduction pathways. Also required is the exposure of collagen culture to a vehicle/negative control. A matter in which the collagen gel in our study proves itself dissimilar to the in vivo environment is the amount by which it may act as a physical barrier to drug diffusion. The average distance between blood vessels is between 100 and 150 μm, and is smaller in regions of the body where there is a higher metabolic need for oxygen such as in the brain or the liver. As such to be biomimetic, the collagen barrier should be approximately between 100 and 150 μm, and yet in our study, the collagen barrier is at least 1 cm or several orders of magnitude higher than that of in vivo conditions. Thus, the drug must also travel several orders of magnitude higher than it would in vivo, rendering a higher drug resistance than expected.

The 3D model is able to prevent choleostatic drugs such as cyclosporine A from affecting the bile transporters found between hepatocytes of the cell culture. Bile canaliculi is a thin tube formed between hepatocytes as a conduit for the excretion of bile, but only when the hepatocytes are properly functioning and, thus, can be used as a measurement of liver function. To determine the ability of a 3D model to form these bile canaliculi, 3D heterospheroids and 2D culture of HepG2 are exposed to CLF. The resulting images, as shown in Figure 2.7, reveal that the 3D model shows a much brighter green fluorescence of the CLF transported into the bile canaliculi, than the 2D culture. This is evident by the fluorescence seen surrounding the cells in the 3D model. Thus, the 3D model is superior to 2D cultures in improving liver functionality. The functioning of the bile canaliculi can be inhibited by the introduction of the choleostatic drug, cyclosporine A. Cyclosporine is a drug which is a competitive inhibitor of bile transporters and, thus, prevents excretion of bile acids such as CLF into the bile canaliculi. Cyclosporine A is exposed to a heterospheroid, and its fluorescence is compared to a non-exposed condition. The non-exposed condition showed greater green fluorescence compared to its exposed counterpart. Similar maintenance of the bile canaliculi when exposed to choleostatic drugs is evident in other 3D models such as the sandwich model or in Matrigel. [58-61] In the future, other such assays of liver function such as the albumin or urea assay should be performed to determine the effect of these drugs on our model.

# CHAPTER 3

# VASCULARIZED MICROFIBER/ELECTROSPUN TUBE

*Aim 2 is to fabricate and characterize chitosan-heparin micro/nanofiber scaffolds seeded with endothelial cells to act as tissue engineered blood vessel as a substrate for angiogenesis*. We hypothesize that heparin immobilized chitosan microfibers or electrospun tube will support enhanced VEGF binding and endothelial cells adhesion for angiogenesis.

## 3.1 Background

Diffusion is capable of distributing molecules of nutrients and gases up to 100 μm. As a result, multicellular organisms with tissues exceeding 100 μm have a vasculature which greatly expands the surface area and the capability of diffusion. Without this vasculature, cells may undergo hypoxia and soon die. As a result, the tumor hijacks the angiogenesis process by releasing pro-angiogenic growth factors to promote angiogenesis and subsequent vascularization of the tumor. The triculture heterospheroid is a model of the cancer, however, to complete the model of cancer angiogenesis, a blood vessel construct needs to incorporated.

We propose two types of blood vessel constructs: chitosan microfibers and electrospun tubes coated with endothelial cells. *In which discrete chitosan micro/microfibers are crosslinked with heparin for fibronectin and VEGF, and seeded with endothelial cells to act as tissue engineered blood vessel as a substrate for angiogenesis.*

The vasculature is composed of a variety of cell types with their own specific functions to maintain the vessel. Endothelial cells compose the inner tunica intima of the

vasculature. For this study, the endothelial lines RAEC and MVEC are used. Although, human umbilical vascular endothelial cells (HUVEC) would be the ideal cell line to use in order to recapitulate human physiology due to the cell line's human origins, their limited lifespan/Hayflick limit and low rate of cell division makes the cell line difficult to coat and successfully grow on the chitosan constructs.

Besides, endothelial cells, cells such as smooth muscle cells, help to maintain the vasculature in normal, healthy tissue; however, in cancer the vasculature grow wild and hoary due to a lack of these cells. [62-64] An example of such cells not included in this model are pericytes. Pericytes, or stellate cells in the liver, are responsible for maintaining and stabilizing blood vessels, as well as providing growth factors and cytokines. [65] However, although certainly present in the normal and cancer vasculature, pericytes are may not be necessary for this model of cancer. Cancer vasculature has a tortuous architecture containing vessels of varying diameters, abnormal vascular branching pattern, and irregular blood flow.[62-64] Reasons for this include differential expression of growth factors throughout the cancer.[62-64]. The cancerous pericyte, is loosely attached to the vasculature, resulting in a failure to maintain and stabilize the blood vessel. [65, 66] What is more, fibroblasts may be able to form vascular lumen with the endothelium and without pericytes, thus, abrogating the need for pericytes. [67, 68]

To serve as a scaffold for the endothelial cells, wet spun chitosan fibers and electrospun chitosan tubes are used. Concerning wetspun chitosan fibers, when chitosan is exposed to an acid it becomes a liquid, however, becomes a solid when the chitosan/acetic acid solution comes in contact with a strong basic solution. This chitosan/acetic acid solution is injected into a strong basic solution of NaOH:EtOH via a 30 gauge syringe

needle, wet spun fibers are formed with circular circumferences of 100-150 μm, similar to that of the aorta.

The manufacture of electrospun chitosan tubes follows similar lines of construction as wetspun chitosan fibers. Briefly, electricity is applied to a chitosan/acetic acid solution such that a circuit is established between a needle of a syringe, from which chitosan is ejected, and a metal plate. The result is the formation of fibers on the micron scale which will together form a mat of chitosan. This chitosan mat is rolled onto a needle to form the tube shape and exposed to a strong basic solution of NaOH:EtOH, before being washed and dried. The application of this basic solution in particular is applied, as opposed to other solutions such as NaOH:$H_2O$, because such a solution has been shown to improve adhesion and proliferation of endothelial cells on chitosan.[69] The chitosan tube is then removed from the needle after drying. The disadvantage of using the chitosan tube is that the size of the syringe and the rolled chitosan mat, make such a construct much larger than the physiological diameters of blood vessels in vivo and therefore such a construct would differ in properties such as flow.

In both cases, the material chitosan used in the construction of the structures is not conducive to cell adhesion as it lacks cell binding sites. Thus, in order to aid in cell adhesion of endothelial cells to the structure as well as promote cell growth and differentiation, the structures are first modified before inoculation of cells. To this end, fibronectin or VEGF is included into the wet spun fiber. Fibronectin is a glycoprotein with RGD binding sequences involved in cellular adhesion. VEGF is a glycoprotein growth factor involved in the vascularization process. The use of VEGF is prohibitive due to both its expense and its short half-life. In order to extend this half-life and raise the local concentration VEGF,

VEGF will be bound to the microfiber mat. Heparin will serve as the binding mediator for both fibronectin and VEGF, and the microfiber mat. Heparin is a natural glycosaminoglycan which is able to bind VEGF due to its negatively charged sulfate groups. Use of covalently bound heparin shows greater adsorption and prolonged release of the VEGF or other growth factors to the surface of a material other than the material by itself. [70-73] As well as serving as a binding agent, there exist a synergy between heparin and VEGF that aids in angiogenesis. [74, 75]

To inoculate the RAEC cells onto the structures, the structures are simply incubated in high density cell containing media for up to 2 hrs while being shook every 15 min. At this point, the cell coated wetspun chitosan fiber does not contain a lumen. To form the lumen within the wetspun chitosan fiber, the chitosan needs to be dissolved out of the structure and so the structure is incubated with a variety of enzymes to perform the degradation. Following dissolution of the chitosan, the natural scaffold, i.e., collagen and other ECM components, will serve to preserve the vessel structure. Chitosanase or chitinase would be the most likely candidates as enzymes used to degrade chitosan, however, are cost prohibitive. Instead cellulase is used as it is far cheaper than chitosanase and has been shown to have similar degrading power to chitosanase by cleaving the chitosan structure at the same β-glycoside bond. [76] Furthermore, lysozyme is used as it also far cheaper than chitosanase and is known to effectively degrade chitosan. Enzymes like cellulase and lysozyme work at an optimal pH which both happen to be around pH 5, however, cells survive in an environment of 7.4. A compromise between these two conditions is met by incubating the cell coated fiber in a solution at pH 6. Such a low pH

will also aid in the dissolution of chitosan as chitosan dissolves into a liquid at a pH lower than 7.3.

The manner in which the endothelial cells will coat the fiber should produce a non-fenestrated blood vessel as endothelial cells should evenly coated the fiber. Although, normal liver vasculature is fenestrated, the liver tumor vasculature is not. The liver tumor vasculature can take on an “arterialized”, i.e., tight, or “capillarized”, i.e., non-fenestrated phenotype, heretofore known as sinusoidal vasculature. [77-79] In this case, the sinusoidal-like vasculature produced by RAEC should more accurately recapitulate the vasculature found in this particular cancer.

These VEGF coated, heparin cross-linked chitosan fibers provide a scaffold for RAEC to form into perfusable blood vessels.

## 3.2 Methods

### 3.2.1 Chitosan

Two percent chitosan solution is made by stirring medium molecular weight chitosan (Aldrich) in $dH_20$ with 1% acetic acid overnight. Chitosan/$dH_20$/acetic acid is then centrifuged at 3000 rpm for 20 min to remove undissolved chitosan. Chitosan solution is decanted from the pellet. Chitosan solution is sterilized through autoclave treatment.

### 3.2.2 Chitosan Film

Chitosan solution is pipetted into 48 well plate and allowed to dry overnight. Chitosan solution is neutralized by the addition of 0.2M NaOH for 10 min. Four conditions tested: tissue culture plate, chitosan, chitosan heparin, chitosan heparin fibronectin. 500 μl of

media added to each well, followed by the addition of 40,000 MVEC cells into each. 10x and 20x phase images taken daily followed by Actin/DAPI staining.

### 3.2.3 Heparin Crosslinking (Chitosan Film)

Films/fiber/tube are incubated in 5mM 1-ethyl-3-(3-dimethylaminopropyl) carbodiimide (EDC) and 2mM n-hydroxysulfosuccinimide (NHS) (Sigma) and 1mg/mL heparin (in those conditions that require heparin) in HEPES buffer at 37ºC overnight.

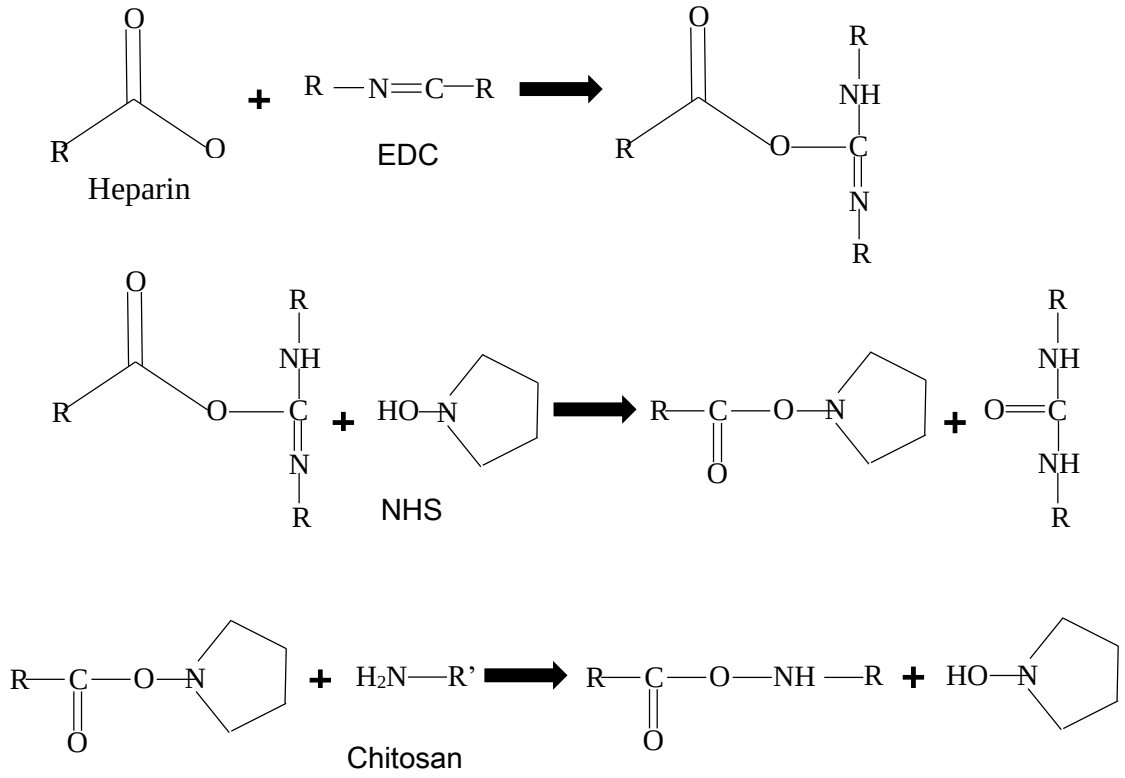


**Figure 3.1** Diagram of EDC/NHS Crosslinking. Diagram of crosslinking process shows how EDC and NHS covalently crosslink heparin to chitosan. [151]

### 3.2.4 Fibronectin Coating

Due to the cost prohibitive nature of VEGF, fibronectin is used for preliminary testing in VEGF's place. Following crosslinking, 10 μg/mL fibronectin solution in $dH_20$ is added to each well and incubated at room temperature overnight.

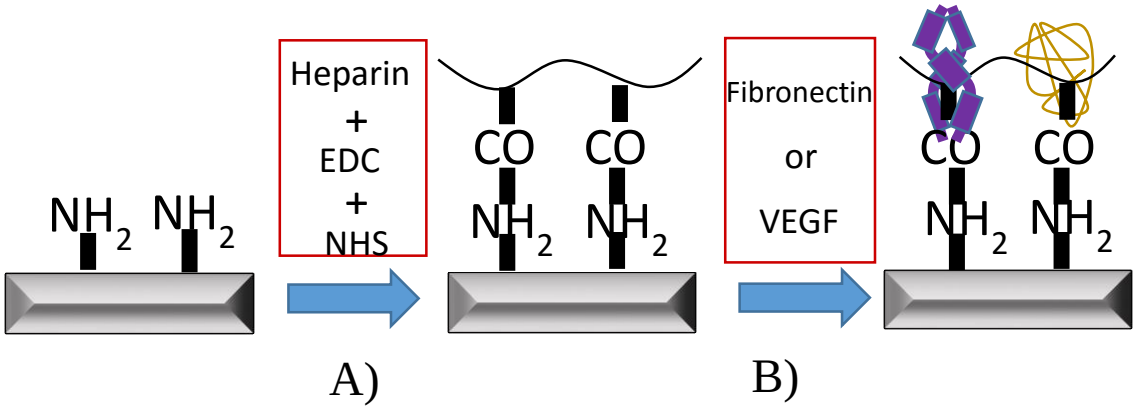


**Figure 3.2** Diagram of Heparin Crosslinking and Fibronectin/VEGF Adsorption. Diagram of heparin EDC/NHS crosslinking and fibronectin/VEGF coating shows A) Heparin EDC/NHS Crosslinking in which amide groups of the chitosan microfiber and carboxyl groups of the heparin are cross-linked with EDC/NHS, and B) Fibronectin/VEGF Coating in which Heparin binding sequences on fibronectin and VEGF cause binding of the two molecules to heparin.

### 3.2.5 Toluidine Blue Staining (Chitosan Films)

Toluidine blue (Sigma Aldrich) is a dye which stains sulfate bearing compounds, e.g., heparin, dark blue, and therefore, detect the presence of such a compound. Heparin cross-linked fibers are incubated in 3 mg/mL toluidine blue dye for 10 min at room temperature. Images of heparin cross-linked fibers are taken before and after 10 min staining. Images analyzed using SigmaScan Pro5 for difference in coloration.

### 3.2.6 FTIR

To determine if crosslinking mechanism between chitosan and heparin occurred, a chitosan film, heparin powder, and chitosan cross-linked heparin film are examined for their chemical groups using Spectrum 100 FT-IR Spectrometer (Perkin Elmer).

### 3.2.7 Sterilization

Film (and subsequent fibers and tubes) are sterilized for 20 min under UV radiation before treatment.

### 3.2.8 Actin/DAPI Staining

Cells fixed with 4% paraformaldehyde for 10 min at room temperature. Cells are washed twice in PBS. 1μg/mL actin phalloidin (Sigma) in PBS is incubated with the sample in the dark for 30 min. Cells are washed twice. 1 μg/mL DAPI (MP Biomedicals) is added in PBS and incubated in the dark for 10 min. Cells are visualized using fluorescent microscopy.

### 3.2.8 Alamar Blue Assay (Chitosan Film)

Cell population can be measured using the Alamar Blue assay, in which the dye resazurin is incubated with the spheroids, aliquots are taken after 1 hr, and then measured with a fluorometer. The absorbance values correlate with the cell population.

10 μM resazurin is added to 500 μL media and incubated at 37$^{o}$C for 1 hr. Samples are collected and 100 μL pipetted into 96 well plate in triplicate. Fluorescent intensity of resazurin was measured using a Gemini XPS fluorescent plate reader at wavelengths 530 nm for excitation and 590 nm for emission. Assay is performed over the course of 3 days.

### 3.2.9 Wetspinning Fiber

Chitosan is a gel below a pH 6 and a solid above pH 6. Exploiting this property, a scaffold can be designed with traits similar to the physical properties of blood vessels in vivo, namely having a similar diameter of 100-150 μm. Chitosan dissolved in acid can be ejected through a syringe into a basic chemical bath, causing the chitosan to precipitate and assume the shape of a blood vessel.

Two percent chitosan solution is wet spun by ejecting solution through a 30 gauge needle into a 1:1 NaOH:EtOH bath stirring at ~350 rpm. Fibers are formed which are removed from the bath, washed in EtOH, and dried overnight.

### 3.2.10 Instron (Tensile Properties)

Uniaxial tensile testing using Instron (Model 3343) is used to generate a stress-strain curve of dry wetspun chitosan fibers in order to determine their mechanical properties. Chitosan fibers, measuring 1 cm, are placed in pneumatic grips with an initial gauge length of 1 cm. Tensile testing is then performed with a 1N load and a crosshead extension rate of 10 mm/min. Stress is calculated by dividing force by cross sectional area which is measured by fiber diameter using caliper. Young's modulus is calculated as the slope of the linear elastic region of the tensile stress-strain curve.

### 3.2.11 Wetspun Fiber Diameter

Using phase microscopy, images are taken and analyzed using SigmaScan Pro5 software for fiber diameter. Wetspun diameters are measured when fiber are dry or wet. Wet wetspun fiber are exposed to water for 10 min before diameters are measured.

### 3.2.12 Toluidine Blue Staining (Fiber)

Toluidine blue is a dye which stains sulfate bearing compounds, e.g., heparin, dark blue, and therefore, detects the presence of such a compound. Heparin cross-linked fibers are incubated in 3 mg/mL toluidine blue dye for 10 min at room temperature. Images of heparin cross-linked fibers are taken before and after 10 min staining. Images are then analyzed using SigmaScan Pro5 for difference in coloration.

### 3.2.13 SEM

Samples are fixed in 2% glutaraldehyde, and after washing and drying, samples are coated with carbon. Scanning electron microscopy (SEM) (Leo 1530 VP) is then used to visualize heparin complexes.

### 3.2.14 VEGF Adsorption (Fiber)

Following incubation in heparin, the fiber and the tube are briefly washed in $dH_20$. The fiber and the tube are then incubated in 10 μg/mL VEGF at room temperature, overnight.

### 3.2.15 Anti-Flk Staining

To determine the ability of heparin to bind angiogenic growth factors such as VEGF, anti-Flk staining is employed to visualize VEGF in red. A chitosan fiber is heparin crosslinked as previously mentioned. The crosslinked fiber is then exposed to 10 μg/mL VEGF overnight. After washing three times with PBS, anti-Flk, PE antibody (BD Pharmingen, 1:50) is added and incubated at room temperature for 2 hrs. After washing twice with PBS, the samples are observed with fluorescence microscopy.

### 3.2.16 Cell Culture (MVEC/RAEC)

Microvascular endothelial cells (MVEC; purchased from VEC Technologies, Rensselaer, NY) and Rat aortic endothelial cells (RAEC; a gift Dr. Eun J. Lee's lab) are cultured in high glucose DMEM, 10% fetal bovine serum (FBS), 1% penicillin/streptomycin, 2 mM L-glutamine, 1% Insulin-Transferin-Selenium (ITS), 10 ng/mL VEGF, and incubated in 10% $CO_2$ at 37$^{o}$C.

### 3.2.17 Cell Coating

To form discrete blood vessels, RAEC are coated onto fibronectin coated, heparin cross-linked chitosan fibers/tube.

In brief, RAEC are passaged, cells are detached with trypsin, re-suspended in media, and subsequently centrifuged at 700 rpm for 5 min to obtain a pellet. The cells are counted using a hematocytometer and approximately 2 million cells are aliquoted into a vial. Fibers or tubes are submerged in the cell media within the vial and are incubated for 2 hrs and shook every 15 min. After incubation, the cell media and fibers or tube are relocated into a p35 Petri dish. An additional 1 mL of media is added and the fibers are allowed to incubate.

# Schematic of immobilization of bioactive molecules

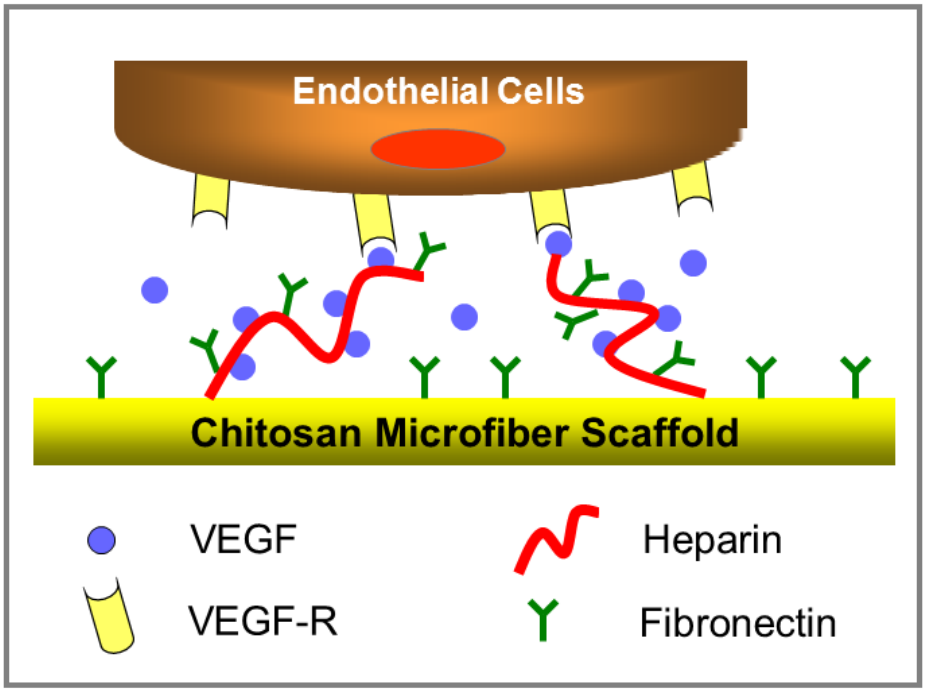


| Bioactive Molecules | Main Function |
|---|---|
| Chitosan | Main structural material (biodegradable, biocompatible, non-toxic); high binding affinity to protein |
| Heparin | Bind to various growth factors (GFs); protect GFs |
| Fibronectin | RGD cell binding domain; Heparin binding domain |
| Growth factors | VEGF to enhance vascularization and survival of endothelial cells |

**Figure 3.3** Diagram of Cell Coating (Theory). Immobilization of heparin to chitosan microfiber scaffold binds VEGF and fibronectin allowing for binding to VEGF-R on endothelial cells.

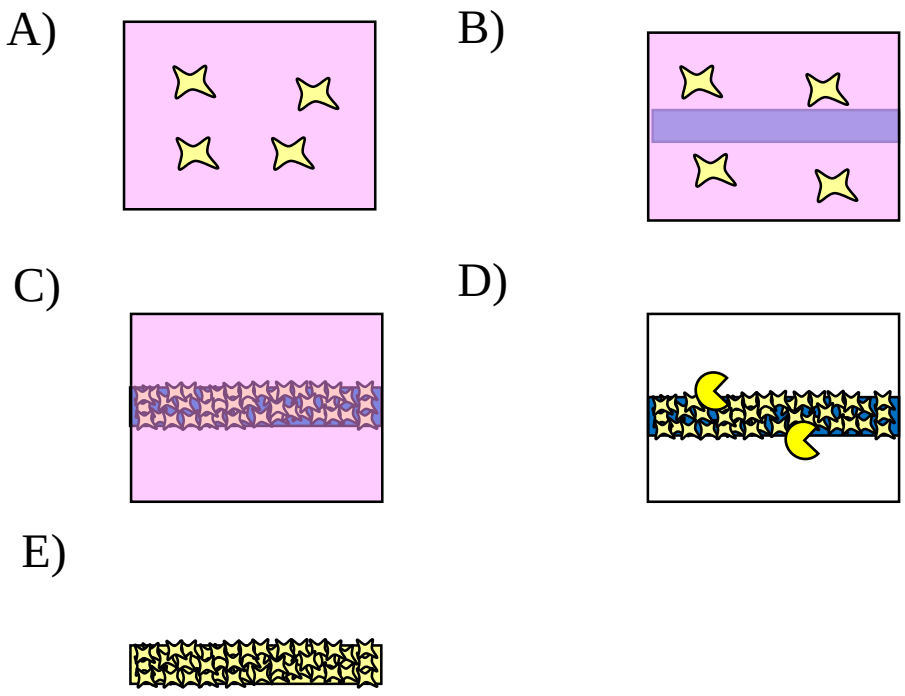


**Figure 3.4** Diagram of Cell Coating (Fabrication). Diagram of cell coating fiber and coring show A) RAEC cells being trypsanized and cells suspended in media, B) heparin/fibronectin coated fiber being added into cell media and left to incubate for 7 days, C) combination of enzymatic and acidic degradation used to dissolve scaffold, and D) the eventual formation of patent blood vessel.

### 3.2.18 LIVE/DEAD Assay

For the Live/Dead Assay, 1 μM calcein AM and 1 μM ethidium homodimer (Invitrogen) are added to the model and then incubated at 37C for 10 min. Following incubation, culture/spheroids are visualized with fluorescent microscopy using a Nikon Eclipse TI-5 microscope.

### 3.2.19 Degradability

To become a perfusable blood vessel, enzymes and acids are used to dissolve the chitosan fiber coated with RAEC cells. Fibers coated with cells are incubated in cellulase (12 μg/mL) (Sigma Aldrich) and lysozyme (8 μg/mL) (MP Biomedicals) in HBSS buffer (pH

6). To visualize the lumen, fibers coated with cells are taken at various time points during incubation.

In order to evaluate the effectiveness of this enzyme mixture, the degradation of the enzyme mixture is compared to chitosanase. Unless otherwise indicated, degradation is always performed by cellulose and lysozyme.

Two methods are employed to determine when the fiber has been sufficiently degraded. The first method is simple phase microscopy in which the fiber is observed and considered successfully degraded once the black line along the edge of the fiber has disappeared. The second method is staining the fiber with trypan blue, since trypan blue stains positively charged materials such chitosan, and observing the degradation of the blue chitosan material.

### 3.2.20 Electrospinning Chitosan Mat and Tube Formation

Electrospun mat is prepared by dissolving 8% medium molecular weight chitosan in trifluoroacetic acid and methylene chloride. A positive voltage of 20 kV is applied to the solution and delivered through a 22 gauge needle at a rate of 5 mL/hr with a syringe pump. The electrospun mat is collected on an aluminum plate (10 cm x 10 cm). The distance between the syringe and the collecting plate is 10 cm. Electrospun mats are stored in a dry environment to remove acetic acid.

Square sections (1 cm x 1 cm) are rolled tightly around a 22 gauge needle to form electospun tubes. The electrospun tubes on 22 gauge needles are neutralized in 1M NaOH for 10 min and washed overnight in $dH_2O$. Electrospun tube is then dried overnight in a chemical hood.

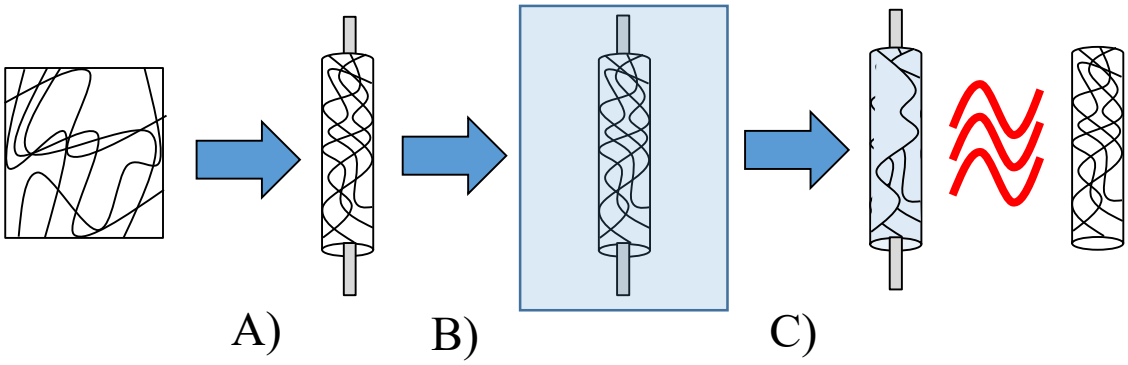


**Figure 3.5** Schematic of Electrospun Mat Tube Fabrication. Schematic of forming electrospun mat into a tube is diagramed. A) shows electrospun chitosan mat being wound tightly around 22 gauge syringe needle, B) shows neutralization of mat in 1M NaOH:EtOH solution for 10 min and subsequent washing in $dH_2O$ overnight, and C) shows the drying and removal of the chitosan mat to form the chitosan electrospun tube.

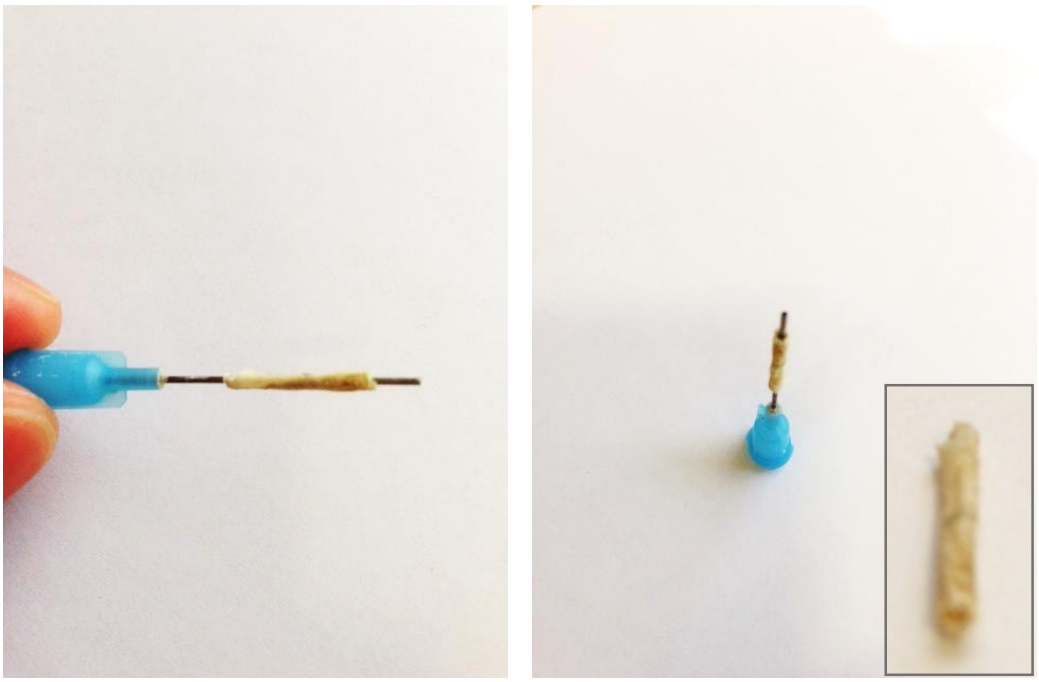

**Figure 3.6** Photographs of Electrospun Mat Tube. Photographs of finished chitosan electrospun tubes show dimensions and presence of a hollow lumen.

### 3.2.21 LIVE and Hoechst Staining

Calcein AM is used to fluoresce living cells and Hoechst dye is used to stain nuclei, in order to determine presence of cells on chitosan electrospun tube. 1 μM calcein AM and 1 μM Hoechst dye are added to the model and then incubated at 37C for 10 min.. Following incubation, culture/spheroids are visualized with fluorescent microscopy using a Nikon Eclipse TI-5 microscope.

### 3.2.22 Vascular Sprouting (Fiber/Tube)

To assess the fiber/tube's ability to allow angiogenesis to occur, the fiber/tube are embedded on Matrigel, and images of the vascular sprouting occurring on the fiber/tube are taken on days 1, 4, and 7. Length of vascular sprouts are measured using SigmaScan Pro5 software. Due to the possibility that fibers from the electrospun tube could unwind and form what appear to be vascular sprouts, a non-cell coated tube is also embedded in Matrigel to serve as a control and determine whether such an event occurs.

## 3.3 Results

### 3.3.1 Toluidine Blue Staining (Film)

Toluidine blue staining of a chitosan (control) film and chitosan cross-linked with heparin film shows that chitosan control film maintains its white coloration following dyeing. In contrast, chitosan cross-linked with heparin film shows blue coloration following dyeing, showing that a negatively charged compound has been bound to the chitosan film

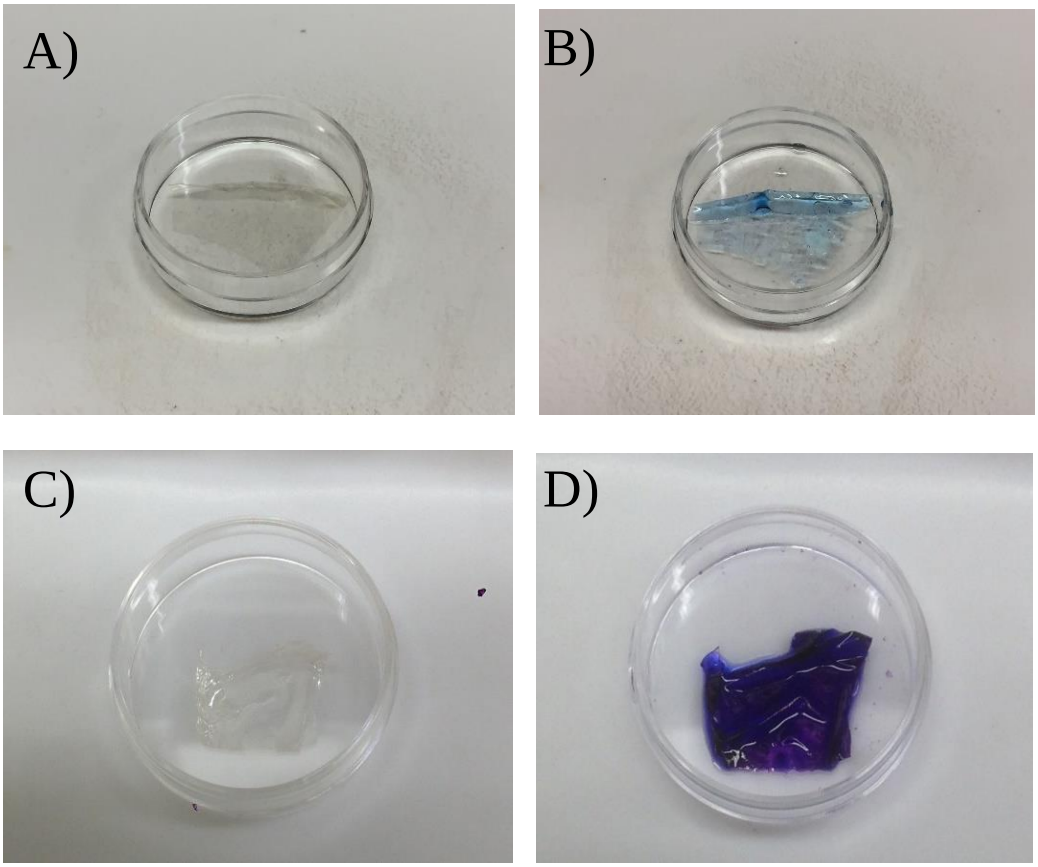


**Figure 3.7** Toluidine Blue Staining of Chitosan/Heparin Films. Toluidine blue staining images are taken. The first two images shows chitosan film (control) A) before staining and B) after staining. The last two images shows chitosan heparin film A) before staining and B) after staining. The control condition shows only pale/opaque coloration, compared to the Prussian blue/purple coloration in the chitosan heparin condition.

### 3.3.2 FTIR

FTIR graph of the chitosan film, heparin powder, and chitosan crosslinked with heparin film shows similarity of absorbance peaks between heparin powder and chitosan cross-linked with heparin film at 1230 $nm^{-1}$ and 1040 $nm^{-1}$. These peaks represent the $SO_3$ assymetric and symmetric groups, which figure prominently in the chemical structure of heparin.

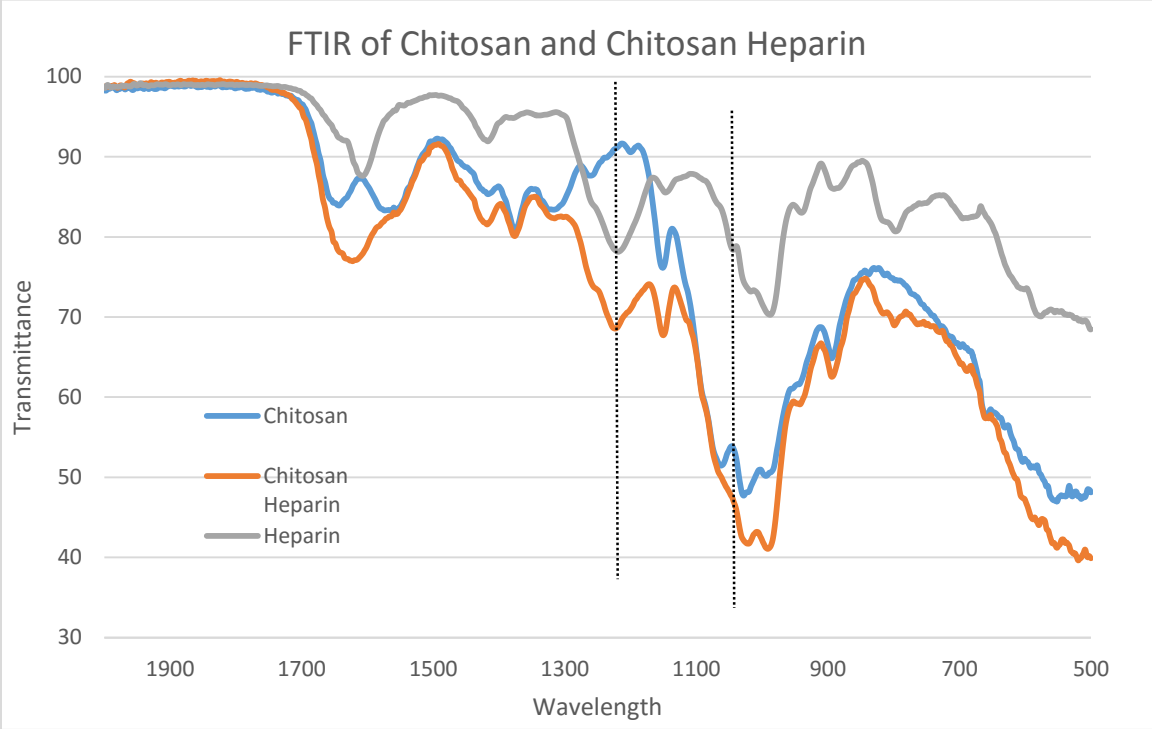


**Figure 3.8** FTIR Graph of Chitosan, Heparin, and Chitosan Heparin Films. FTIR graph of chitosan film, heparin powder, and chitosan crosslinked with heparin film, shows similarity between chitosan crosslinked with heparin and heparin powder at 1230 $nm^{-1}$ and 1040 $nm^{-1}$, which correspond to sulfate groups known to be present in heparin. N=4.

### 3.3.3 Phase Imaging

The surface properties of a material affects cell viability. As evidenced below the varying tissue culture and modified chitosan surfaces results in continued adherence to the surface after six days for tissue culture plate and chitosan heparin fibronectin conditions; and sloughing off the surface after six days for chitosan and chitosan heparin conditions.

The tissue culture plate is chemically treated to be hydrophilic and therefore ideal for cell adhesion. Chitosan, though known to be biocompatible, lacks surface binding proteins like RGD in collagen/gelatin, and therefore cells fail to adhere to chitosan unless modified appropriately. Chitosan heparin couples the already lackluster cell adhesion properties of chitosan with heparin; the most negatively known natural substance. Heparin is a

glycosaminoglycan with several negatively charged sulfate groups which can act by electrostatically repelling cells, which are negatively charged. Chitosan heparin fibronectin is modified with fibronectin which negates many of the poor cell adhesion properties of chitosan and heparin. Fibronectin is a glycoprotein which in conjunction with heparin has been shown to a have a synergistic effect on cell adhesion and cell viability.

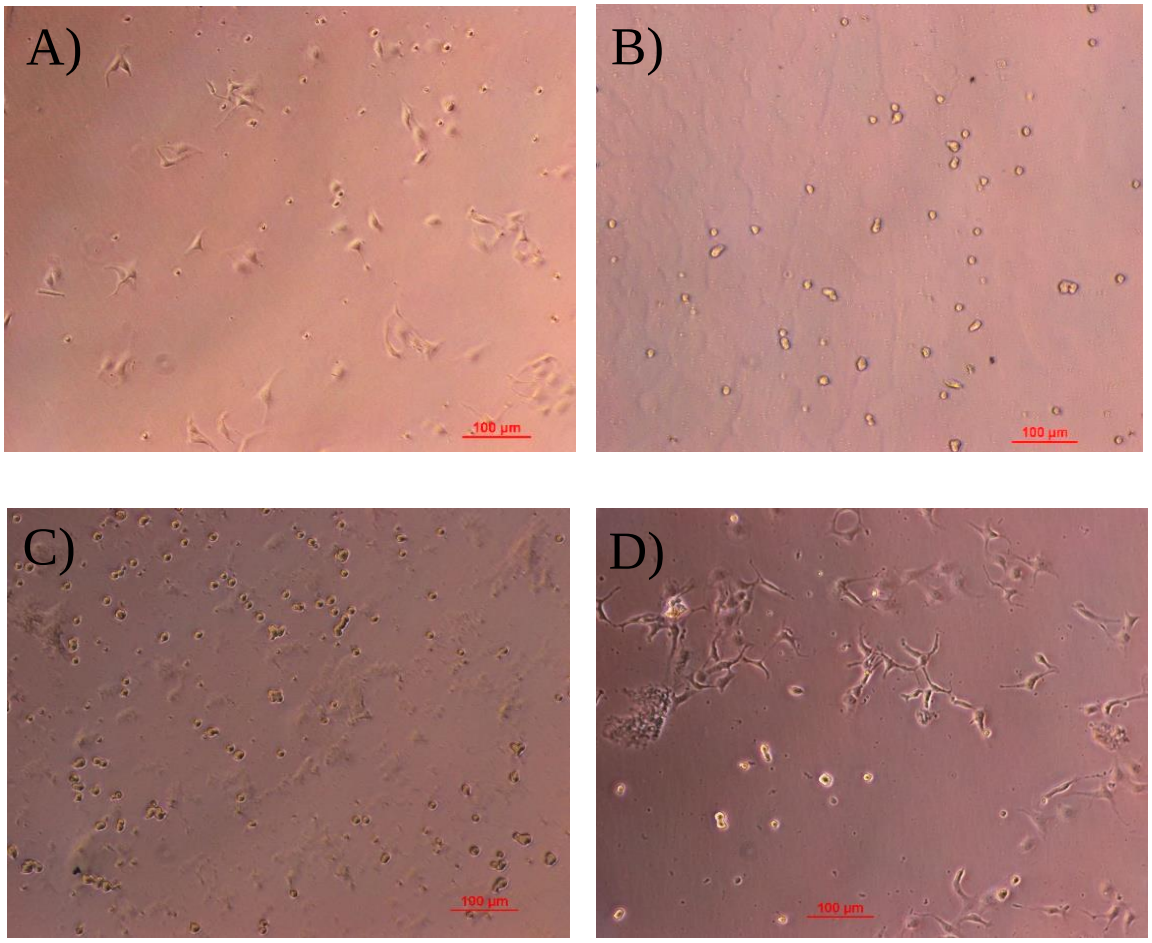


**Figure 3.9** Phase Images of MVEC Seeded on Chitosan Modified Films. Phase imaging of various chitosan films shows cells at 10x magnification on day 1 on A) Tissue Culture Plate, B) Chitosan, C) Chitosan Heparin, and D) Chitosan Heparin Fibronectin. Chitosan and Chitosan Heparin films show little cell adhesion. Chitosan Heparin Fibronectin film shows cell adhesion and spreading.

### 3.3.4 Actin/DAPI Staining (Chitosan Film)

Actin/DAPI Staining is performed 1 day after MVEC coating on film. Initial attachment of cells can be seen in Figure 3.10 A) the tissue culture plate and Figure 3.10 D) the chitosan heparin fibronectin conditions evident by the stained actin and nuclei. Although, cells have attached to both, cells in the chitosan heparin fibronectin condition shows greater cell spreading.

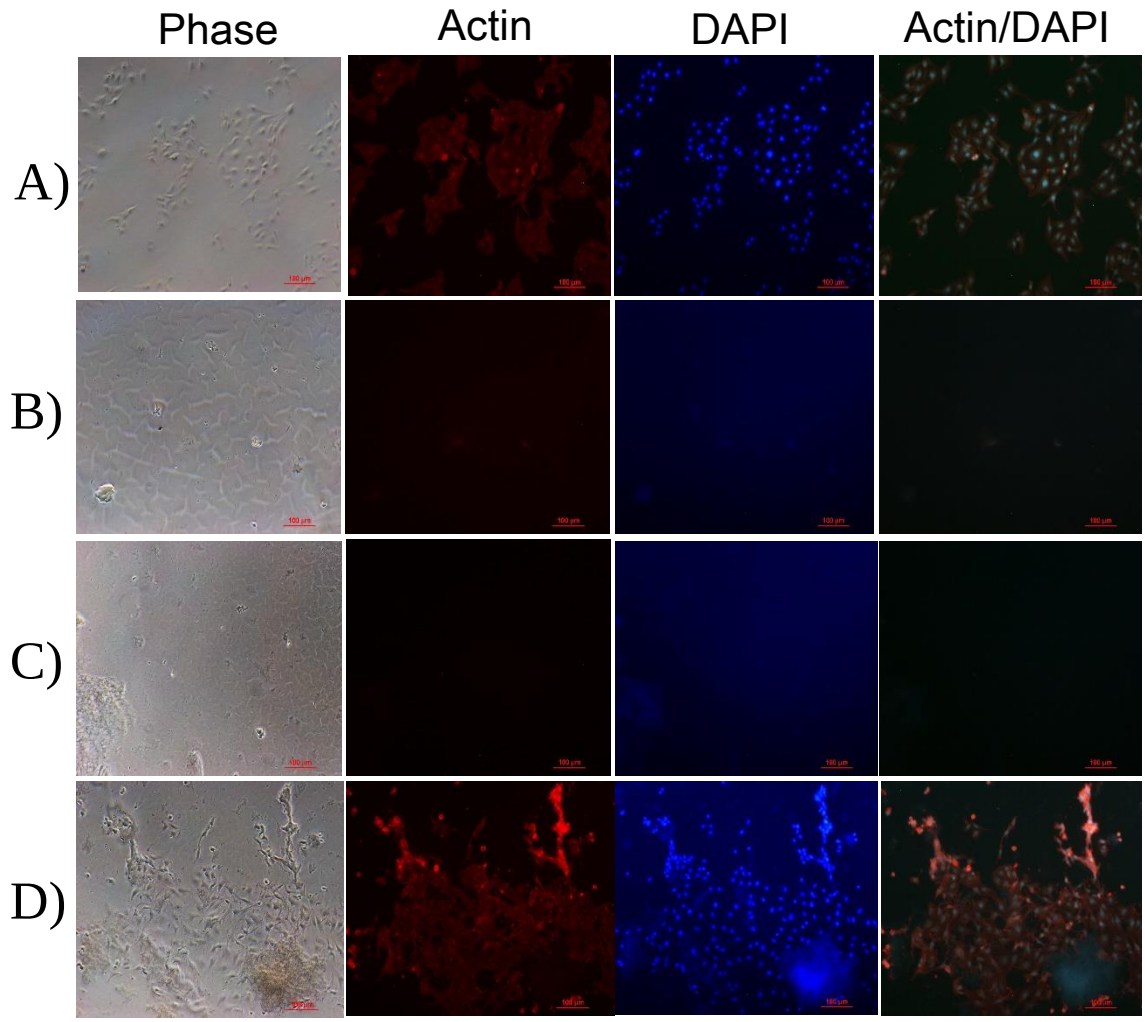


**Figure 3.10** Fluorescent Images of Actin/DAPI Staining of MVEC Seeded on Chitosan Modified Films. Fluorescent imaging of Actin/DAPI staining of various chitosan films at 10x magnification for A) Tissue Culture Plate, B) Chitosan, C) Chitosan Heparin, and D) Chitosan Heparin Fibronectin, after 1 day of culture. Chitosan and Chitosan Heparin films

Less cell attachment can been seen in Figure. 3.10 B) the chitosan and Figure. 3.10 C) the chitosan heparin conditions as no stained actin or nuclei are witnessed.

### 3.3.5 Alamar Blue Assay (Chitosan Film)

Alamar Blue Assay shows the relative cell population growth for the three conditions. Chitosan heparin fibronectin conditions shows greater cell population growth and are significantly larger than chitosan and chitosan heparin conditions on day 1. These results support conclusions in Phase and Actin/DAPI imaging, as cells must attach to a surface in order to receive pro-viability signals. Tissue culture plate and chitosan heparin fibronectin conditions shows adhesion and chitosan and chitosan heparin conditions did not, the cells in the tissue culture plate and chitosan heparin fibronectin conditions were able to attach, spread, and grow, whereas those cells in the chitosan and chitosan heparin conditions were unable to attach, spread, and grow, initially.

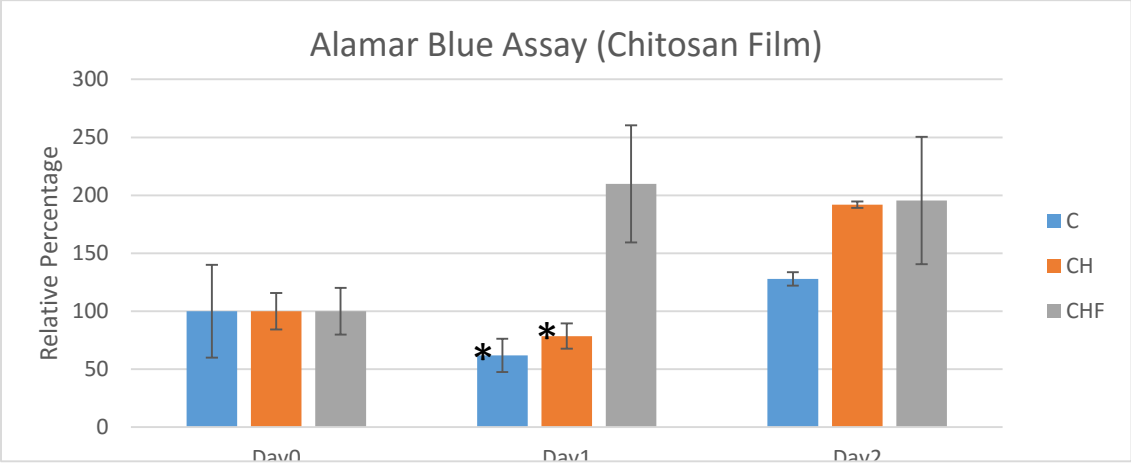


**Figure 3.11** Cell Viability of MVEC Seeded on Chitosan Modified Films. Graphs show the Alamar Blue Assay of MVEC inoculated on varying Chitosan Films. C= chitosan, CH= chitosan with cross-linked heparin, and CHF= chitosan with cross-linked heparin and coated with fibronectin. Chitosan Heparin Fibronectin film shows significant difference compared to Chitosan and Chitosan Heparin on day 1. Chitosan Heparin Fibronectin film shows no significant difference compared to Chitosan and Chitosan Heparin films on day 2. Values represent averages ± SD (n=4, *P<0.05) when comparing C and CH to CHF.

### 3.3.6 Instron (Tensile Properties)

Instron testing is used to measure the mechanical properties of the wetspun chitosan fibers, showing a Young's modulus of 1767.7 ± 470.8 MPa and ultimate strength to be 51.3 ± 17.8 MPa. Overall, the chitosan fiber was brittle.

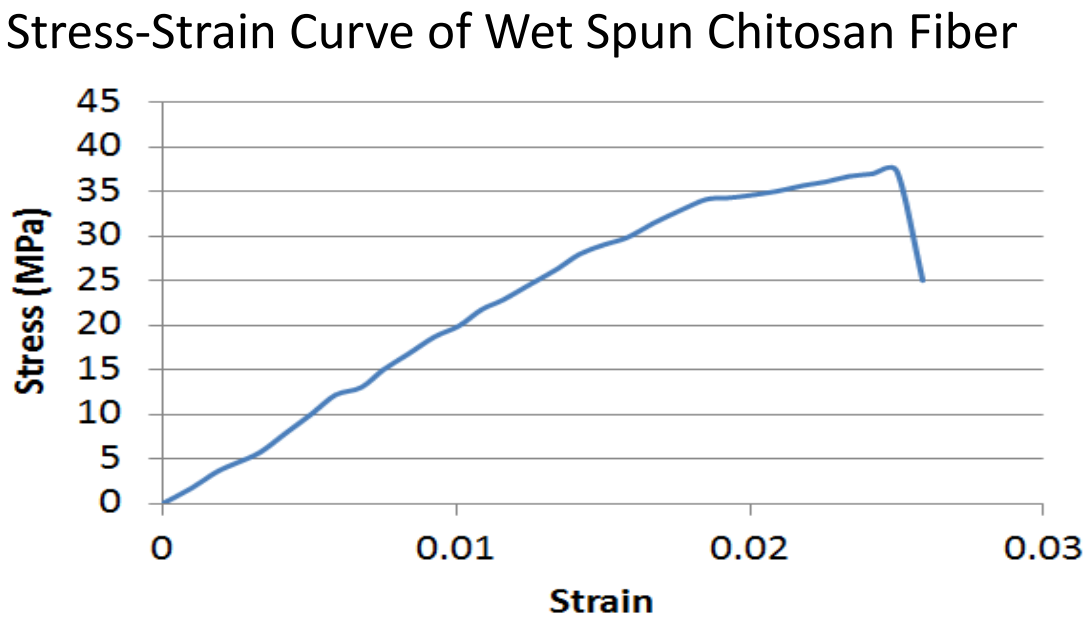


**Figure 3.12** A representative graph of Stress-Strain Curve of Wetspun Fiber. Graph shows the stress-strain curve of a wetspun chitosan fiber. Instron shows Young's modulus of the chitosan microfiber to be 1767.7 ± 470.8 MPa and ultimate strength to be 51.3 ± 17.8 MPa. (n=4)

### 3.3.7 Wetspun Fiber Diameter (Dry)

The diameter of the wetspun fibers using different gauge needles (30G vs 20G) and with or without the presence of flow (stir bar rotating a 350 rpm) is determined using SigmaScan Pro 5 to measure the distances. The average diameter for 30G with flow is 206.57 ± 24.47 μm, for 30G without flow is 393 ± 96.57 μm, for 20G with flow is 531.93 ± 132.1μm, and for 20G without flow is 1123.86 ± 274.43 μm. Overall, there is a trend such that smaller gauge needles (30G) and flow allow for a smaller wetspun diameter size.

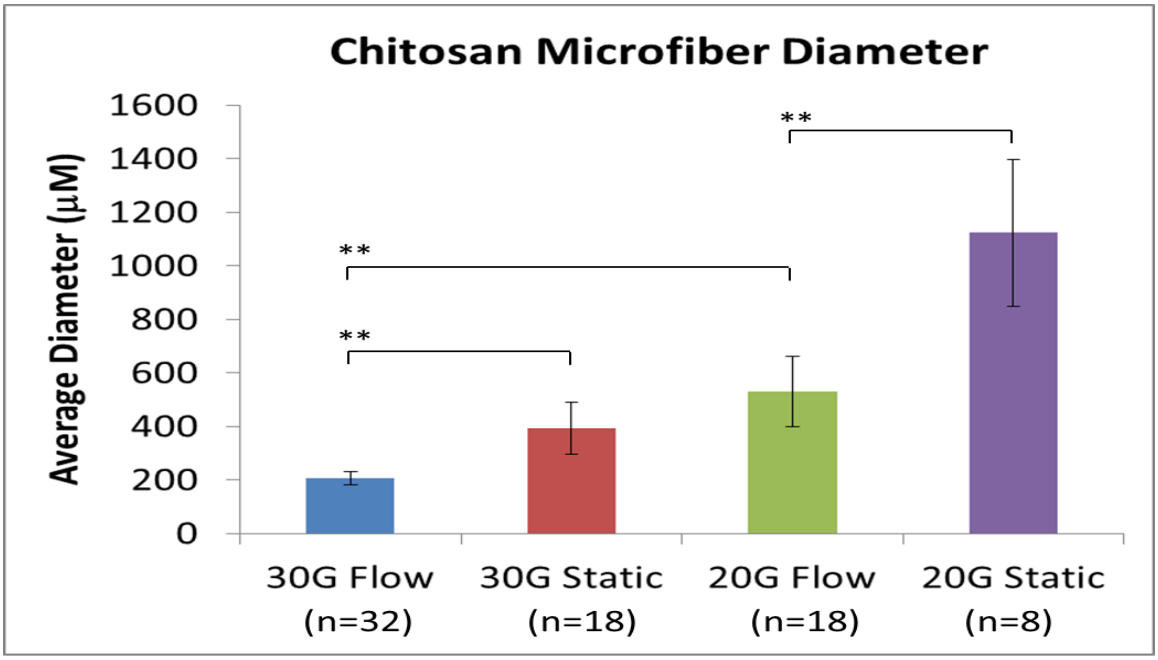


**Figure 3.13** Histogram of Average Diameter of Chitosan Wetspun Fiber. Histogram of the average diameters of the chitosan wetspun fibers shows that smaller gauge needles and flow conditions result in smaller diameters. N indicated in histogram, ** $P < 0.05$.

### 3.3.8 Swelling Test

Wetspun chitosan fibers are kept dry or made wet, and their respective diameters are measured for a chitosan control condition and a chitosan heparin crosslinked condition. The chitosan control condition shows a normalized swelling percentage of 192 ± 24.2, while the chitosan heparin crosslinked condition shows a normalized swelling percentage of 154 ± 24.8. Thus, the chitosan heparin crosslinked condition shows less swelling than the chitosan control.

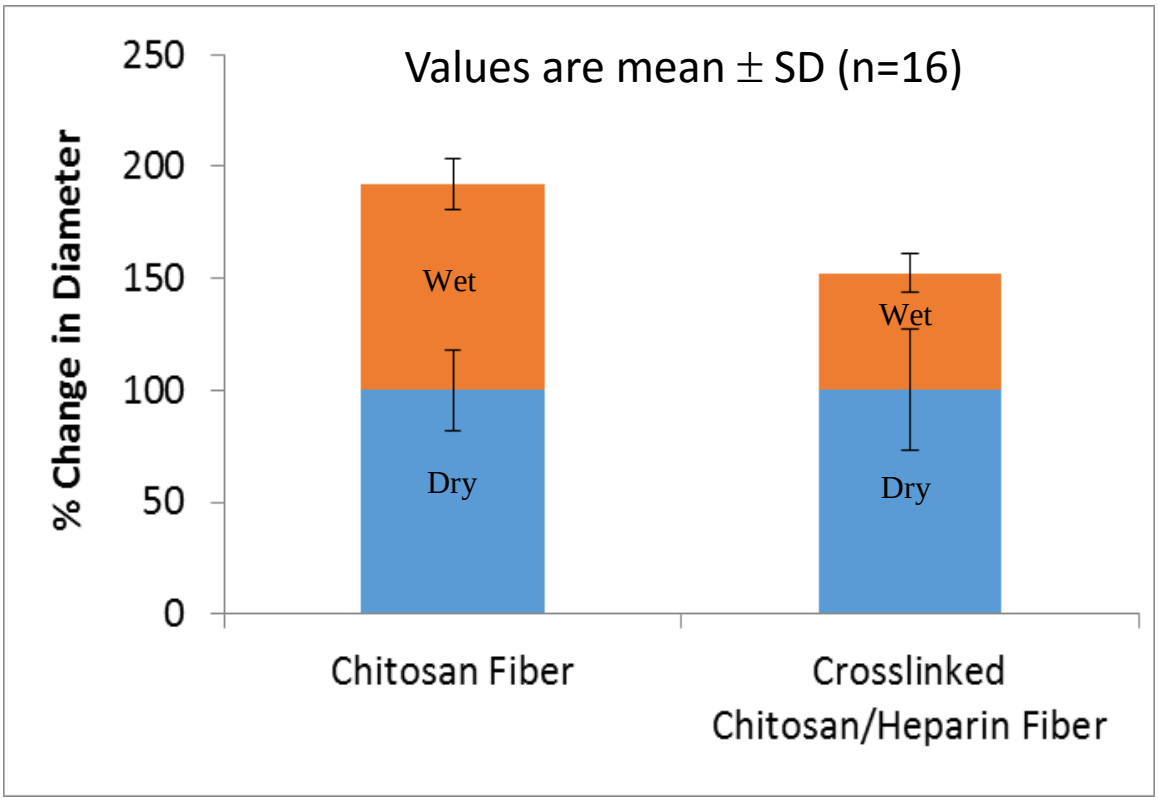


**Figure 3.14** Histogram of Chitosan/Chitosan Heparin Wetspun Fibers under Dry and Wet Conditions. Histogram of chitosan control wetspun fibers and chitosan heparin crosslinked wetspun fibers shows average diameters of the fibers when dry and when wet.

### 3.3.9 Toluidine Blue Staining (Fiber)

Toluidine blue staining of chitosan heparin fibers shows a change in coloration from naturally clear fibers to the dark blue/violet colored fibers shown in Figure 3.6. The change in color is an indication that the toluidine blue dye is bound to the sulfate groups of heparin, thus, showing the successful covalent crosslinking of heparin to the chitosan fiber.

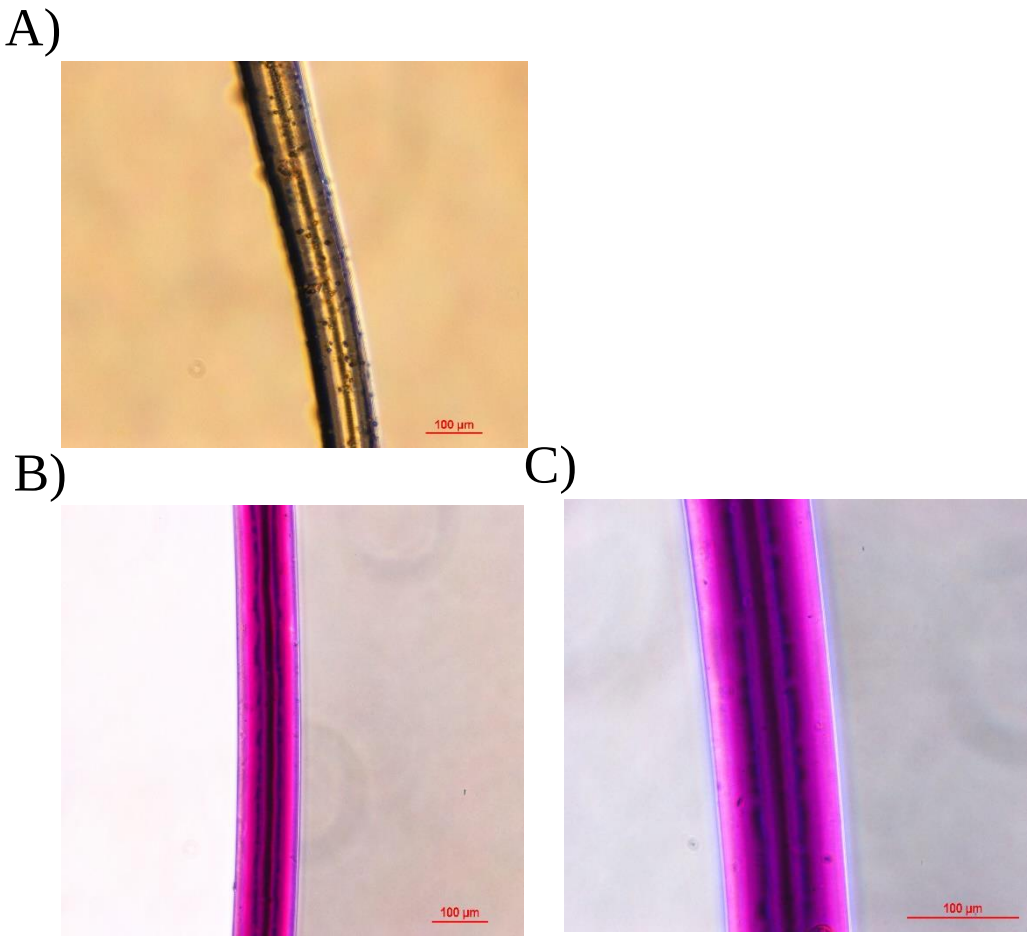


**Figure 3.15** Toluidine Blue Staining of Chitosan/Chitosan Heparin Fibers. Toluidine blue staining images of fibers show A) 10x magnification of control chitosan fibers, B) 10x magnification of heparin cross-linked chitosan fibers, and C) 20x magnification of heparin cross-linked chitosan fibers. Chitosan control fibers remain opaque in color even after staining, whereas heparin crosslinked fiber show a Prussian blue/purple coloration.

### 3.3.10 SEM

Heparin/fibronectin coated fibers are carbon coated and visualized to show complexes on chitosan fibers.

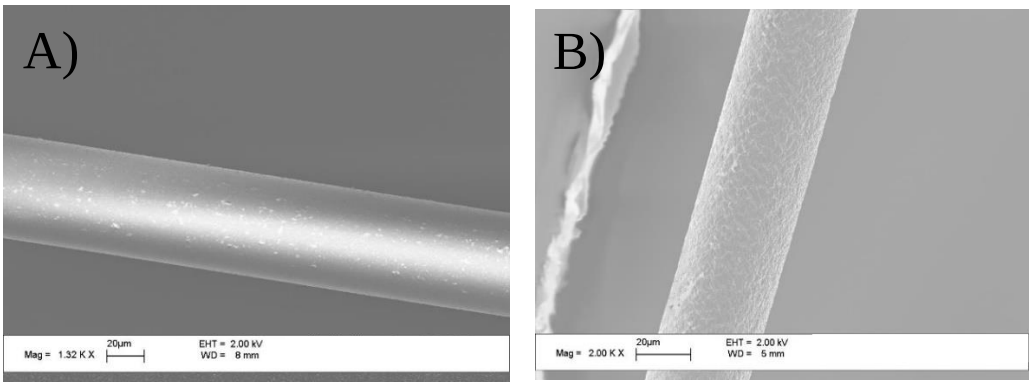


**Figure 3.16** SEM Images of Chitosan/Chitosan Heparin Fibers. SEM Images of A) Control (Non-coated) fiber, B) Heparin/fibronectin coated fibers, show the presence of complexes present in the heparin/fibronectin condition which are not present in the control condition.

### 3.3.11 Anti-Flk Staining

Anti-Flk (fetal liver kinase 1) staining of a control chitosan and a chitosan heparin/VEGF coated fiber shows little red fluorescence for the control and strong red fluorescence for the heparin/fibronectin coated fiber, indicating high VEGF binding affinity to the chitosan-heparin complex fibers.

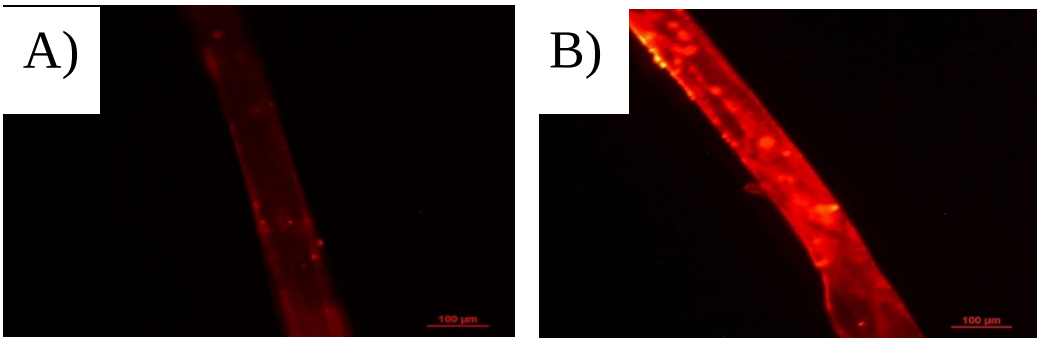


**Figure 3.17** Anti-Flk Staining of Chitosan/Chitosan Heparin VEGF Fibers. Anti-Flk staining of A) control (non-coated) and B) heparin/VEGF coated fibers shows little red fluorescence for the control and considerable fluorescence for the heparin/fibronectin coated fiber

### 3.3.12 Phase Microscopy (MVEC Coated Chitosan Fibers)

MVEC cells are placed on chitosan fibers and images are taken thereafter to determine that MVEC cells able to adhere to fiber and will continue to adhere to the fiber after a long duration, i.e., 6 days. In Figure 3.18 A), two images of MVEC coated chitosan fibers after 1 day show that the cells were able to adhere. In Figure 3.18 B), two images of MVEC coated chitosan fibers (taken on the same chitosan fibers, but different locations) shows that cells still adhere to the fiber after 6 days.

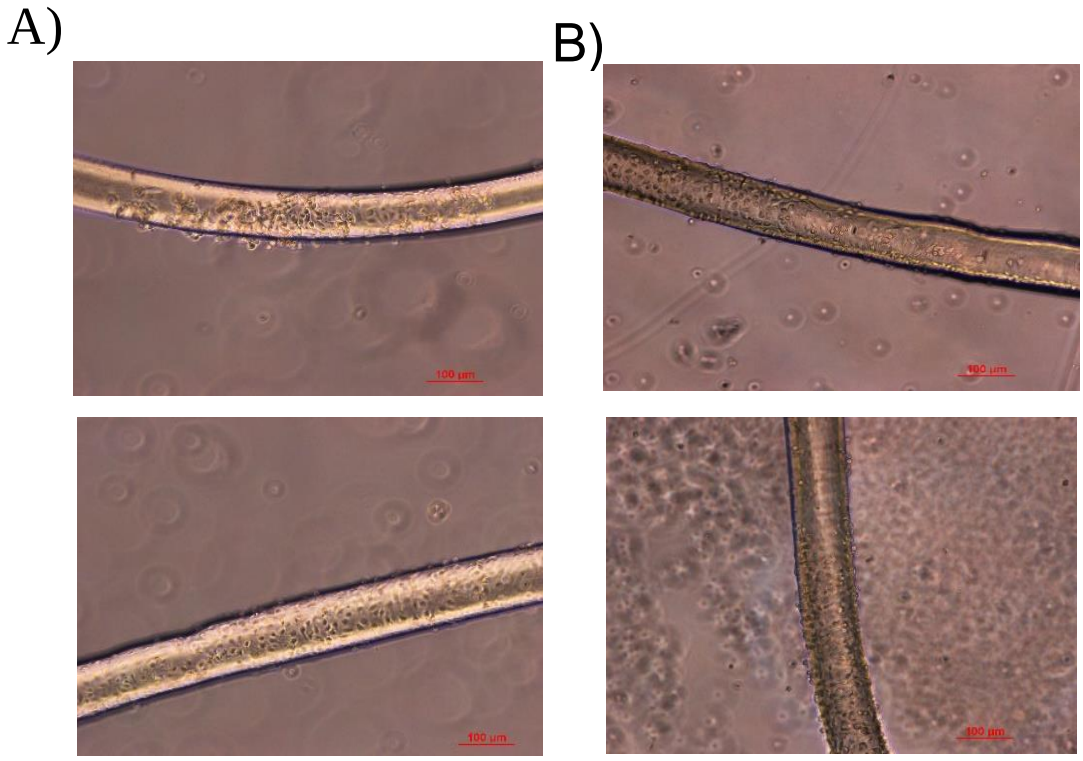


**Figure 3.18** Phase Images of MVEC Coated Fibers. Phase imaging of MVEC coated chitosan fibers (coated with fibronectin, no heparin crosslinking) A) after 1 day and B) after 6 days, shows that cells continue to remain on fibers.

### 3.3.13 Live/Dead Staining (Fibers)

Live/Dead staining of RAEC coated chitosan fibronectin fibers reveals that the fiber is able to maintain cell viability of the RAEC coated fibers after 3 days. Calcein AM/LIVE staining in Figure 3.19 B) shows considerable green fluorescence compared to ethidium homodimer staining in Figure 3.19 C) which shows only background red fluorescence. This shows that the fiber is an appropriate scaffold to maintain the RAEC cells and allow for their continued growth and migration across the entirety of the fiber.

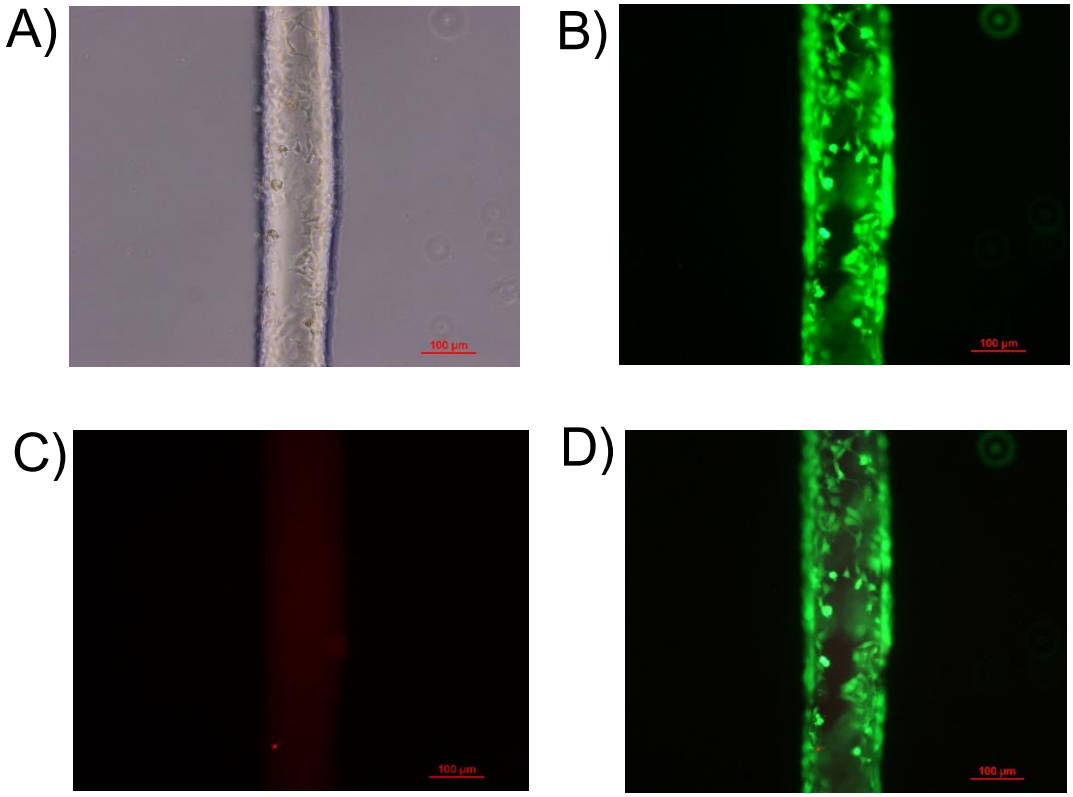


**Figure 3.19** LIVE/DEAD Images of RAEC Coated Fibers. Live/Dead Staining Imaging of MVEC Coated Fiber at 10x magnification shows A) phase image, B) Live image, C) Dead image, and D) Live/Dead merged image.

### 3.3.14 Degradability

Images of the chitosan fiber are taken at various time points following exposure to the enzyme. Trypan blue stained chitosan fibers without cells are used as a preliminary test to determine when the fiber is sufficiently degraded before cell coated fibers are used. Cells coating the fibers would affect the properties of degradation due to a combination of their physical presence preventing the admission of acids and enzymes toward the fiber, and excretion of metabolites which may interact with the fiber over the course of incubation. Regardless, of this fact, this preliminary test is invaluable as the enzyme/acid bath is harmful to the cell coated on the fiber, and so by determining the absolute minimal amount of time necessary for fiber degradation, a greater cell viability can be had. As shown by the images in Figure 3.20 A) and Figure 3.20 D) , the fiber does not degrade evenly, rather parts of it degrade, while other parts remain insoluble as evident by the areas of blue that remain. Furthermore, the phenomena of swelling occurs as shown between the images in Figure 3.20 A) and Figure 3.20 B), in which the diameter of the fiber is shown to expand more than 200%. Overall, although, total degradation did not occur in an organized manner, the parts of the chitosan that did dissolve seem to have dissolved by around 30 min.

For cell coated degradation tests, the point at which the chitosan fiber is sufficiently degraded is herein considered to be when the straight black edge of the chitosan fiber is no longer seen. However, a difficulty with degradation is the swelling of the fiber resulting in the construct bursting at 30 min in Figure 3.21 C) and releasing cells into the surrounding medium at 45 min in Figure 3.21 D).

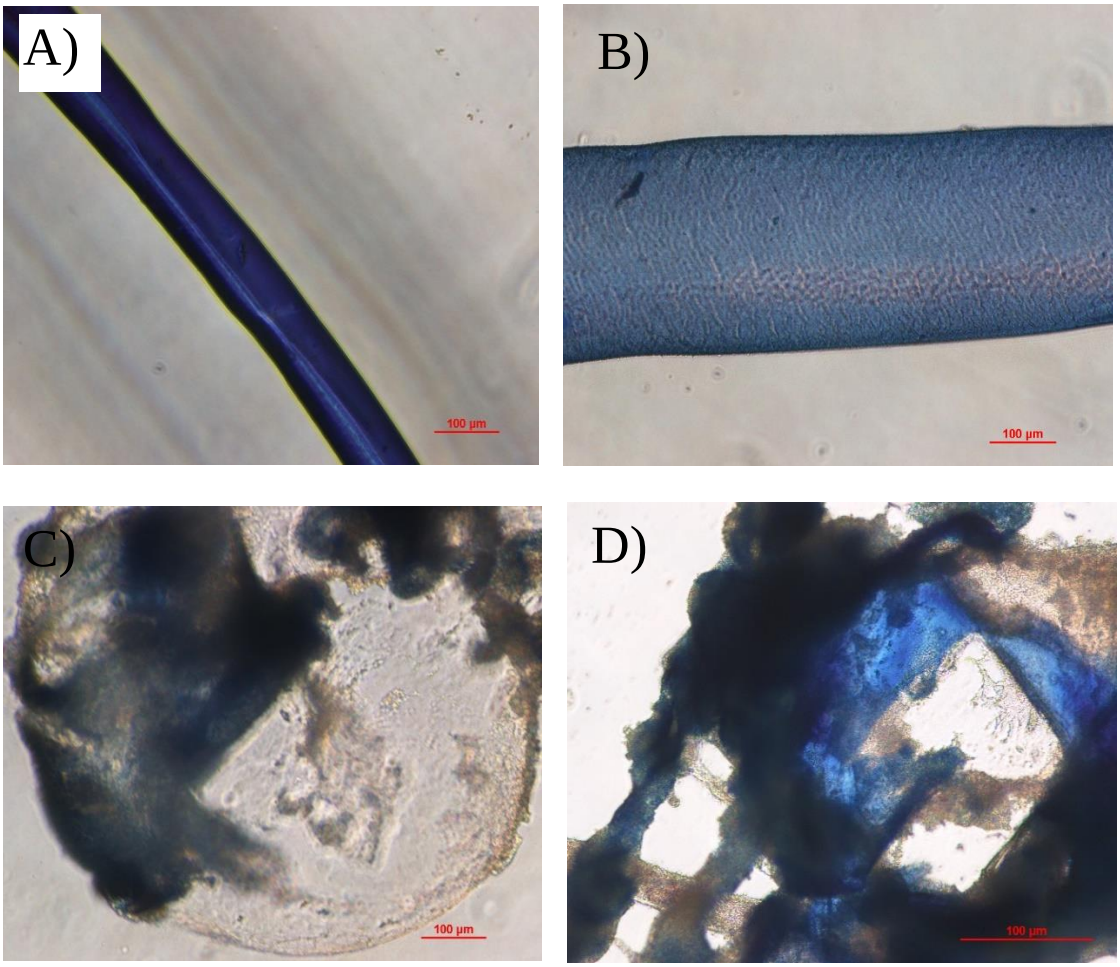


**Figure 3.20** Trypan Blue Staining of Non-Cell Coated Chitosan Fiber during Degradation. Trypan blue stained non-cell coated fibers in HBSS pH5.5 with lysozyme and cellulase are imaged at 4x magnification at A) 0min, B) 30min, C) 60min, and D) 90 min, showing uneven dissolution.

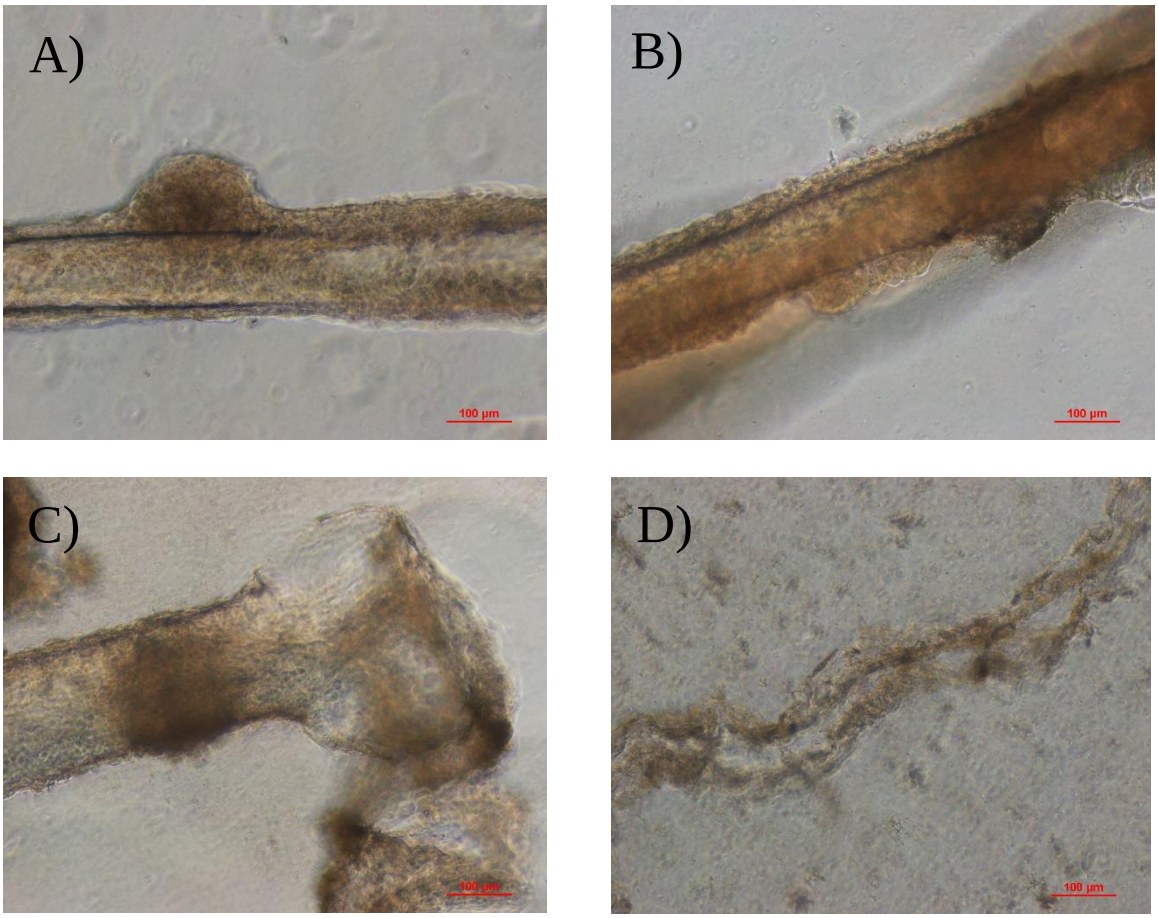


**Figure 3.21** Phase Imaging of Cell Coated Chitosan Fiber during Degradation. Degradation of the chitosan fiber with the passage of time at 10x magnification show the effect of cellulase and lysozyme on the chitosan fiber after A) 0 min, B) 15 min, C) 30 min, and D) 45 min, showing bursting after 30 min and cell ejection off scaffold.

### 3.3.15 LIVE/Hoechst Staining (Tube)

Live staining using Calcein AM and nucleus staining using Hoechst, reveals live cells in green and their nucleus in blue. As can be seen in Figure 3.22, by comparing phase with fluorescent images, almost all of the cells show green fluorescence and nucleus staining, showing that cells were able to attach to the electrospun tube and remain viable.

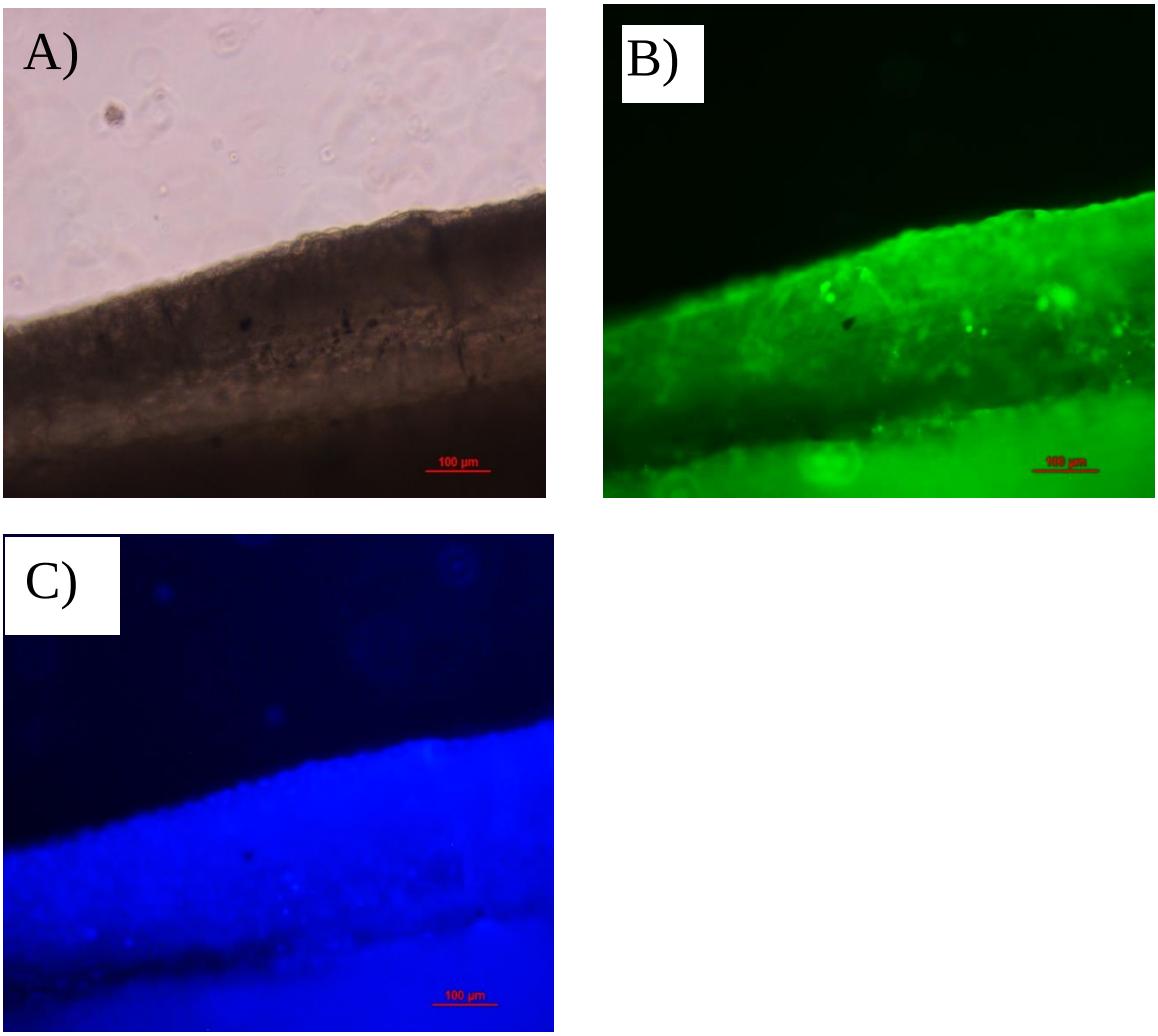


**Figure 3.22** LIVE/Hoechst Staining of Cell Coated Tube. Calcein AM and Hoechst staining is performed on a RAEC cell coated tube at 10x magnification. A) shows phase image, B) shows green/Live image, and C) shows blue/nucleus image. Fluorescent coloration shows presence of cells on the tube.

### 3.3.16 Vascular Sprouting (Fiber/Tube)

A non-cell coated tube is embedded in Matrigel and phase images show that after six days that no sprouts can be seen as shown by Figure 3.23. By contrast, both the tube and the fiber after being embedded in Matrigel for six days are both able to promote vascular sprouting are evident by the images in the Figure 3.24 and Figure 3.25.

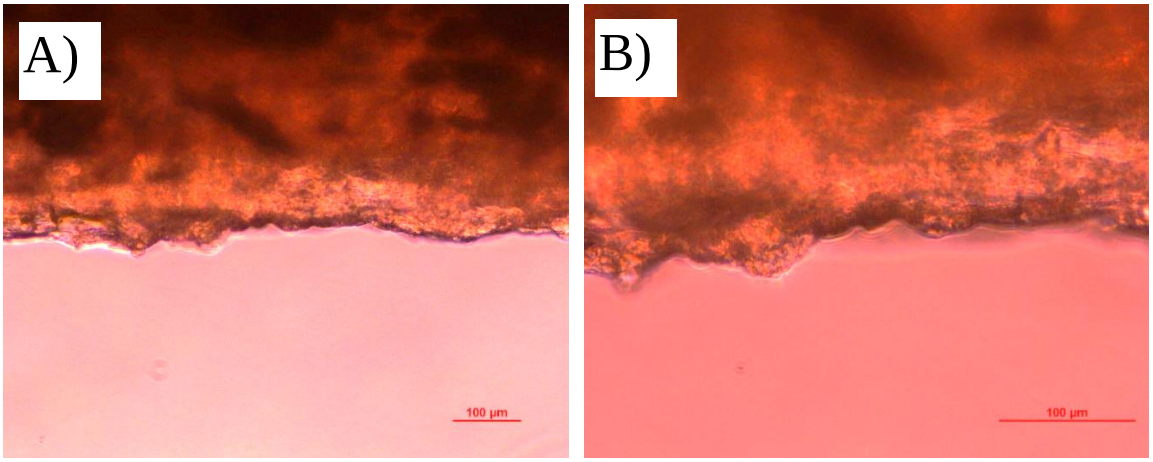


**Figure 3.23** Phase Images of Non-Cell Coated Tube. Non-cell coated tube is embedded on Matrigel and A) 10x or B) 20x magnification images are taken after 6 days, showing absolutely no sprouting.

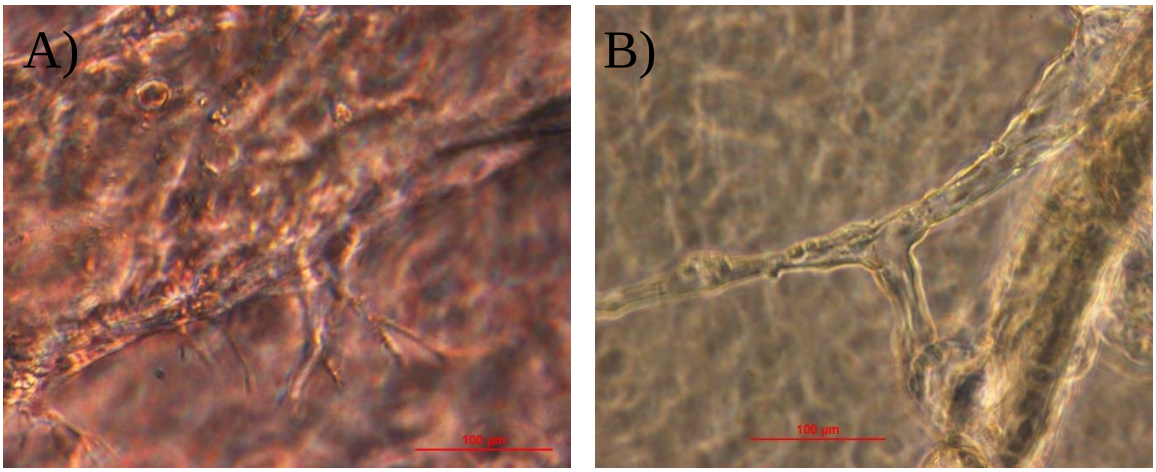


**Figure 3.24** Phase Images of Vascular Sprouting from Cell Coated Fiber. Vascular sprouting is seen emerging from the RAEC cell coated fiber after 6 days at a magnification of 20x. A) shows sprouting angiogenesis, while B) shows maturation of the vessel by the addition of multiple cells.

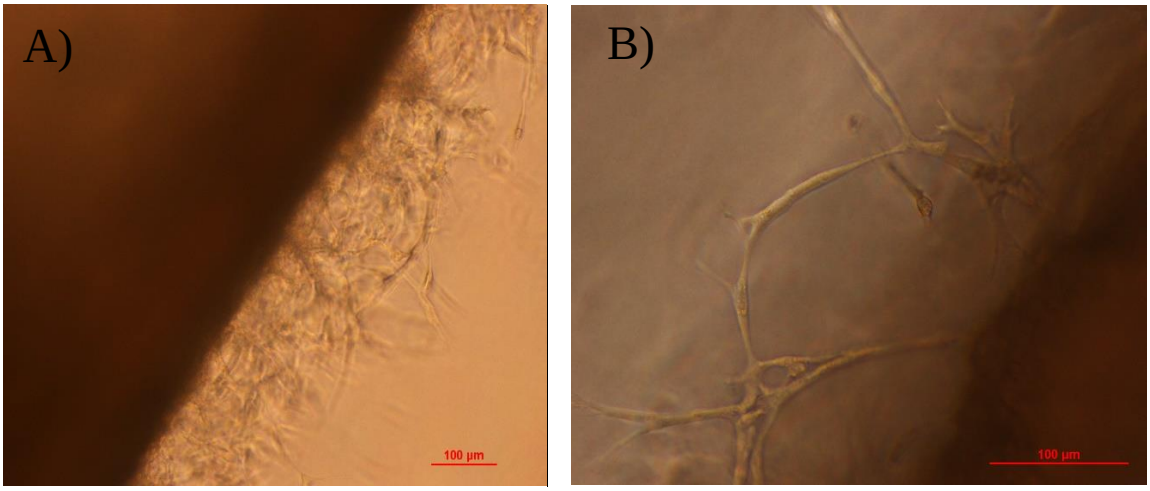


**Figure 3.25** Phase Images of Vascular Sprouting from Cell Coated Tube. Vascular sprouting is seen emerging from the RAEC cell coated tube after 6 days at a magnification of A) 10x, showing sprouting angiogenesis, and B) 20x, showing vascular looping.

## 3.4 Discussion

### 3.4.1 Toluidine Blue Staining and FTIR

Toluidine blue staining and FTIR are used on a heparin cross-linked film to determine that heparin has successfully been crosslinked to the chitosan. A film is used instead of a fiber as the fiber is not large enough to provide a sample large enough for study, however, it can be reasonably assumed that employing the same crosslinking technique on the film as the fiber will yield the same results.

Toluidine blue is a dye that binds to sulfate groups, such as those found heparin, but not found in chitosan. In Figure 3.7 C) and D) and Figure 3.15 B) and C), an unmodified chitosan film and an unmodified wetspun chitosan fiber are both exposed to toluidine blue dye, resulting in only pale/opaque coloration. In contrast to Figure 3.7 A) and B) and Figure 3.15 A) chitosan heparin film and chitosan heparin fiber are both exposed to toluidine blue

dye and shows a blue/purple coloration. Thus, the Toluidine blue assay shows that the fiber is successfully cross-linked with heparin.

FTIR measures absorbance of wavelength which correlate to the chemical groups on the material. The most distinguishable chemical groups on heparin are sulfate, which has a wavelength at 1240 $nm^{-1}$ and 1040 $nm^{-1}$ representing $SO_4$ assymetric and symmetric stretching, respectively. [80] As can be seen in Figure 3.12, there are large peaks at wavelengths ~1200 $nm^{-1}$ and ~1000 $nm^{-1}$ on the heparin cross-linked chitosan film which is similar in magnitude to powdered heparin, but is absent in the unmodified chitosan film, showing that heparin has been successfully incorporated in the chitosan heparin film.

### 3.4.2 Cell Adhesion

A preliminary test using chitosan film is employed to determine the ability of cross-linked heparin and adsorbed fibronectin to promote cell attachment. Chitosan is a natural, biodegradable, biocompatible, and anti-bacterial material, however, lacks binding sites to promote cell attachment. [81-83] To promote cell attachment, chitosan is chemically modified with RGD sequences, CAG sequences, or in this study using EDC/NHS with heparin. [72, 84-87] Heparin is a large negatively charged glycosaminoglycan which is used to attract growth factors such as fibronectin or VEGF; which in turn help promote cell binding. [70]

Having confirmed heparin attachment to the film via the aforementioned Toluidine blue staining and FTIR, fibronectin is adsorbed to the chitosan heparin film. To determine the ability of the various films to promote cell adhesion, four conditions are studied: a control in which cells are plated on the tissue culture plate; chitosan in which cells are plated on an unmodified chitosan film; chitosan heparin in which cells are plated on

chitosan film covalently cross-linked with heparin, and chitosan heparin fibronectin in which cells are plated on a chitosan film covalently cross-linked with heparin and followed by the adsorption of fibronectin. Chitosan and chitosan heparin films show the least cell attachment and proliferation as shown by phase and fluorescent images in Figure. 3.9 and Figure 3.10. As stated before chitosan has no cell binding sites. As for chitosan heparin, heparin is known to be the most negatively charged glycosaminoglycan and cells tend to have a slight negative charge. As such the two ionically repel each other, resulting in an initial lack of cell attachment. However, heparin also contains binding sites for VEGF, a growth receptor present on the endothelial cells which allows for some binding. By contrast, chitosan heparin fibronectin shows the greatest cell attachment. Fibronectin is a glycoprotein which contains the RGD peptide sequence which promotes binding of integrins a5b1 on endothelial cells and, thus, has the binding capabilities to allow for greater cell attachment. [88] Furthermore, the combination of heparin and fibronectin has been shown not only to improve cell proliferation, but to improve function of pancreatic cells, cardiomyocytes, and sciatic nerves. [74, 89, 90]

### 3.4.3 Proliferation

Cell proliferation of cells grown on the four conditions was measured over three days. Tissue culture plate (TCP) and chitosan heparin fibronectin (CHF) showed the most proliferation, while chitosan and chitosan heparin showed the least amount of proliferation according to the Alamar Blue assay as shown in Figure 3.11. The cell population of chitosan and chitosan heparin initially decreased from day 0 to day 1, however the population increased from day 1 to day 2. For day 2, chitosan heparin shows a cell population almost rivaling that of chitosan heparin fibronectin. To explain the rebound in

cell population it must be noted that the medium used for the endothelial cell culture contains the growth factor VEGF. Although, the chitosan and heparin contain no binding sites for cells, heparin can bind VEGF. Chitosan heparin contains heparin which binds to VEGF and is used in other studies to not only promote endothelial cell attachment, but improve cell differentiation, and capillary tube length. [75, 91]

### 3.4.4 Mechanical Properties

Mechanical properties of the tissue engineered scaffold can affect the properties of cells seeded on them. For endothelial cells, high stiffness can lead to dysfunction in vivo and expression of angiogeneic growth factors. [92-94] The measured Young's modulus of the chitosan fiber is 1767.7 MPa or 1.7GPa as shown by Figure 3.11. By comparison, soft tissue has a Young' modulus ~3kPa, collagenous bone has a Young's modulus ~30kPa, and a tissue culture plate/glass has a Young's modulus >1 GPa. [95] Thus, the chitosan fiber is highly stiff and high stiffness causes an increase in endothelial permeability and lowered cell-cell adhesion. [96] The lowering of cell-cell adhesion presents a problem, as will be reviewed in greater detail in the degradation section, as this would lower the burst pressure for the endothelial cell coated fiber. Though, the high stiffness may contribute to low burst pressure, the lowered cell-cell adhesion allows for greater angiogenesis as cells are freed to remodel into vascular sprouts. [97] A possibility not discussed here is that the chitosan fiber is tested when dry, however, because the chitosan fiber is experimented upon when wet, the stiffness represented by Figure 3.12 may be erroneous as a wet fiber's stiffness is expected to decrease.

Another area of contention is the plastic deformation region. It is assumed by the short strain occupied by the plastic deformation region that the material is brittle. However,

an alternative theory for the short strain region is slip, by which the chitosan fiber in the grips slips out.

### 3.4.5 VEGF Binding

To determine the ability of heparin to attach VEGF onto the fiber, immunofluorescent staining of VEGF using Flk-1 is employed. A control/non-treated fiber and a chitosan heparin VEGF fiber are exposed to the immunofluorescent Flk-1 antibody as shown in Fig. 3.17. The chitosan heparin VEGF conditions show considerable red fluorescence compared to the control fiber, showing that VEGF is successfully bound to the heparin coated fiber. Although, not used ostensibly in this model, VEGF attachment nevertheless occurs as it is a critical component of the endothelial cell media and so can attach to both heparin and fibronectin. More importantly, the application of VEGF to the chitosan fiber can be used in later studies, to promote angiogenesis.

### 3.4.6 Cell Coating Fiber

Imaging techniques are used to determine the ability of the wetspun fibers to adequately maintain cell adhesion and viability of cells coated on them. Phase imaging, as shown in Figure 3.18 A) and B) reveal that the cells are able to adhere onto the wetspun fiber after one day and remain even after six days. Furthermore, as shown by Figure 3.18 B), endothelial cells show a parallel and cobblestone morphology similar to that seen in vivo. [98] More importantly, after six days most of the fiber is covered by the cells and, thus, a non-fenestrated tissue engineered construct following degradation of the chitosan should be produced. A Live/Dead cell staining of the wetspun fibers, as shown by Figure 3.19,

reveals that most of the cells remaining on the fiber are green/Live and few red/Dead, showing that the scaffold is able to maintain cell viability.

The purpose of this cell coating is to create a tissue engineered blood vessel which will undergo angiogenesis and connect with the spheroid, much as angiogenesis occurs between blood vessels and solid tumor in vivo. To show that angiogenesis occurs, phase images are taken of the cell coated fiber and tube after embedding on Matrigel. For the cell coated fiber, sprouting angiogenesis can be seen in Figure 3.23 A), and vascular looping in which vascular sprouts combine can be seen in Figure 3.23 B). Thus, the cell coated fiber has successfully promoted angiogenesis.

Despite, the success seen in promoting sprouting angiogenesis and vascular looping, vascular sprouts fail to mature as they appear not to contain lumens.

### 3.4.7 Degradation

The purpose of the blood vessel is to provide a conduit for blood to flow. Thus, the most important feature of the tissue engineered blood vessel is the presence of a hollow lumen. Although, this study is more concerned with using the tissue engineered blood vessel to distribute anti-cancer drugs, the importance of the feature remains the same. This tissue engineered blood vessel differs from other such constructs in that the scaffold is only employed to give shape to the cells and afterwards is removed allowing for the construction of a discrete tissue engineered blood vessel. Cells are coated on a chitosan fiber and cells are allowed to grow and take the shape of a vessel. After which, the chitosan fiber is removed or cored. In order to core the chitosan, a combination of acidic and enzymatic degradation is employed.

Manual removal of the chitosan is difficult because of the minute nature of the tissue engineered blood vessel and because the chitosan scaffold and cells have an affinity for one another meaning that removal of the chitosan will also remove many of the cells. Chemical removal via acidic and enzymatic degradation is employed instead. The first technique to chemically remove chitosan is via acidic degradation. As mentioned previously, chitosan dissolves below a pH 7.3 and a precipates above the value, and so by exposing the solid chitosan fiber to an acidic environment, the fiber will dissolve into a liquid and out of the construct. The second technique to chemically remove the chitosan is via enzymatic degradation. Enzymes have the ability to degrade specific materials with an extremely high affinity. Chitosanase or chitinase, therefore would be the most likely candidate with which to degrade chitosan, however the enzyme is cost prohibitive. This does not necessarily preclude the use of enzymes to degrade the chitosan as other enzymes such as cellulase can have nearly the same effectiveness at degrading the material. [76, 99] In this case, it is hypothesized that the enzyme cellulase degrades chitosan as both chitosan and cellulase have the β 1,4-glycosidic linkage between monomers.[99]

When fibers are exposed to pH 5.5 with 12.5mg/mL cellulase, the chitosan fiber begins to degrade. To assess when the chitosan fiber has completely degraded a variety of techniques are employed including: trypan blue staining, and phase morphology.

The use of trypan blue to determine when the chitosan has degraded obviates from the usual use of the dye, as the dye is used to stain dead cells blue. In this case, trypan blue has an affinity for positively charged materials such as chitosan and so stains the outline of the chitosan fiber in blue as exhibited by Figure 3.20. When this trypan blue dyed fiber is exposed to acidic/enzymatic degradation conditions, the fiber swells as shown in Figure

3.20 A) and B). The reason for this is that the fiber can be considered a hydrogel. When in an acidic solution, the amide groups will obtain a positive charge resulting in electrostatic repulsion between the polymers of chitosan. The resulting network of polymers will allow the free flow of $H_2O$ into the network, forming a hydrogel and causing the structure to swell with $H_2O$.

A simpler method to determine degradation is observation under microscope. The generality that straight/smooth lines don't exist in nature also applies in this study as the manufactured fiber, even when encased in cells, still has a straight/smooth outline. Thus, once the straight/smooth line is no longer seen, it can be assumed that the manufactured fiber has been sufficiently dissolved.

There are limitations to using chemical degradation to core the chitosan fiber as the cells in the construct must remain viable and the construct must remain intact. For acidic degradation, a pH of 6 is used and no lower due to concerns over cell viability in a low pH environment. The medium used to expose the cell coated fiber is Hank's Buffered Saline Solution (HBSS) due to the nutrients present to keep the cells viable and the calcium present to maintain the cell-cell contacts with which to keep the construct intact. When the cell coated fiber is exposed to the acid, it swells. This swelling has the ability to break the cell-cell contacts which results in the destruction of the construct. In order to reduce this, the construct must resist the outward force of the swelling. What is more swelling is not consistent as only part of the construct burst, while the remainder remained intact as shown by Figure 3.21 C).

As such the fiber cannot be hollowed at present time. Since, the fiber is not hollowed successfully and so any experiments to determine cell viability following acid

and enzymatic treatment are not performed. Solutions to the problem could be the inclusion of additional cell types, most notably smooth muscle cells and fibroblasts. Circumferential and longitudinal strength in the blood vessel lies within the tunica media and tunica adventitia, the middle and outer layers of the blood vessel. Within the tunica media are smooth muscle cells where most of the circumferential strength lies and within the tunica adventitia are fibroblasts where most of the longitudinal strength lies. [100] By including one or both cell types onto the endothelial cell coated tube, additional strength could be rendered to oppose the outward swelling force.

### 3.4.8 Cell Coated Tube

As an alternative to the fiber, a cell coated tube is proposed. The tube is constructed by wrapping a chitosan electrospun mat around a 22 gauge syringe needle, neutralizing the mat with NaOH, followed by washing, and drying. After removal from the needle, the tube is processed in the same manner as the fiber in order to crosslink the structure and coated it was cells. It must be noted that unlike the fiber, the size of the tube is much larger and, thus, cannot recapitulate the diameter of the blood vessel in vivo. Although, this would alter the fluid dynamics of flow within the tissue engineered blood vessel, this project employs the tissue engineered blood vessel solely as a means of delivery and such an enlarged diameter should not present a problem.

To ensure that such a construct could support the viability of cells presented on it, cells on electrospun tubes are visualized using Live/Calcein and Hoechst/nucleus staining. Phase imagery is unable to determine presence of cells on the electrospun tube due to the non-transparent nature of the chitosan electrospun mat. As such fluorescent imagery must be used to visualize the cells instead, however, not red fluorescence such as that emitted

by ethidium homodimer as the chitosan electrospun mat is autofluorescent for the color red. The results of this experiment as shown in Figure 3.22, show numerous nuclei on the surface of the tube in Figure 3.22 C), proving that the tube allows for cell coating, and the equally numerous green stained cells shows that the tube is able to maintain cell viability in Figure 3.22 B).

To determine the ability of such a construct to promote angiogenesis, a cell coated tube is embedded on Matrigel. After a week of incubation in the Matrigel, vascular sprouts can be seen along the sides of the vascular construct, as shown in Figure 3.24, thus, showing that such a construct can support angiogenesis. The early steps of angiogenesis are evident as seen in Figure 3.24 A), in which tiny finger-like protrusion can be seen emerging from the vessel bed. Further steps in angiogenesis are seen in Figure 3.24 B), in which the ends of the vascular sprouts combine together to form a vascular loop.

Although, early steps in angiogenesis can be witnessed in such a model, the vascular sprouts never form mature lumens. This can be remedied in the future by the inclusion of a second coating of fibroblast cells or the introduction of flow through the tube. [101-104] In order to stabilize the vascular sprouts, mural cells are required to interact with the endothelial cells. The most notable of these is the pericyte, as mentioned previously, however in vivo and in vitro it is also known that the fibroblast can also serve to stabilize the structure and can aid in the vascularization of the spheroid. [105, 106] Hence, a second cell coating of fibroblasts done in a similar manner to that of the first coating of endothelial cells, should be able to promote the mature vascularization of the cell coated tube. Another manner to promote mature vascularization is the introduction of flow inside the tube. Although the mechanism by which flow promotes vascularization is

unknown, the presence of flow is known to promote maturation of vessels in vitro, as well as in wound healing and development.

# CHAPTER 4

# VASCULARIZED CANCER MODEL

*Aim 3 is to construct a biomimetic and vascularized liver cancer model, in which multicellular cancer spheroids and chitosan-heparin micro/nanofiber scaffolds seeded with endothelial cells are combined .recapitulating tumor angiogenesis such that a vasculature is formed to allow passage of a drug into the spheroid.* . We hypothesize that this model can be used to characterize the effect of drugs on vascular sprouts, anastomosis, migration, and transportation of drugs through cancer.

## 4.1 Background

As mentioned previously, anti-angiogenic drugs have failed alone as a cancer treatment, however, co-administration with chemotherapy drugs has been shown to greatly improve clinical outcomes. [5, 6, 107, 108] Thus, co-administration has breathed new life into anti-angiogenic drug therapies, but at the same time has illuminated a problem with cancer research: in vitro versus clinical results.

Clinical results should be predicted during the initial phases of drug testing, however, aren't and can be blamed on broad assumptions. The drug testing process, in brief, begins with in vitro testing, followed by animal studies, and finally followed by clinical trials. Clinical trials are the most expensive phase of drug testing and most telling as human beings, for which these drugs are being tested for, are being tested upon. However, because of their cost/ethical considerations, clinical trials are usually reserved later in the process in hopes that in vitro and/or animal testing will root out those drugs that are dangerous and/or ineffective. But sometimes, these hopes are misplaced as it is possible

that in vitro and/or animal testing will deem a drug safe/effectual that is later determined by clinical trials as dangerous/ineffective. An equally valid scenario is the opposite, when in vitro and/or animal testing will deem a drug unsafe/ineffective, when clinical trials show the drug to be safe/effectual. In either case, the disparity between the results of in vitro and/or animal testing with that of clinical trials can be blamed on broad assumptions made during the course of in vitro and/or animal testing, however, as mentioned in the introduction, this is not the case.

Nowhere is the contradiction between in vitro and clinical results more noticeable than in Manov et al. and Abou-Alfa et al. In clinical trials performed by Abou-Alfa et al., co-administration of sorafenib and doxorubicin shows a mean overall survival of the patients of 13 months compared to 3 months when sorafenib is administered alone. [109] In an in vitro experiment performed by Manov et al., co-administration of sorafenib and doxorubicin in a Hep3B/HepG2 model, showed an increase in cell viability. [110] The results of this in vitro experiment run counter to clinical results, however, can be explained by the molecular mechanisms by which each drug causes apoptosis. Doxorubicin can cause apoptosis via the sustained upregulation of the MAPK/ERK pathway. [111] Sorafenib can cause apoptosis via the downregulation of the MAPK/ERK pathway via B-Raf blockage. [6, 112] Thus, the two drugs counteract each other. Sorafenib, though, has other means by which to cause apoptosis, namely via the anti-angiogenic strategy in which hypoxia/ischemia induces apoptosis. In the model system devised in Manov et al., hypoxia is lacking as it is a 2D monoculture and so the culture is always sufficiently oxygenated. Admittedly, Manov et al. noted this fault in the model and are justified in that the purpose of their experiment was to investigate the effects of these two drugs and their counteracting

mechanism. However, if the purpose of such a model is not to determine the effect of molecular mechanisms and instead is used for in vitro drug testing, then this in vitro model would predict co-administration of doxorubicin and sorafenib to be ineffectual. In order to address the problems involved in in vitro testing, a new model must be constructed that incorporates various aspects of cancer including vasculature and hypoxia into its design.

Hypoxia is an important aspect that needs to be incorporated into an in vitro model's design and is difficult to recreate in a 2D model, thus, requiring a 3D model. The effect of hypoxia on cancer has become a focus of research in recent years due to the wide range of effects hypoxia has on cancer. Through a series of mutations, a cell begins to grow uncontrollably and forms the nascent tumor. [1, 113] Initially, simple diffusion is able to transport nutrients and gases throughout the nascent tumor. However, when the tumor reaches the size of ~1 $mm^3$, transport of nutrients and gases via simple diffusion is no longer possible resulting in a hypoxic/necrotic core within the tumor. [2, 114] The hypoxic conditions results in the modulation of various signal transduction pathways. Under the normal conditions of oxia, the transcription factor HIFa interacts with Von Hippel Landau (VHL) factor and becomes ubiquitylated for proteosomal degradation. However, during hypoxia HIFa is transported into the nucleus where it dimerizes with HIFb, interacts with hypoxia related elements (HRE), and transcribes tumor angiogenic factors. [11, 13, 115-118] Specifically, VEGF is transcribed which causes sprouting angiogenesis to relieve hypoxia in the affected area. When, anti-angiogenic drugs are used to halt the angiogenesis process, critical nutrients and oxygen are deprived from the tumor resulting in tumor starvation and hypoxia which leads to tumor necrosis. [12, 119, 120] The tumor hypoxia/ischemia brought on as a result of anti-angiogenic drug exposure is evident in

clinical and in vivo studies, however, is absent in Manov et al., thus explaining why a combination of sorafenib and doxorubicin showed growth instead of cell population decline.

However, the hypoxia following exposure to the anti-angiogenic drug leads to drug resistance. Hypoxia leads to the stabilization of HIF-a, which is able to dimerize with HIF-b and forms a complex which activates gene expression. [11, 13, 115] Most notable of the genes expressed is MDR-1 which transcribes the drug efflux protein P-gp. Also, hypoxia can lead to acquired drug resistance, when the hypoxia leads to the upregulation of alternative pro-angiogenic signals pathways such as PI3K/Akt. [6, 108] Overall, hypoxia leads to drug resistance and an accurate model should mimic both the initial decrease in viability due to tumor starvation/hypoxia and the drug resistance due to the hypoxia resulting from exposure to the anti-angiogenic drugs.

*To mimic tumor angiogenesis and hypoxia, a biomimetic and vascularized liver cancer model is fabricated in which multicellular cancer spheroids and chitosan-heparin micro/nanofiber scaffolds seeded with endothelial cells are combined together on Matrigel .recapitulating tumor angiogenesis such that a vasculature is formed to allow passage of a drug into the spheroid.*

Due to the abnormal growth of cancer and the failure of angiogenesis to meet the oxygen/nutrient needs of the growing cancer, differential regions of oxia and hypoxia are created within the tumor. A spheroid is able to mimic these differential regions of oxia and hypoxia given its geometry; in which cells on the outer layer cells are exposed to oxygen and nutrients, while those cells of the interior fail to receive oxygen and nutrients. Liver cancer is known to be highly vascularized, thus, in order to create a highly vascularized

model, the spheroid's ability to create a region of hypoxia is taken advantage of. The hypoxic/necrotic core of the spheroid causes the upregulation of a variety of tumor associated factors, specifically VEGF. Local blood vessels react by undergoing remodeling, in which the basement membrane of the vessel disintegrates, endothelial cell junctions dissolve, and the endothelial cells remodel to form a vascular sprout. [121, 122] The vascular sprout will grow along the chemotactic gradient of tumor angiogenic factors toward the source of hypoxia/tumor and proceed to form blood vessels in the region until oxia is restored.

Ideally, such a model would be able to mimic the path an anti-angiogenic drug takes from the bloodstream through the tumor vasculature and into the tumor. Our model should accomplish this as the hypoxia derived from the spheroid's geometry is like the solid tumor and will cause vascular sprouting and angiogenesis from the endothelial cells coating the cell coated tube which will proceed to form a vasculature with the spheroid. Angiogenesis should bridge the spheroid and the cell coated tube, and would be able to allow the passage of drugs into the spheroid. Part of this tumor vasculature is exhibited in the previous section in which vascular sprouts are seen emerging from the cell coated tube and would ideally vascularize the spheroid. However, that takes time and due to the limited lifespan of in vitro models it is not possible for vascular sprouts from the cell coated tube to vascularize the spheroid. Thus, the spheroids must be pre-vascularized and form their own vascular sprouts which can anastomize with the vascular sprouts and bridge the cell coated tube with the spheroid. To pre-vascularize the spheroids, endothelial cells are added to the cell media used in forming the hanging droplets to create triculture spheroids made of HepG2, fibroblast, and endothelial cells.

Ostensibly, a model of cancer angiogenesis would minimally require the cancer cells in question and endothelial cells, however, fibroblasts aid in cell survival and to promote vascular sprouting. In regards to angiogenesis, fibroblasts provide soluble growth factors such as VEGF and interact with endothelial cells to promote vascular sprouting and networking. [67, 101, 123-127] Besides, producing vascular sprouts, endothelial cells, much like fibroblasts, can improve urea metabolism, albumin metabolism, and bile canaliculi/CLF staining of HepG2 cells co-cultured with it. [22, 128-132]

To aid in the formation of vascular sprouts to form from the triculture spheroids, the triculture spheroids will be cultured on Matrigel. Matrigel is collagen IV and other extracellular matrix components derived from the Engelbreth-Holm-Swarm (EHS) mouse sarcoma and promotes the vascularization of endothelial cells. Hence when endothelial cells are cultivated in heterospheroids on Matrigel, the endothelial cells will form vascular sprouts that emanate from the spheroid, much like how vascular sprouts would emanate from the aortic ring in the aortic ring assay. Anti-angiogenic drugs affects angiogenesis, preventing vascular sprout growth. Thus, when our model is exposed to an anti-angiogenic drug, the vascular sprouts will stop growing or even regress and so the model can be used to assess the anti-angiogenic capability of a drug. For this study, the anti-angiogenic drug sorafenib is used. Sorafenib/Nexavar blocks VEGF and PDGF receptors, prevent HIFa and VEGFa expression, and block the Raf/MEK/ERK signal transduction pathway. [6, 133, 134]

Vascular regression is the remodeling and pruning of the vasculature as a result of drug exposure as mentioned previously, or naturally. The natural occurrence of vascular regression would affect this model by causing vascular sprouts to retract before they can

anastomize with each other and/or form lumens. The presence of fibroblasts and paracrine factors elicited by the fibroblasts is able to stabilize the vascular sprout by expressing the pro-stabilization factor Ang-1. [135] Given presence of fibroblasts in our model, the vascular sprouts should be able to remain stable and grow overall in the absence of drugs. Furthermore, due to the unregulated expression of VEGF and other growth factors, and irregular oxygen supply in cancer, it is a question whether vascular regression even occurs in cancer. [136] Thus, natural vascular regression should not present a problem for the vascular sprouting assay.

Besides physically connecting spheroids and cell coated tube, the model must also prove itself perfusable, such that an anti-angiogenic drug can travel from the tube into the spheroid. In animal studies proving that an implanted model is perfusable requires a simple injection of a fluorescent dye into the bloodstream. If the implanted model has connected with the surrounding native vasculature and if the vasculature within the model contains a lumen, then upon dissection of the animal, the fluorescent dye should be revealed within the model's vasculature network. An in vitro model does not have the same option as it is difficult, using tools available to the common laboratory, to inject fluorescent dye into such a system due to the diminutive size of the vasculature and a lack of a point of entry. The cell coated tube abrogates this problem as the cell coated tube is large enough such that a pipette is able to inject fluorescent compounds inside.

As an additional experiment, the triculture spheroid on Matrigel can be used as an alternative to the rat/mouse aortic ring assay. Assays of the effect of an anti-angiogenic drug on endothelial cells usually employ the rat/mouse aortic ring assay, an in vitro assay in which an aortic ring is excised from the organism and grown on Matrigel with or without

the vehicle, followed by the measurement of the length or area of the vascular sprouts. [137] Although, the aortic ring assay is the standard model, it is not without problems. The aortic ring assay measures the effect of a vehicle on rodent endothelial cells, which may or may not be similar to human endothelial cells. Also, the aortic ring assay may lack consistency as the population of cell types may differ due to the variation inherent amongst specimens. Even the sex of the rodent may effect angiogenesis as male specimens are more angiogenic than female specimens. The most notable problem with the aortic ring assay, especially when used to measure the effect of anti-angiogenic cancer drugs is the fact that the aortic ring is an aortic ring without the presence of cancer cells. Cancer cells are critical to the process of tumor angiogenesis and have been shown in vitro to aid in the process of angiogenesis and vascularization in vitro due to cell-cell contact and/or release of growth factors. [78, 138-140] More importantly, endothelial cells can interact with the cancer cells altering the metabolism of cultures reacting various drugs. [141] To remedy some of the problems inherent with the aortic ring assay, an alternative model is proposed by incorporating endothelial cells into our previous heterospheroid model of cancer. Such a model would be an improvement over the aortic ring model in that 1) each spheroid would have a consistent population of cells relevant to cancer angiogenesis, 2) wouldn't require the use of animal models or surgical procedures to remove the aortic ring, and 3) include cancer cells to provide cues for angiogenic growth.

## 4.2 Methods

### 4.2.1 Culture (HUVEC)

Human umbililcal vascular endothelial cells (HUVEC; ; a gift Dr. Eun J. Lee's lab) are cultured in endothelial cell growth medium (EGM-2 Bulletkit Lonza) containing basic fibroblast growth factor (bFGF), EGF, insulin-like growth factor-1 (IGF-1), VEGF, hydrocortisone, ascorbic acid, heparin, gentamicin, and amphotericin-B. All cultures are incubated in 10% $CO_2$, 37$^{o}$C incubator.

### 4.2.2 Hanging Drop Method-Triculture Spheroid

Triculture spheroids are fabricated using the hanging drop method, as described previously in Section 2.2.2. To obtain triculture spheroids, 1,000 HepG2, 1,000 growth arrested 3T3-J2 fibroblast cells, and 1,000 endothelial cell (RAEC or HUVEC) in 30 μL droplets, containing RAEC or HUVEC media depending on endothelial cells used, are plated on a 100 mm Petri dish and inverted. Spheroids are harvested after 7 days.

### 4.2.3 Vascular Sprouting (Length)

When cultured in spheroids and grown on Matrigel, endothelial cells have the potential to form vascular sprouts. The length of these sprouts can be used to assay the effect of various drugs on the vascularization of a tumor. The spheroids are incubated on the surface of Matrigel and sprouting is allowed to occur over the course of 7 days. The spheroids are then exposed to various concentrations of a drug (sorafenib: 0μM, 5μM, and 10μM). Images are taken at 10x magnification and length of sprouts analyzed using SigmaScan Pro5.

### 4.2.3 Vascular Sprouting (Immunohistochemistry)

To ensure that the vascular sprouts are indeed the product of endothelial cell induced angiogenesis and not one of the other cell types masquerading as vascular sprouts, such vascular sprouts are stained for CD31, an antibody pertinent to endothelial cells. Triculture spheroids are harvested after 7 days. Collagen gel (1.2 mg/mL) and 10x DMEM is allowed to gel at 37$^{o}$C for 30 min and spheroids are embedded on top of the gel. Sprouts are allowed to grow on the collagen gel surface for another 7 days. The culture is then fixed with 4% paraformaldehyde for 10 min before being stained with FITC mouse anti-human CD31 (BD Pharmingen) (1:50) in PBS overnight at 4$^{o}$C.

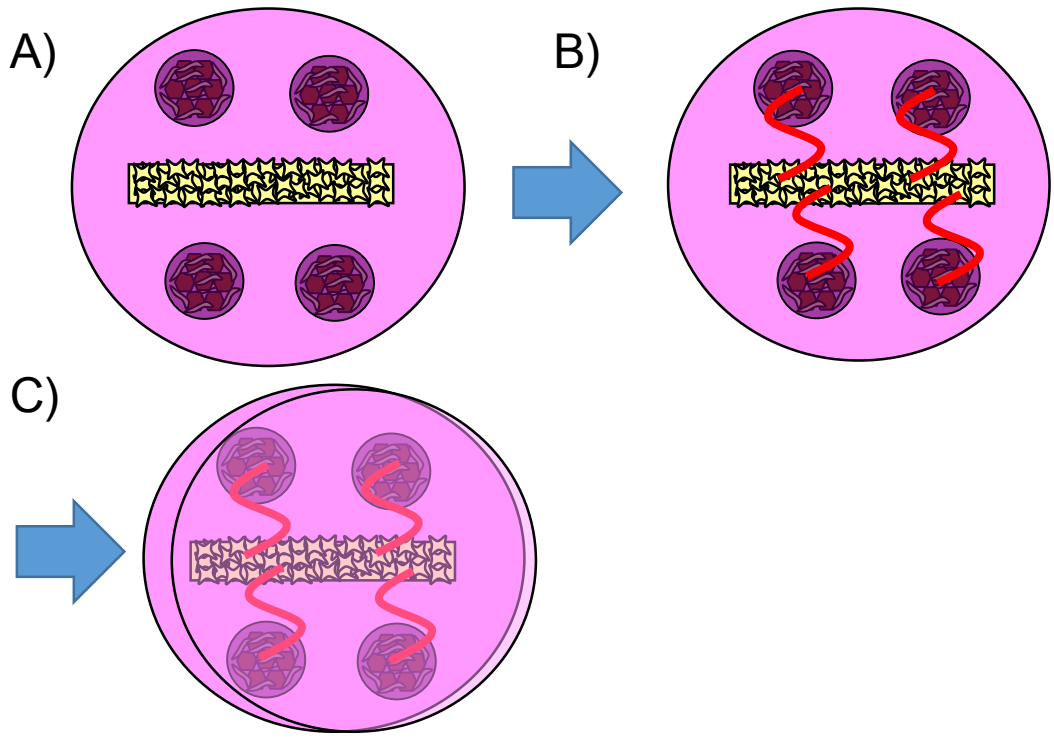


**Figure 4.1** Design of Vascularized Model. Design of vascularized model is featured showing the fabrication of the model, starting with A) the embedding of both spheroids and vascular tube on Matrigel, B) spheroid and vascular tube forming vascular sprouts, and C) the addition of a second layer of Matrigel.

### 4.2.5 Anastomosis

Vascular sprouting is shown to independently occur in the triculture spheroids and the cell coated tube. When placed together in the same culture, it is possible for these vascular sprouts emanating from the triculture spheroid and cell coated tube to interact with each other in what is known as anastomosis. To record this event, triculture spheroids and cell coated tube are embedded together on Matrigel and monitored over the course of time for interactions between the vascular sprouts.

### 4.2.6 Migration

Migration of spheroids toward the fiber/tube is evident in some circumstances. By taking images at various time intervals, the migration can be monitored.

### 4.2.7 Fluorescent Dextran/Doxorubicin Injection

To prove that vascular sprouts of the spheroid and the cell coated tube have anastomized and formed a lumen, FITC dextran (70kDa) or doxorubicin is injected into the cell coated tube. If a lumen is formed between the cell coated tube and spheroid, and no physical leakage has occurred, then fluorescent dextran/doxorubicin should only be viewed in the regions of the cell tube, the vasculature between the tube and the spheroid, and within the spheroid itself. Note, doxorubicin, as well as being a chemotherapy drug, is slightly fluorescent for the color red and, thus, can be used to show the distribution of the drug throughout the model.

## 4.3. Results

### 4.3.1 Vascular Sprout (Drug Testing)

Images of vascular sprouts emanating from the spheroid were taken and length of sprouts are measured by SigmaScan Pro5. For all conditions the vascular sprouts in the 0uM/control condition showed continued sprout length growth. In contrast, vascular sprouts in drug exposed (5μM and 10μM conditions) show a decrease sprout length growth. For the 10μM condition, there cease to be any vascular sprouts present by day 4. There is a significant difference (n=10, **p<0.005) between the 0μM/control and the drug exposed conditions for each of the following days.

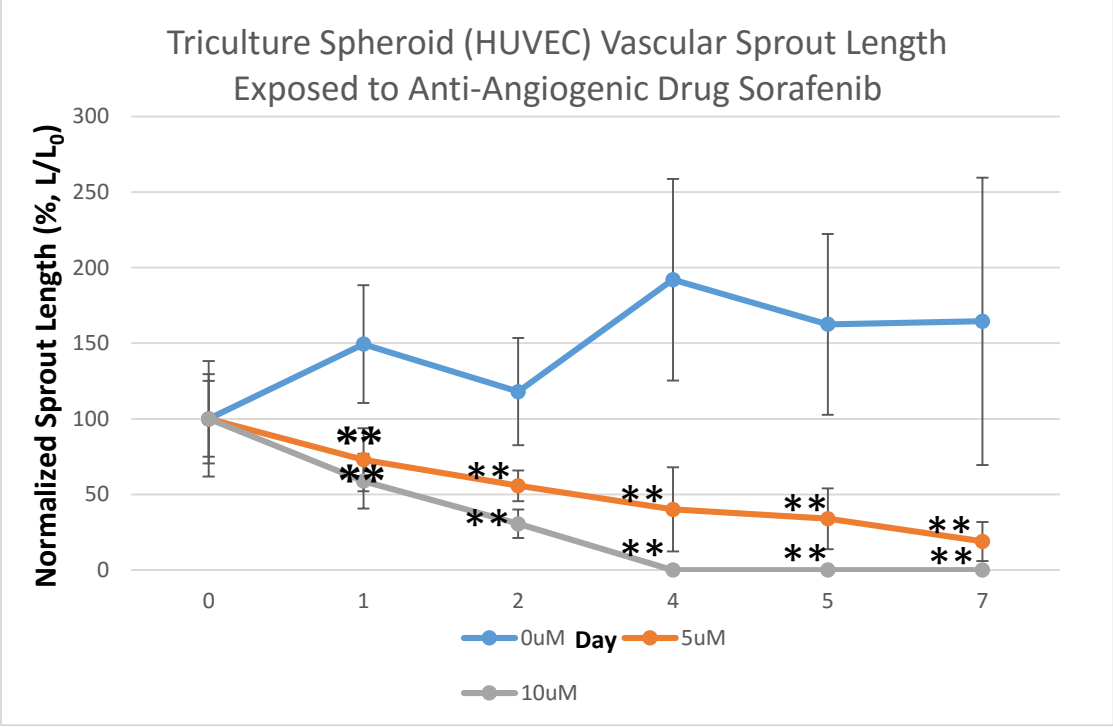


**Figure 4.2** Triculture Spheroid (HUVEC) Vascular Sprout Length Exposed to Anti-Angiogenic Drug Sorafenib. Lengths of the vascular sprouts in HUVEC triculture spheroid when exposed to sorafenib shows for 0μM/control condition increas whereas 5μM and 10μM conditions shows decreased growth. Sprout length is normalized to day 0 average before drug treatment. Values represent averages ± SD (n=10, *P<0.05, ** P<0.005, when comparing 5 μM and 10 μM to 0 μM.

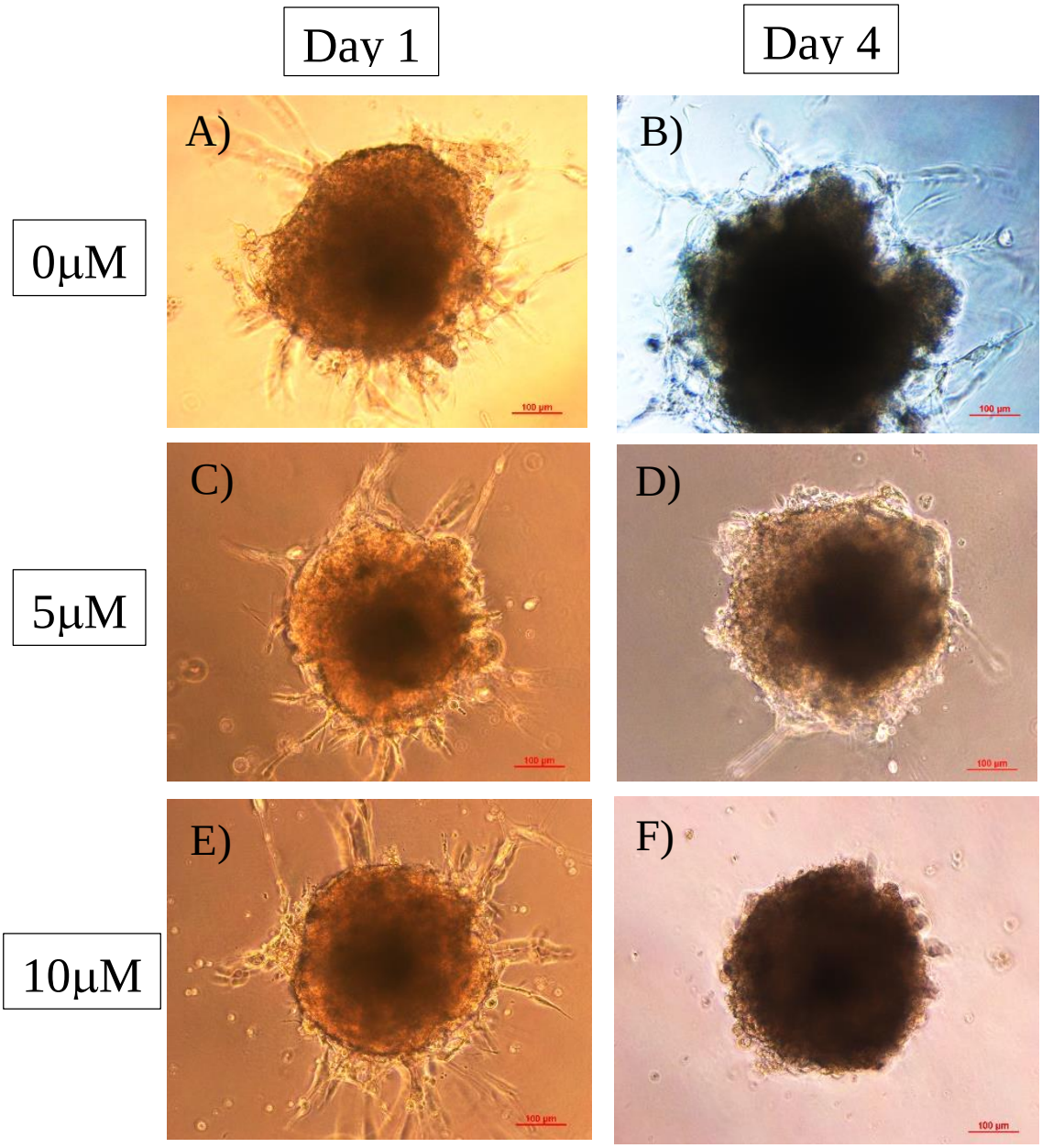


**Figure 4.3** Phase Images of Triculture (HUVEC) Spheroids and Vascular Sprouts Exposed to Sorafenib. Images of vascular sprouts from HUVEC triculture spheroids show vascular sprouts before and after exposure to drugs on day 1 an day 4. A) shows the 0μM/control, and B) shows the control after 4 days revealing increased growth. C) shows the before and D) shows the after image of HUVEC triculture spheroids exposed to 5μM sorafenib. E) shows the before and F) shows the after image of HUVEC triculture spheroids exposed to 10μM sorafenib. Greater concentration of sorafenib shows greater decrease of sprout length.

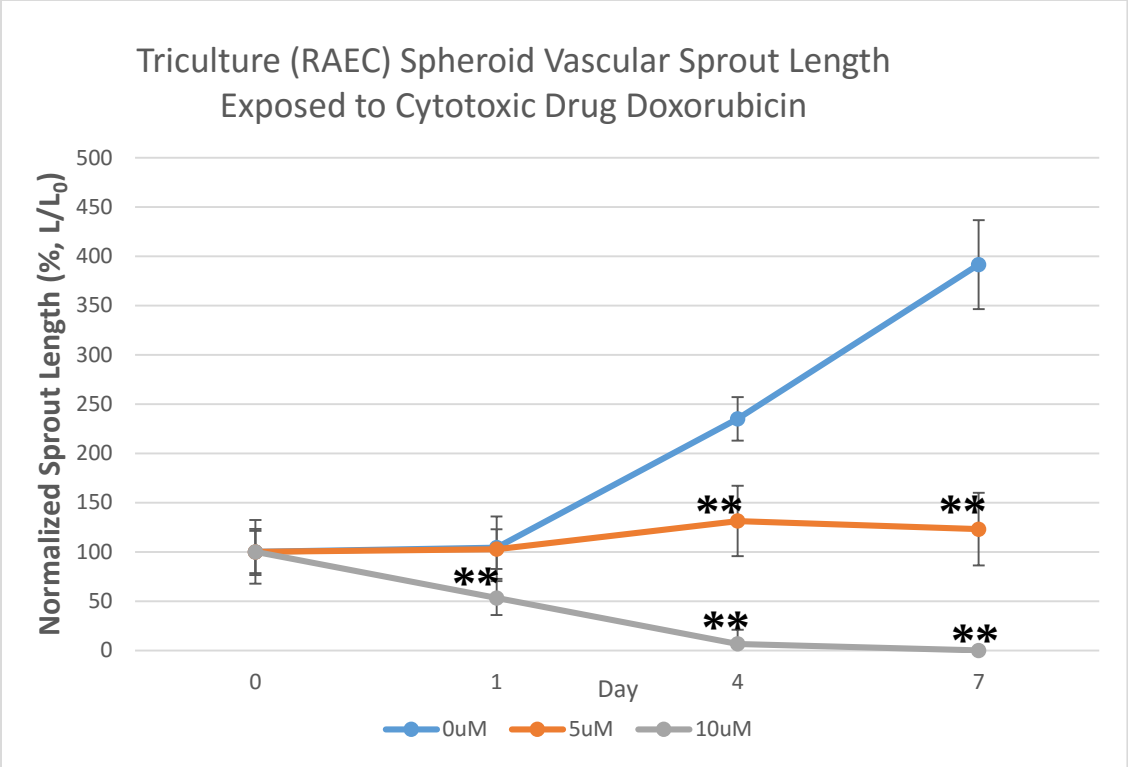


**Figure 4.4** Triculture Spheroid (RAEC) Vascular Sprout Length Exposed to Cytotoxic Drug Doxorubicin. Length of the vascular sprouts in RAEC triculture spheroid when exposed to sorafenib shows for 0μM/control condition increased growth whereas 5μM and 10μM conditions shows decreased growth. Sprout length is normalized to day 0 average before drug treatment. Values represent averages ± SD (n=10, *P<0.05, ** P<0.005), when comparing 5 μM and 10 μM to 0 μM.

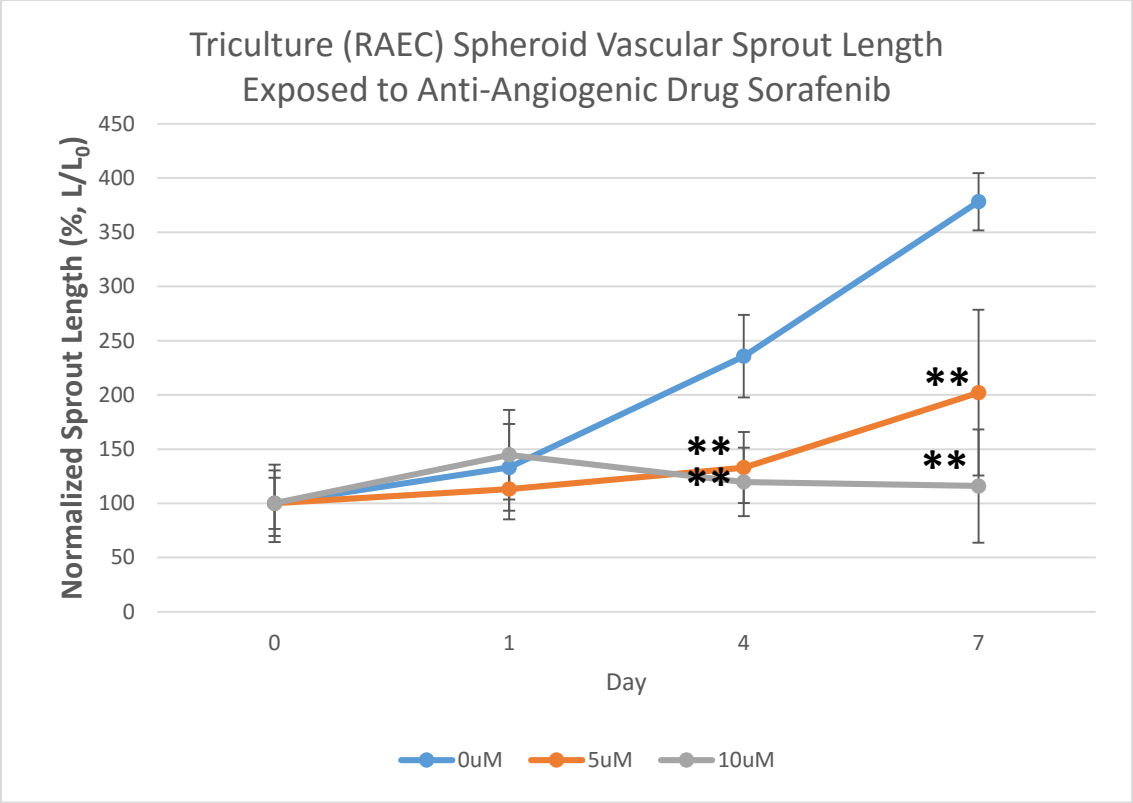


**Figure 4.5** Triculture Spheroid (RAEC) Vascular Sprout Length Exposed to Anti-Angiogenic Drug Sorafenib. Length of the vascular sprouts in RAEC triculture spheroid when exposed to doxorubicin shows for 0μM/control condition increased growth whereas 5μM and 10μM conditions shows decreased growth. Sprout length is normalized to day 0 average before drug treatment. Values represent averages ± SD (n=10, *P<0.05, ** P<0.005), when comparing 5 μM and 10 μM to 0 μM.

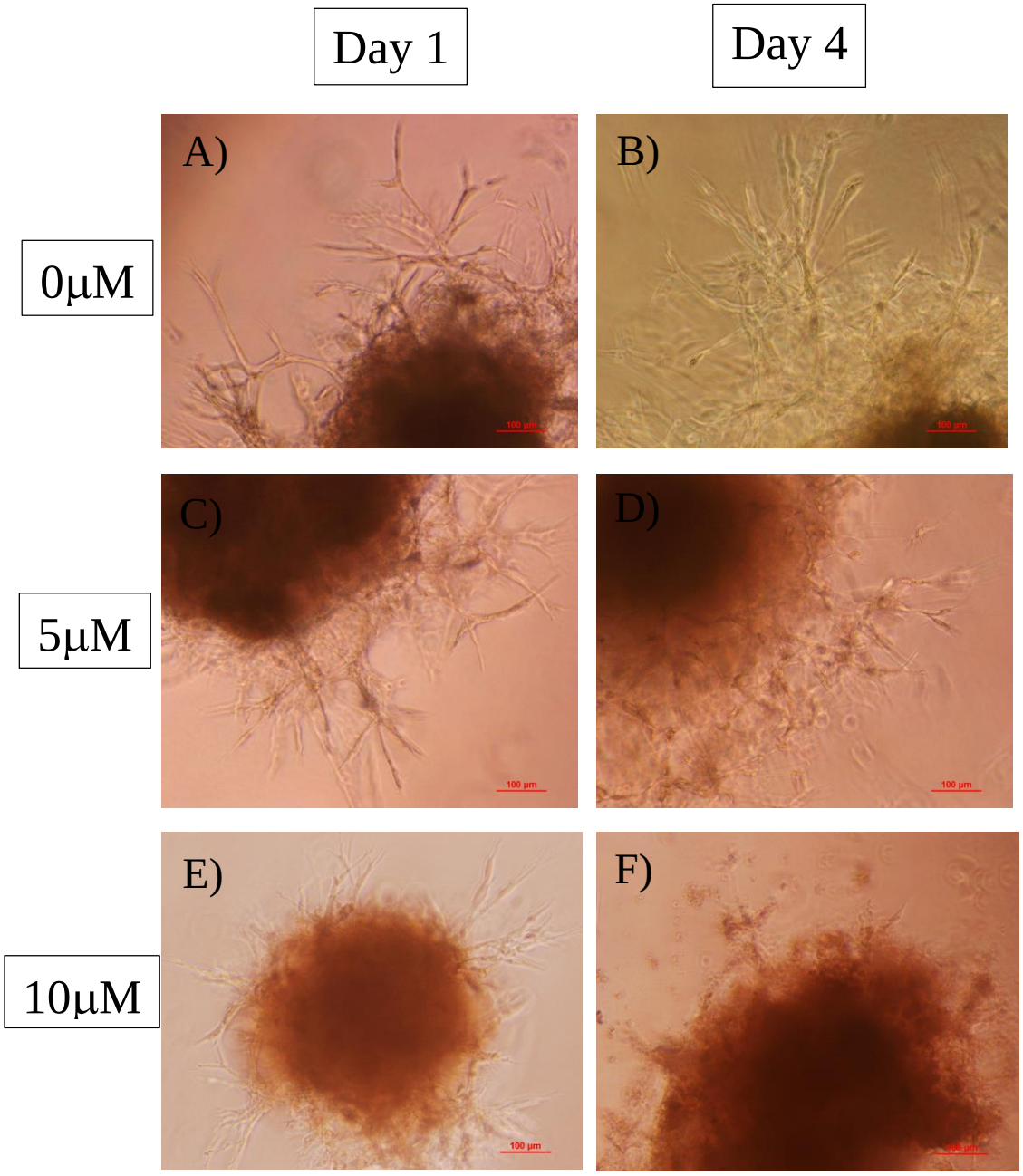


**Figure 4.6** Phase Images of Triculture (RAEC) Spheroids and Vascular Sprouts Exposed to Sorafenib. Images of vascular sprouts from RAEC triculture spheroids show vascular sprouts before and after exposure to drugs on day 1 and day 4. A) shows the control, and B) shows the control after 4 days revealing increased growth. C) shows the before and D) shows the after image of RAEC triculture spheroids exposed to 5μM sorafenib. E) shows the before and F) shows the after image of RAEC triculture spheroids exposed to 10μM sorafenib. Greater concentration of sorafenib shows greater decrease of sprout length.

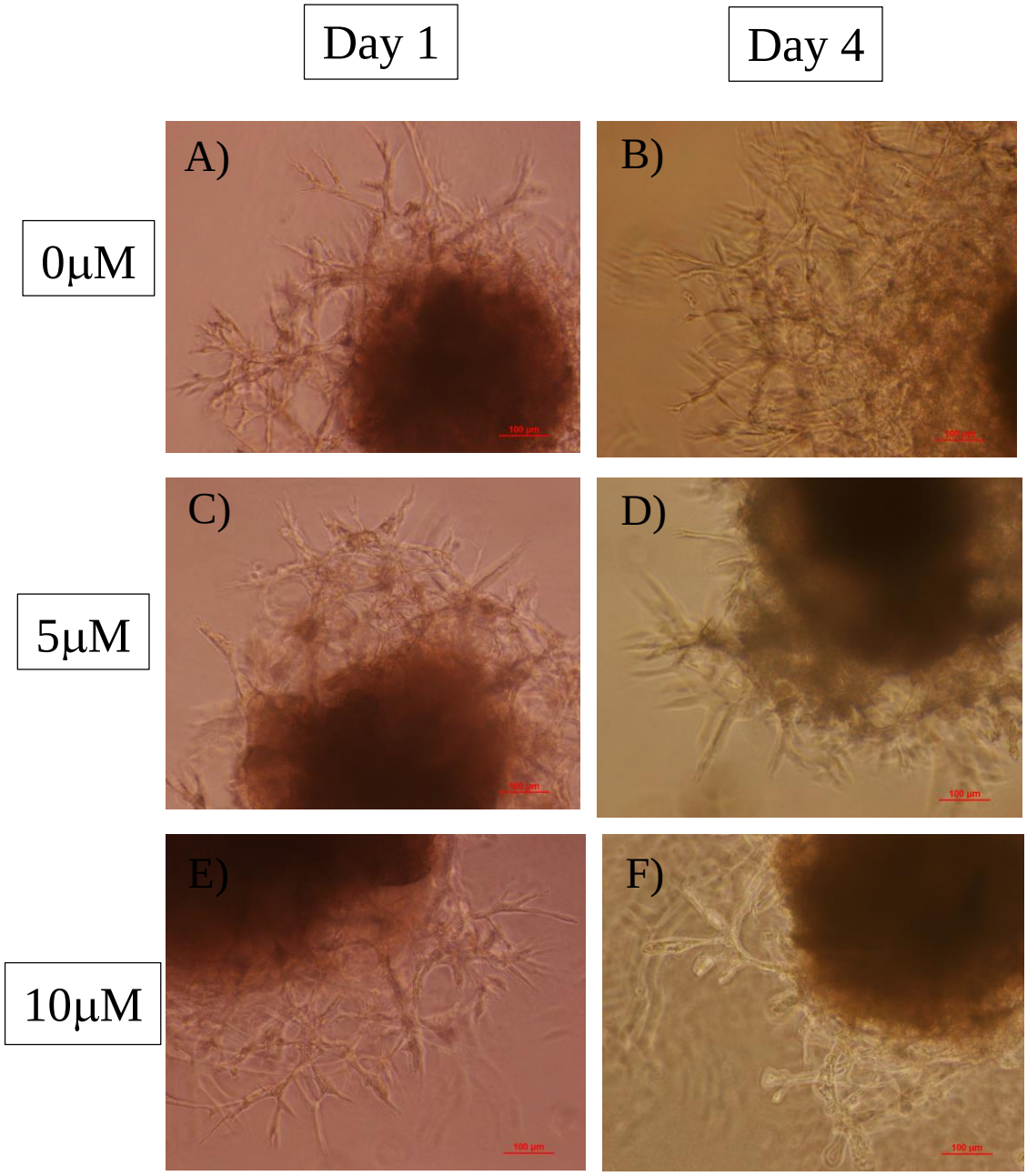


**Figure 4.7** Phase Images of Triculture (HUVEC) Spheroids and Vascular Sprouts Exposed to Doxorubicin. Images of vascular sprouts from RAEC triculture spheroids show vascular sprouts before and after exposure to drugs on day 1 and day 4. A) shows the before and B) shows the after image of RAEC triculture spheroids exposed to 10μM sorafenib. C) shows the before and D) shows the after image of RAEC triculture spheroids exposed to 5μM doxorubicin. E) shows the before and F) shows the after image of RAEC triculture spheroids exposed to 10μM doxorubicin. Greater concentration of doxorubicin shows greater decrease of sprout length.

### 4.3.2 Vascular Sprout (Immunohistochemistry)

CD31 staining of the triculture spheroids containing HUVEC cultured on Matrigel fluoresces for endothelial cells. On what is presumed to be the vascular sprouts, a majority of the cells fluoresce and therefore can be assumed to be endothelial cells. Non-green fluorescing cells are present alongside the endothelial cells on the vascular sprouts as evident by DAPI stained images.

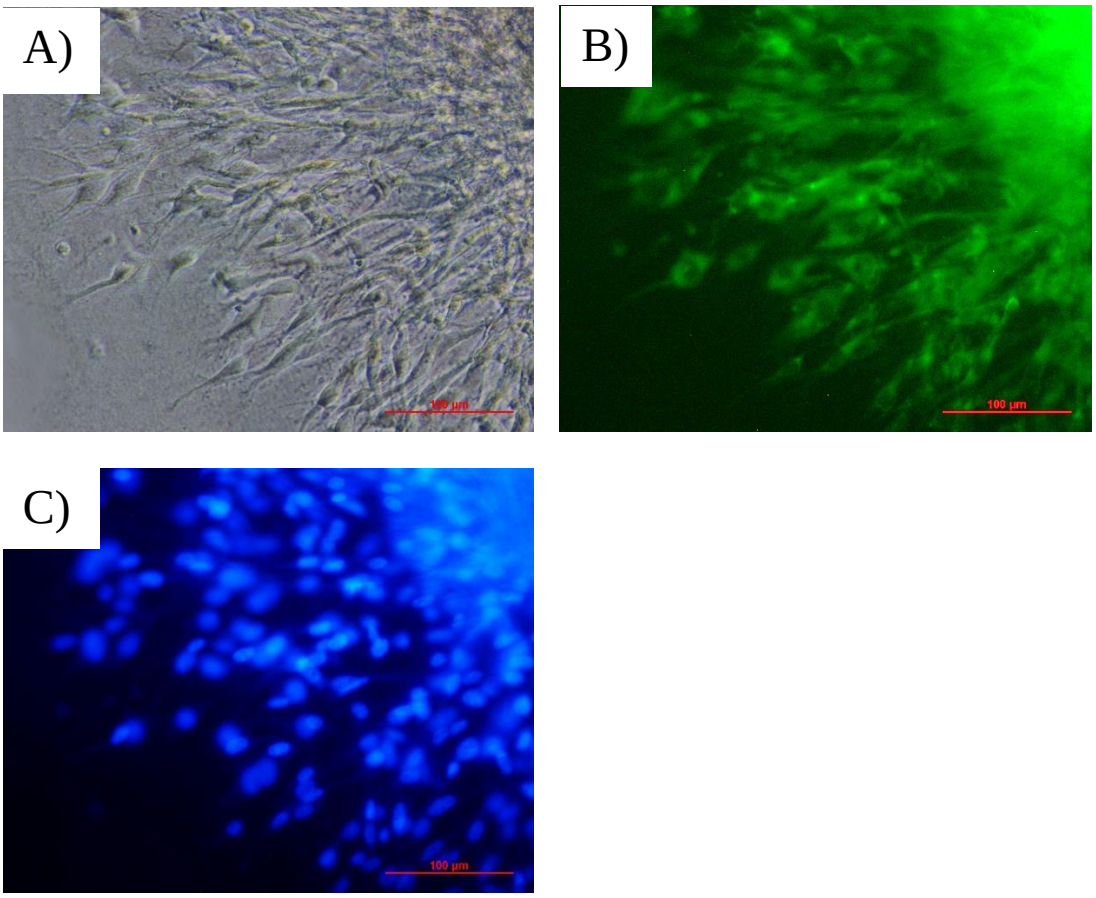


**Figure 4.8** CD31 and DAPI Images of Triculture (HUVEC) Spheroids and Vascular Sprouts. Vascular sprouts radiating from HUVEC triculture spheroids on collagen gel are visualized at 20x magnification. A) shows phase image, B) shows CD31 stained image, and C) shows DAPI stained image, showing the presence of endothelial cells.

### 4.3.3 Vascular Sprout (Live/Dead)

Images of triculture spheroids show Live/Dead imaging after the addition of 10μM doxorubicin or 10μM sorafenib. Following exposure to either drug, spheroids show considerable red fluorescence or cell death.

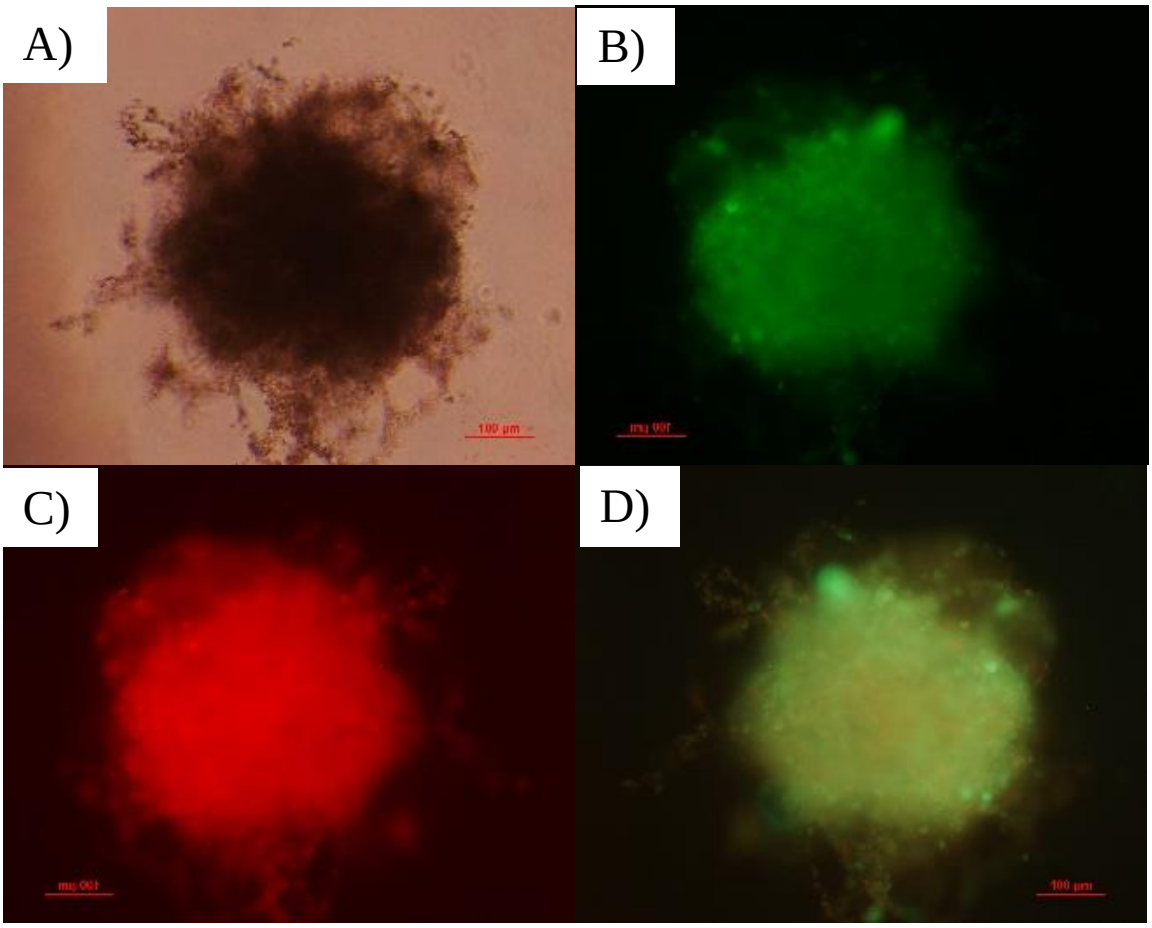


**Figure 4.9** LIVE/DEAD Assay of Triculture (RAEC) Spheroids following Exposure to Doxorubicin. RAEC triculture spheroids are exposed to anti-cancer drugs and images are taken at 10x magnification. 10 μM doxorubicin exposed conditions are shown in the first four images. A) shows the phase image, B) shows the live image, C) shows the dead image, and D) shows live/dead image. Considerable red fluorescence compared to green fluorescence shows that doxorubicin has caused apoptosis.

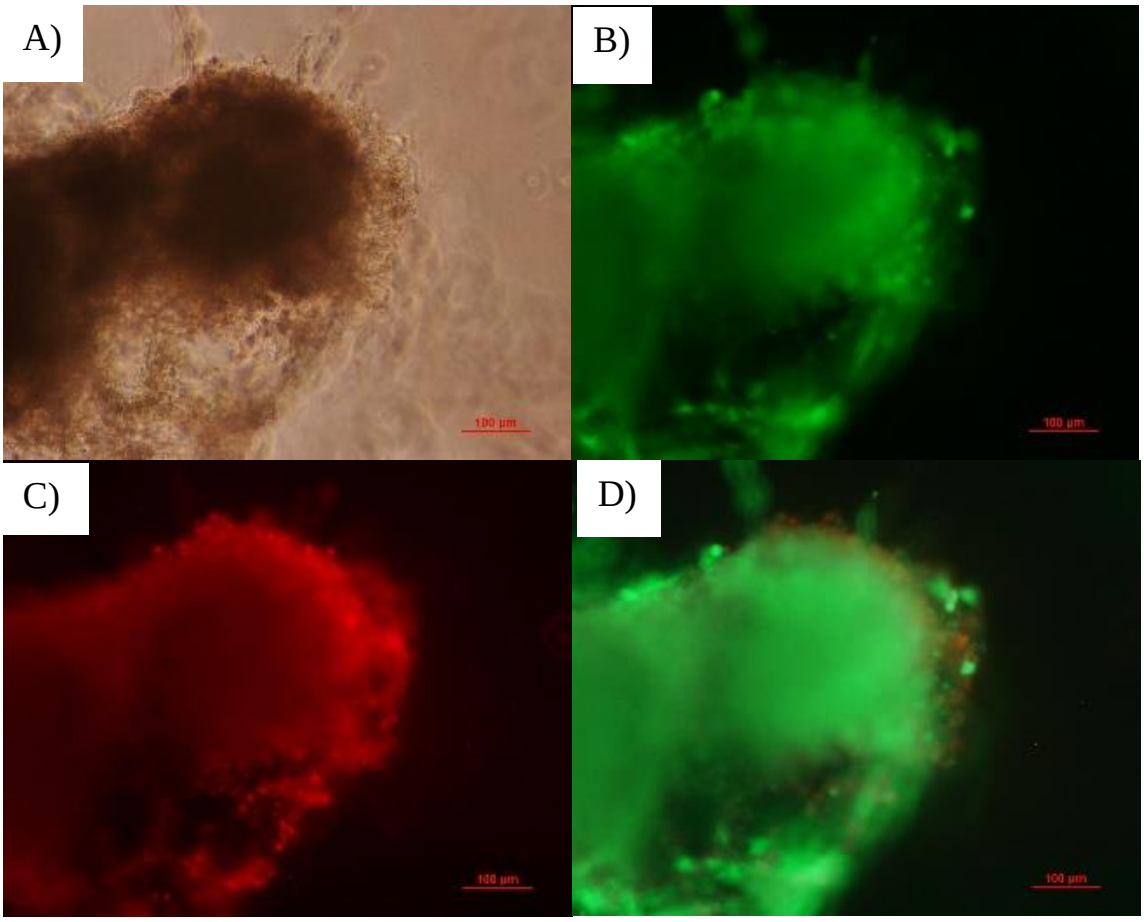


**Figure 4.10** LIVE/DEAD Assay of Triculture (RAEC) Spheroids following Exposure to Sorafenib. RAEC triculture spheroids are exposed to anti-cancer drugs and images are taken at 10x magnification. 10μM sorafenib exposed conditions are shown in the last four images. A) shows the phase image, B) shows the live image, C) shows the dead image, and D) shows the live/dead image. Considerable red fluorescence compared to green fluorescence shows that sorafenib has caused apoptosis.

### 4.3.4 Anastomosis

Anastomosis is seen occurring between vascular sprouts of the triculture spheroids and the vascular sprouts of the cell coated fiber/tube. Over the course of time, vascular sprouts can be seen independently manifesting from the triculture spheroid and cell coated fiber/tube, until the multiple sprouts are seen conjoining with one another. Conjoined vascular sprouts can be seen as enlarged compared to the size of singular sprouts.

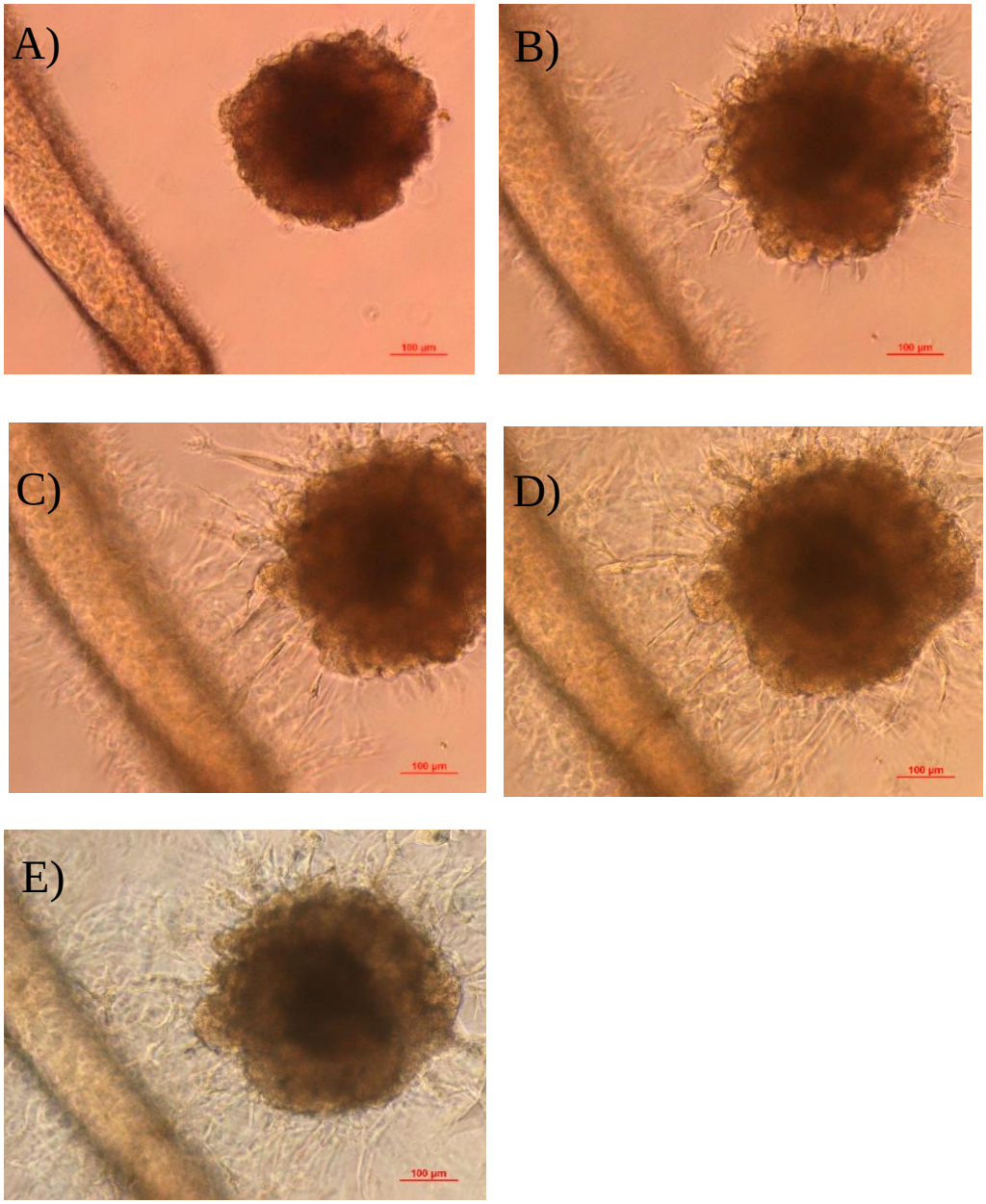


**Figure 4.11** Anastomosis Between Cell Coated Fiber and Triculture Spheroid. Anastomosis between spheroid and cell coated fiber can be seen at 10x magnification after day A) 1, B) 2, C) 3, D) 5, and E) 7 embedding on Matrigel. Vascular sprouts deriving from the spheroid and the cell coated fiber can be seen interacting with one another.

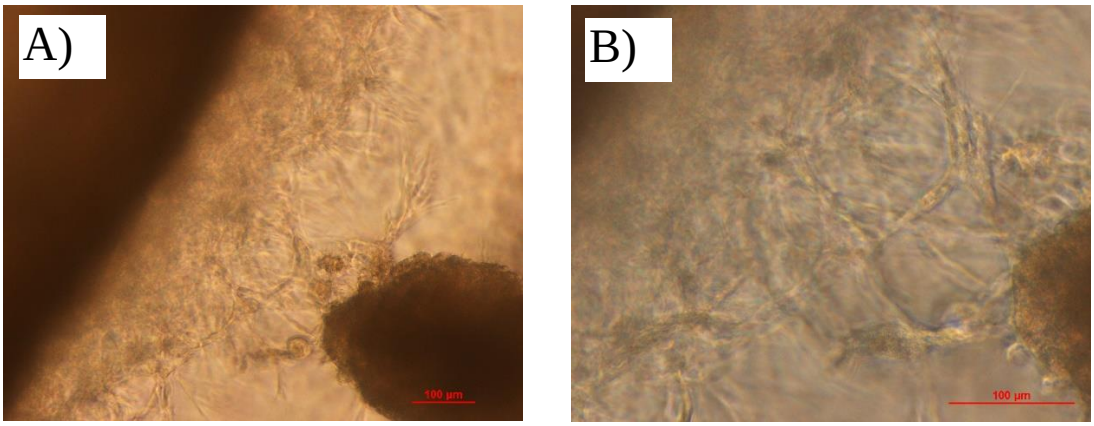


**Figure 4.12** Anastomosis Between Cell Coated Tube and Triculture Spheroid. Anastomosis between spheroid and cell coated tube can be seen at A) 10x and B) 20x magnification after day 6.

### 4.3.5 Migration

10x phase images of single spheroid and fiber is monitored over the course of several days and shown in Figure. 4.13. As can be seen the spheroid is able to migrate closer to the fiber moving approximately 100 μM distance. 10x phase images of a single spheroid and tube is monitored over the course of several days and shown in Figure. 4.14. As can be seen, the spheroid is able to migrate onto the tube after 14 days, after which the spheroid loses shape and melds with the tube.

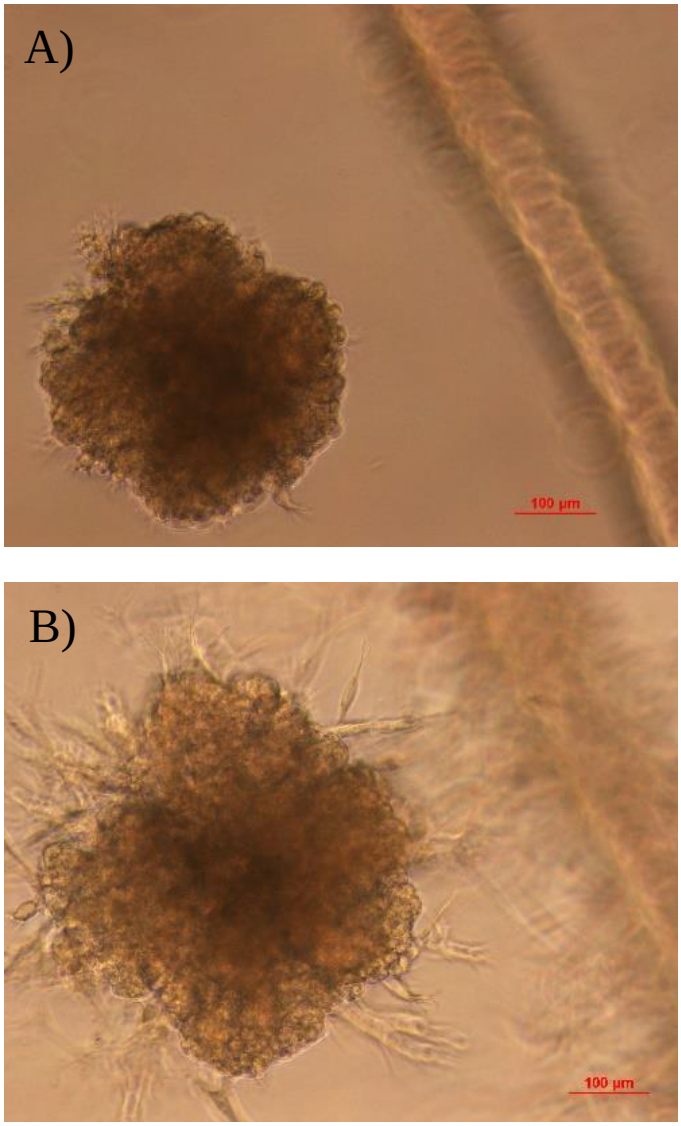


**Figure 4.13** Migration of Triculture Spheroid to Cell Coated Fiber. Migration of HUVEC triculture spheroid toward cell coated fiber can be seen on A) 1 day and B) 3 days, after embedding on Matrigel, showing the spheroid moving closer to the fiber.

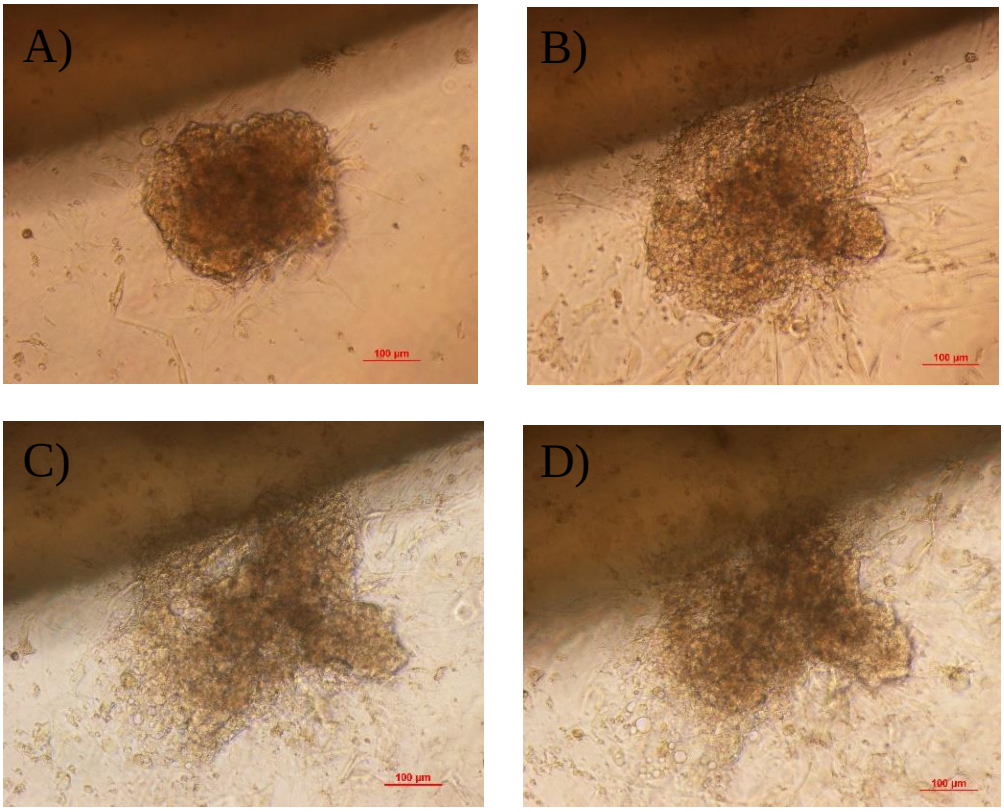


**Figure 4.14** Migration of Triculture Spheroid to Cell Coated Tube. Migration of HUVEC triculture spheroid toward cell coated tube can be seen on A) 1 day, B) 3 days, C) 7 days, and D) 14 days after embedding on Matrigel, showing the spheroid merging with the tube.

### 4.3.6 Fluorescent Dextran Injection

10x images of an area including spheroid and tube shows the distribution of fluorescent dextran within the region. Images are that of the region 10 min after injection of the FITC dextran into the cavity of the tube. Failure of green fluorescence to appear solely in the lumen of the cell coated tube, spheroid, and vasculature shows some non-specific diffusion, which is expected. Some fluorescence can be seen with the vascular sprouts showing the emergence of a nascent lumen. However, these vascular sprouts are not seen in the area of the spheroid.

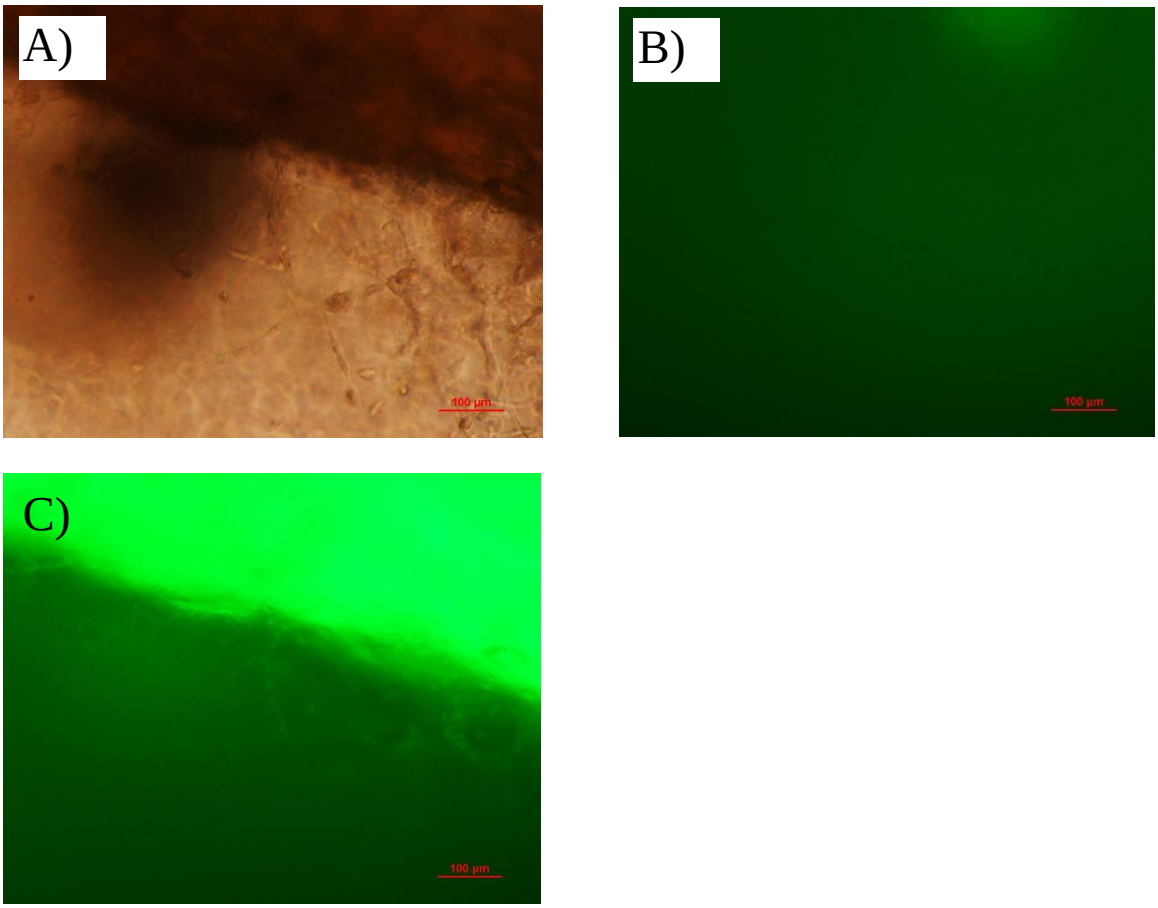


**Figure 4.15** Images of Vascularized Cancer Model Following Injection of FITC Dextran. Injection of FITC dextran can be seen at 10x magnification. A) shows phase image, B) shows green fluorescent image before injection of FITC dextran, and C) shows green fluorescent image 10 min after injection of FITC dextran. Green fluorescence can be seen in region of vascular sprouts.

### 4.3.7 Doxorubicin Injection

10x images of an area including spheroid and tube shows distribution of doxorubicin within the region. Images are that of the region 10 min after injection of doxorubicin into the cavity of the tube. Like fluorescent dextran, doxorubicin, evident by red fluorescence, can be seen throughout the model. Red fluorescence can be seen within the spheroid, however, none can be seen in the vascular sprouts.

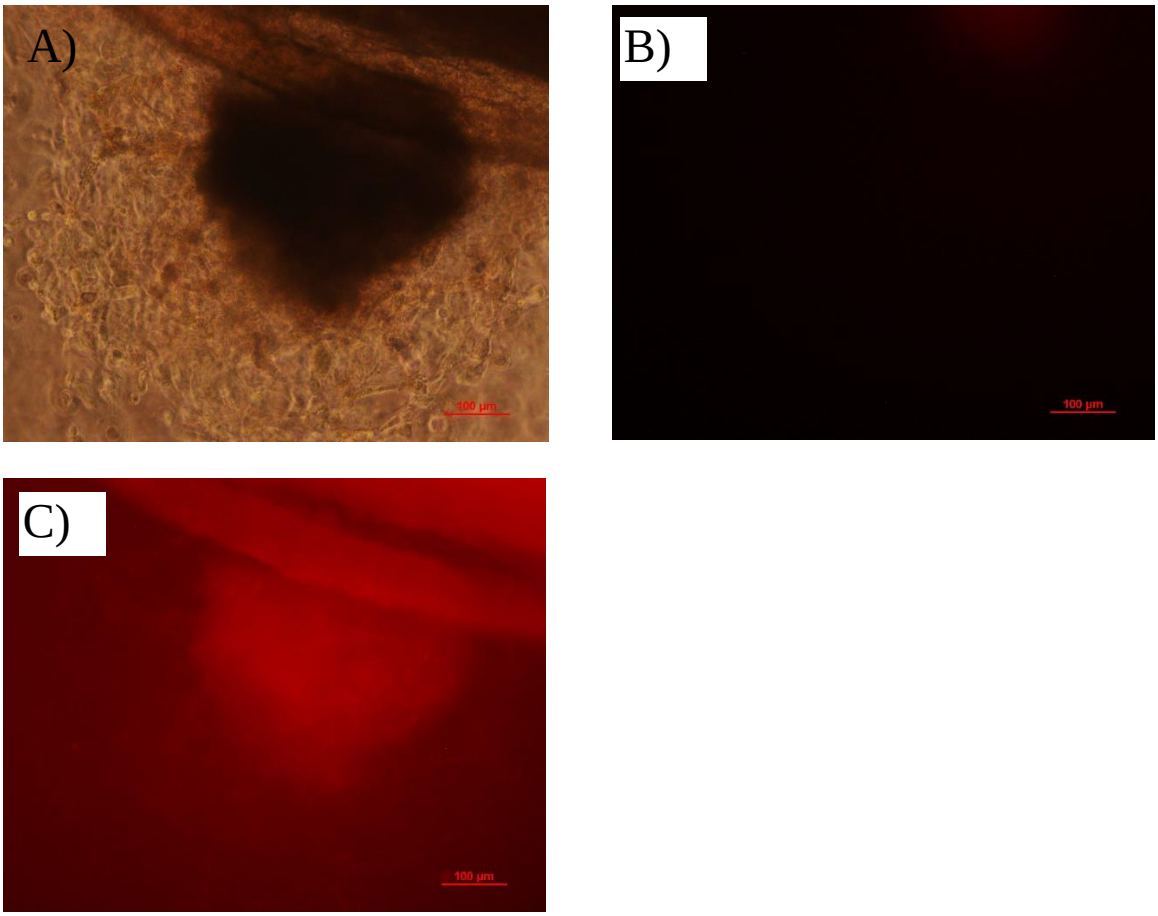


**Figure 4.16** Images of Vascularized Cancer Model Following Injection of Doxorubicin. Injection of doxorubicin can be seen at 10x magnification. A) shows phase image, B) shows red fluorescent image before injection of doxorubicin, and C) shows red fluorescent image 10 min after injection of doxorubicin. Red fluorescence can be seen in spheroid region.

## 4.4 Discussion

### 4.4.1 Model Overview

When the cell coated electrospun tube is embedded on Matrigel with triculture spheroids, three scenarios occur between the tissue engineered blood vessel and the spheroids. The first scenario is that the tissue engineered blood vessel and spheroids do not interact. The second scenario is anastomosis in which sprouting angiogenesis occurs between the spheroid and tissue engineered blood vessel, resulting in the interaction between the vascular tips. The third scenario is migration in which the spheroids migrate toward the tissue engineered blood vessel. All three scenarios occur with varying degrees within the model and mimic cancer within the human body.

### 4.4.2 Vascular Sprout Assay

Triculture spheroids formed from HepG2, fibroblast, and endothelial cells are embedded on Matrigel and are allowed to sprout before exposure to anti-cancer drugs. Such a model can be used as an alternative to the rat aortic ring assay and to test this, the lengths of the vascular sprouts are measured at different time points and with different concentrations of drugs. Two types of triculture spheroids are tested, those which contain the endothelial cell type RAEC and those that contained the endothelial cell type HUVEC. RAEC are used in this circumstance to help compare the triculture spheroid with the rat aortic ring assay. HUVEC are used in this circumstance to help connect the vasculature of the spheroid with that of the cell coated tube. In the future, triculture spheroids should contain all human cells in order to not only connect the vasculature of the spheroid with the cell coated tube, but provide an in vitro human cell assay alternative to the rat aortic ring assay.

In the rat aortic ring assay, a rat aorta is exposed to a vehicle and the length or area of the vascular sprouting is measured. In order to validate our model, vascular sprouting is also measured after exposure to a vehicle. In this case, our model is the triculture spheroid on Matrigel, and our vehicle are the drugs sorafenib and doxorubicin. As shown by Figure. 4.8, sprouts are seen emerging from the spheroid and stain for CD31 confirming the sprouts as endothelial in origin. However, no negative control was performed to determine whether these sprouts autofluoresce for color green as a sign of CD31 expression. In our model it is assumed that the vascular sprouts are the product of endothelial remodeling to form stalk and tip cells, rather than fibroblasts expanding. In order to determine whether these sprouts are endothelial or fibroblast cells, a negative control should have been performed in which heterospheroids are incubated on Matrigel to determine if similar sprouting can be seen. Given that the fibroblasts have been treated with mitomycin C to arrest growth and that vascular sprouts can be seen stained for CD31 as evident by Figure 4.8, it can be assumed that vascular sprouts are the product of endothelial cell remodeling. In the future, to further verify the identity of these sprouts, GFP-HUVEC can be used and if green fluorescence is witnessed in the region of the sprouts, prove the presence of endothelial cells.

When RAEC triculture spheroids are exposed to doxorubicin and sorafenib, the vascular sprouts in the vehicle conditions decrease, while the control condition continues to increase. Comparing the drug efficiency based on vascular sprouts shows that doxorubicin showed a greater decrease in vascular sprouting compared to sorafenib. This is contrary to what is expected as sorafenib is typified as an anti-angiogenic drug and, thus, specifically acts on the vasculature, whereas doxorubicin is typified as a cytotoxic drug. Furthermore, in animal models, doxorubicin is shown to have no effect on the vasculature

of orthotopic and subcutaneous human xenografts. [142] However, sorafenib acts mainly on the vasculature by affecting blocking VEGF and PDGF receptors, and affects angiogenesis, the formation of new vessels from pre-existing vessels. Sorafenib is not a vascular disrupting drug and therefore does not destroy the pre-existing vasculature. Doxorubicin by contrast is a cytotoxic drug and would destroy the pre-existing vasculature, as well as other cells. As to why doxorubicin seems to be effective in this in vitro model, but seems to have no effect in the animal model, can be explained in terms of tumor drug delivery. As mentioned previously the tumor vasculature is tortuous and as such it is difficult to effectively deliver drugs to the tumor and for that matter the vasculature itself. Our model does not have any barrier to prevent the doxorubicin from affecting the vascular sprouts, and as such the effective concentration of doxorubicin is much higher. Similarly the rat aortic ring assay does not have any such barrier either and so our model is therefore no better or worse in that regard. A simple solution to this dissimilarity would be to add a second layer of gel to serve as a barrier and, thus, lower the effective concentration of doxorubicin.

### 4.4.3 Anastomosis

Anastomosis is the ideal condition to meet the requirement of Aim 3 as we seek to join the potential vasculature within the spheroids with the cell coated fiber/tube carrying the drug in question. HUVEC spheroids are incubated on Matrigel with either a cell coated fiber or tube, and show the hallmarks of anastomosis. In Figure 4.11 and Figure 4.12, both the spheroids and the fiber/tube are able to form vascular sprouts, though not in any specific direction as evident by the “sun” like formation of sprouts around the spheroids. Eventually, over the course of 7 days, vascular sprouts will continue growing until they

meet each other as evident in Figure 4.11 C). Upon closer inspection at 20x magnification on day 6 as shown by Figure 4.12 B), the vascular sprouts from two different sources will interact with one another, resulting in the anastomosis of the spheroid to the cell coated fiber/tube. However, due to either a lack of pericytes and/or flow, no lumen is witnessed to form inside this vasculature. In the future, these properties need to be included.

A manner in which this model may differ from in vivo conditions is the origin of the vasculature within the liver cancer. In this model, the liver cancer is modeled by the triculture HUVEC spheroids and the origin of the vasculature within this model of the liver cancer is HUVEC cells that originate from the cell media of the hanging drop. This arrangement does not recapitulate the most common origin narrative of the tumor vasculature. Briefly, tumors grow to a size such that oxygen is no longer able to diffuse properly, resulting in hypoxia and the upregulation of pro-angiogenic factors which causes vascular sprouting from a local blood vessel to restore oxia. Hence, the vasculature's origin is from outside the liver cancer and this seems to have been proven by Ghanekar et al. in which a male human cancer xenograft is implanted into a female rat. [143] The vasculature from the xenograft positively stains for rat CD31 and not only that, fluoresces for female chromosomes, showing the origin of the vasculature is from the rat, or outside the cancer. The local blood vessel in our model is the cell coated tube which should therefore provide the vasculature for the spheroid, however, due to the limited lifespan of an in vitro model it may not be possible for this to occur. The process of cancer vascularization takes years in human beings and weeks in the rat. Therefore, in order to speed up the process, HUVEC cells are included into the spheroids.

Although, the local blood vessel narrative is the most widely held narrative regarding vascular origins, there may be alternative narratives involving cancer stem cells and bone marrow endothelial progenitor cells. In the cancer stem cells/tumor progenitor cell narrative, cancer stem cells/tumor progenitor cells, stem cells present within the tumor can differentiate into endothelial cells. [144, 145] Similarly, in the bone marrow endothelial progenitor cells narrative, bone marrow derived endothelial progenitor cells travel through the blood stream and can colonize in the tumor where they differentiate into the endothelial cells. [146, 147] Based on these alternative narratives, it may be possible to justify our model.

### 4.4.4 Migration

Migration is not an ideal condition to meet the requirement of Aim 3 as a vasculature is not formed between the spheroid and fiber/tube as would be formed between the solid tumor and the blood vessel in vivo. HUVEC spheroids are incubated on Matrigel with either a cell coated fiber or tube, and show the hallmarks of migration. In Figure 4.13 and Figure 4.14, the spheroids and the cell coated tube do not form as many vascular sprouts as the anastomosis condition, rather the spheroids migrate toward the cell coated fiber or tube over the course of several days. Migration can be explained by the presence of fibroblasts within the spheroids and endothelial cell coated on the tube. Fibroblasts migrate toward sources of VEGF and endothelial cells provide a source of VEGF. Thus, the fibroblasts surrounding the spheroid may cause the entirety of the spheroid to migrate toward the endothelial cells on the cell coated tube. Similar phenomena are witnessed in transwell membranes in which the membranes coated with VEGF and/or endothelial cells. [148]

Altering the stiffness of the gel in which spheroids are embedded may prevent migration. Addition of collagen gel or other ECM analogue would increase stiffness and increase of hydrogel stiffness is known to prevent migration in other spheroid cultures. [149] However, a difficulty in manipulating stiffness of Matrigel, is that the concentration of protein within the Matrigel is unknown and differs amongst manufacturers and batches.

### 4.4.5 Fluorescent Injection

Fluoresecent FITC-dextran and doxorubicin are injected into a model containing HUVEC triculture spheroids and RAEC cell coated tubes incubated on Matrigel for 7 days, and serve as proxies of anti-angiogenic drugs entering into the model. The results show the capricious nature of the model. In the FITC-dextran images in Figure 4.15 C), green fluorescence can be seen to enter the vascular sprouts, proving the existence of a nascent lumen. However, in the doxorubicin images in Figure 4.16 C), none of the vascular sprouts have red fluorescence within. Similarly, in the doxorubicin images, red fluorescence can be seen in the area encompassing the spheroid, but in FITC dextran images, green fluorescence cannot be seen in the area encompassing the spheroid. Neither FITC dextran, nor doxorubicin are specific dyeing agents and so there is no more reason why one should be seen in a particular site versus the other. The images testify to the capricious nature of the model, in that sometimes vascular sprouts will form a lumen allowing FITC-dextran inside, while sometimes a spheroid will have vascularized allowing doxorubicin inside. Nevertheless, that these fluorescent compounds are able to enter into the vascular sprouts and spheroid show some success for the model in that a drug could enter through the vascular sprouts and that a drug could enter into the spheroid, though separately. Ideally, the fluorescent compound acting as a proxy for a drug should have entered through the

vascular sprout and then into the spheroid. Overall, the results of this experiment, confirm our hypothesis as the fluorescent compound, acting as the anti-cancer drug, is successfully transported from the cell coated tube, acting as the blood vessel, into the spheroid, acting as the spheroid.

# CHAPTER 5

# CONCLUSION

The purpose of this study is to develop an in vitro model of liver cancer that recapitulates aspects of cancer in vivo as a platform to anti-cancer drugs. To accomplish this goal, the study is divided into three different aims.

The first aim is to develop spheroids as an anti-cancer drug platform. To this end homospheroids containing HepG2 cells are developed using the hanging drop method. Such a culture is able to maintain cell viability of the HepG2 cells. When homospheroids are exposed to the anti-cancer drug doxorubicin, the culture shows a greater resistance to the drug than a 2D monolayer, similar to resistance expected in vivo. When spheroids are cultured with HepG2 and fibroblast cells together as heterospheroids, they show a greater resistance to doxorubicin than homospheroids without collagen gel. When both types of spheroids are cultured in collagen gel, they both show high viability following drug exposure, but no significant difference. The difference between homospheroids and heterospheroids with or without collagen gel shows that the collagen gel may mask any of the effect of the fibroblast toward drug resistance. Similarly, cytochrome p450 activity is preserved in collagen gel after exposure to the anti-cancer drug as compared in the non-gel condition. A question not answered in this study is whether the collagen gel as a physical barrier or as a substrate is responsible for drug resistance/increased viability.

The second aim of our study is developing chitosan based microfiber scaffolds as a tissue engineered blood vessel to promote angiogenesis. The material chitosan is not conducive to binding cells, so must be chemically modified to allow cell adhesion. To this

end, chitosan is crosslinked with EDC/NHS to heparin and adsorbed with fibronectin. To test this, chitosan film is first modified. To confirm heparin's binding to chitosan, toluidine blue staining and FTIR are used to analyze heparin crosslinked chitosan films, and shows its presence. A cell adhesion study using phase imagery, Actin/DAPI staining, and Alamar blue assay shows that chitosan film crosslinked with EDC/NHS to heparin and adsorbed with fibronectin is able to promote cell adhesion and proliferation. Similar modification to a chitosan wetspun fiber shows similar results in that cells are able to adhere to the construct as shown by phase imagery and Actin/DAPI staining. A chitosan wetspun fiber crosslinked with EDC/NHS to heparin and adsorbed with VEGF is immunostained with anti-Flk-1 and shows that the fiber is able to bind VEGF. VEGF is a critical growth factor in angiogenesis, but is expensive, and so fibronectin is used instead for the present study. For future studies, the use of VEGF would be used to promote angiogenesis as it aids in the formation of vascular sprouts. In order to hollow out a lumen within the construct to allow distribution of anti-cancer drugs similar to distribution of anti-cancer drugs in vivo, a combination of acidic and enzymatic degradation is employed. Non-cell coated and trypan blue stained fibers are exposed to acidic and enzymatic degradation conditions as a preliminary to cell coated fiber experiments and shows that the fiber does not degrade evenly. When cell coated fibers are exposed to acids and enzymes, swelling/bursting occurs which breaks the construct. Due to the inability to degrade chitosan fiber without destroying the cell construct as a result of present circumstance, an alternative method is proposed using chitosan electrospun mats to form tubes. Chitosan electrospun mats are manufactured by rolling the mat around a needle followed by neutralizing, washing, drying, and removal to form a tube. The tube is treated similarly to the fiber and shows the ability to maintain cell

viability as shown by live and Hoechst staining. Furthermore, when embedded in Matrigel, the tube is able to promote vascular sprouting and angiogenesis.

The third aim of our study is to construct a vascularized liver cancer model using spheroids and cell coated tube. As such triculture spheroids and cell coated tube are embedded on Matrigel. Triculture spheroids, combining HepG2, fibroblasts, and endothelial cells, embedded on Matrigel result in vascular sprouts which can be used to help form a physical connection between the spheroid and the tube. Besides this, triculture spheroids on Matrigel can be used as an alternative to the aortic ring assay. Vascular sprouts emanating from the triculture spheroid can be used as a measure of how anti-cancer drugs affect angiogenesis. The anti-cancer drugs doxorubicin and sorafenib are both able to halt vascular sprouting growth and/or reverse it, similar to the aortic ring assay.

Spheroids are either observed to anastomize, in which vascular sprouts from both the spheroids and tube interact with one another, or migrate, in which the spheroid migrates onto the tube. When fluorescent compounds FITC dextran and doxorubicin are injected into the system, the fluorescent compounds are shown in some of the vascular sprouts and within the spheroid region showing the presence of a nascent lumen.

Overall, the model shows varying degrees of success as a drug cancer model by showing greater resistance similar to cancer in vivo. Aim 1 shows success as a model in that spheroids with different cell types and in collagen gel are able to resist the anti-cancer drug. Homopsheroids are able to resist drugs better than 2D cultures due to their geometry and gel system. Both homospheroids and heterospheroids are shown to promote drug resistance in collagen gels.

For Aim 2, chitosan wetspun fibers require alternative methods to form a tissue engineered blood vessel with a lumen, however, at present chitosan electrospun tubes show success in being a platform for cells as well as containing a lumen. Chitosan film is shown to be chemically modified with EDC/NHS to heparin and adsorbed with fibronectin and able to adhere and proliferate cells. The chitosan wetspun fiber shows similar results. When the fiber is degraded to form a lumen, the fiber is shown to swell and ultimately, cause bursting of the cells coated on the construct. Unable to form a tissue engineered blood vessel using the chitosan wetspun fiber, an alternative chitosan electospun mat tube is used instead. Processed similarly to the chitosan wetspun fiber, electrospun tubes are able to adhere cells and form vascular sprouts on Matrigel.

For Aim 3, spheroids and cell coated tube are combined together on Matrigel in order to form a vascularized liver model. Triculture spheroids exhibit vascular sprouts which after exposure to anti-cancer drugs, show retarded growth, similar to that of the aortic ring assay. Triculture spheroids on Matrigel with cell coated tubes, show anastomosis and migration. Anastomosis between the cells coating the tube and the spheroid is the desired outcome in order to form a vascularized liver model as it mimics angiogenesis in vivo in which blood vessels vascularize the tumor. Migration is an undesired event as it does not mimic angiogenesis and better models the phenomena of vascular co-option. Fluorescent compounds are injected into the model to illuminate the path by which these drugs travel through the model, as well as expose any open lumens. When fluorescent compounds FITC-dextran and doxorubicin are injected into the model, they show the presence of nascent lumen in the vascular sprouts and presence in the spheroid showing the possibility of lumens within the spheroid.

For future studies, further characterization studies can be employed on the vascularized cancer model to determine the mechanism by which combination therapy of sorafenib and doxorubicin is able to prolong overall survival in patients. Various theories exist as to why combination therapy works. The obvious theory is that combination therapy simply works because of the additive effects of multiple types of anti-cancer drugs. However, especially with anti-angiogenic drugs, the anti-angiogenic drugs may be able to restore the vasculature in what is known as vascular normalization.[150] As previously mentioned, blood vessels within cancer are leaky, as a result the concentration of anti-cancer drugs inside the cancer decreases. One of the reasons for the leaky vessels is the overabundance of VEGF. Anti-angiogenic drugs affect VEGF and, thus, may result the restoration/normalization of the vessels such that anti-cancer drugs more readily enter into the tumor. To characterize this in the model, the model is exposed to sorafenib and the vasculature that exists between the spheroids and tube is monitored following the injection of doxorubicin. The intensity of the red fluorescence representing the doxorubicin concentration within the vasculature is then used to determine whether the sorafenib has caused vascular normalization.

Overall, the vascularized liver model shows limited success. The vascularized model is able to form connections between the spheroid and the cell coated tube which could be used for the transport of anti-angiogenic drugs such as sorafenib into the spheroid, similar to what is expected in cancer when the drug is transported into the tumor. However, the advent of migration in the model confounds this expectation. Of course, each spheroid represents a single tumor and the varied fates demonstrated by each of the spheroid of either anastomizing, migrating, or remaining still, may make the model representative of

the fate of tumors in the entire body. Although, this would make the model biomimetic, it would be troublesome to study the effects of the co-administration of doxorubicin and sorafenib as the model is not consistent throughout.

## REFERENCES

[1] Boyle P, Levin B. World Cancer Report 2008. Lyon, France. WHO Press; 2008.

[2] Folkman J. Angiogenesis and apoptosis. Seminars in Cancer Biology. 2003;13:159-67.

[3] Stevenson CE, Nagahashi M, Ramachandran S, Yamada A, Bear HD, Takabe K. Bevacizumab and breast cancer: what does the future hold? Future Oncology. 2012;8:403-14.

[4] Llovet JM, Bruix J. Systematic review of randomized trials for unresectable hepatocellular carcinoma: Chemoembolization improves survival. Hepatology. 2003;37:429-42.

[5] Keating GM, Santoro A. Sorafenib: a review of its use in advanced hepatocellular carcinoma. Drugs. 2009;69:223-40.

[6] Gauthier A, Ho M. Role of sorafenib in the treatment of advanced hepatocellular carcinoma: An update. Hepatology Research. 2012;43:147-54.

[7] Faivre S, Raymond E, Boucher E, Douillard J, Lim HY, Kim JS, et al. Safety and efficacy of sunitinib in patients with advanced hepatocellular carcinoma: an open-label, multicentre, phase II study. Lancet Oncology. 2009;10:794-800.

[8] Frenette C, Gish R. Targeted systemic therapies for hepatocellular carcinoma: clinical perspectives, challenges and implications. World Journal of Gastroenterology. 2012;18:498-506.

[9] Kerbel RS. Reappraising antiangiogenic therapy for breast cancer. Breast. 2011;20 Supplemental 3:S56-60.

[10] Selvakumaran M, Yao KS, Feldman MD, O'Dwyer PJ. Antitumor effect of the angiogenesis inhibitor bevacizumab is dependent on susceptibility of tumors to hypoxia-induced apoptosis. Biochemical Pharmacology. 2008;75:627-38.

[11] Rohwer N, Cramer T. Hypoxia-mediated drug resistance: novel insights on the functional interaction of HIFs and cell death pathways. Drug Resistance Updates. 2011;14:191-201.

[12] Bergers G, Hanahan D. Modes of resistance to anti-angiogenic therapy. Nature Reviews Cancer. 2008;8:592-603.

[13] Rapisarda A, Melillo G. Role of the hypoxic tumor microenvironment in the resistance to anti-angiogenic therapies. Drug Resistance Updates. 2009;12:74-80.

[14] Pritchard JF, Jurima-Romet M, Reimer ML, Mortimer E, Rolfe B, Cayen MN. Making better drugs: Decision gates in non-clinical drug development. Nature Reviews Drug Discovery. 2003;2:542-53.

[15] DiMasi JA, Hansen RW, Grabowski HG. The price of innovation: new estimates of drug development costs. Journal of Health Economics. 2003;22:151-85.

[16] Marsden MD, Zack JA. Studies of retroviral infection in humanized mice. Virology. 2015;479-480:297-309.

[17] Hirschhaeuser F, Menne H, Dittfeld C, West J, Mueller-Klieser W, Kunz-Schughart LA. Multicellular tumor spheroids: an underestimated tool is catching up again. Journal of Biotechnology. 2010;148:3-15.

[18] Brophy CM, Luebke-Wheeler JL, Amiot BP, Khan H, Remmel RP, Rinaldo P, et al. Rat hepatocyte spheroids formed by rocked technique maintain differentiated hepatocyte gene expression and function. Hepatology. 2009;49:578-86.

[19] Verma P, Verma V, Ray P, Ray AR. Formation and characterization of three dimensional human hepatocyte cell line spheroids on chitosan matrix for in vitro tissue engineering applications. In Vitro Cellular and Developmental Biology Animal. 2007;43:328-37.

[20] Luckert C, Schulz C, Lehmann N, Thomas M, Hofmann U, Hammad S, et al. Comparative analysis of 3D culture methods on human HepG2 cells. Archives of Toxicology. 2016.

[21] Lu HF, Chua KN, Zhang PC, Lim WS, Ramakrishna S, Leong KW, et al. Three-dimensional co-culture of rat hepatocyte spheroids and NIH/3T3 fibroblasts enhances hepatocyte functional maintenance. Acta Biomaterialia. 2005;1:399-410.

[22] Bhatia SN, Balis UJ, Yarmush ML, Toner M. Effect of cell-cell interactions in preservation of cellular phenotype: cocultivation of hepatocytes and nonparenchymal cells. FASEB Journal. 1999;13:1883-900.

[23] Bhandari RN, Riccalton LA, Lewis AL, Fry JR, Hammond AH, Tendler SJ, et al. Liver tissue engineering: a role for co-culture systems in modifying hepatocyte function and viability. Tissue Engineering. 2001;7:345-57.

[24] Chia SM, Lin PC, Yu H. TGF-beta1 regulation in hepatocyte-NIH3T3 co-culture is important for the enhanced hepatocyte function in 3D microenvironment. Biotechnology and Bioengineering. 2005;89:565-73.

[25] Seo SJ, Kim IY, Choi YJ, Akaike T, Cho CS. Enhanced liver functions of hepatocytes cocultured with NIH 3T3 in the alginate/galactosylated chitosan scaffold. Biomaterials. 2006;27:1487-95.

[26] Nishikawa M, Kojima N, Komori K, Yamamoto T, Fujii T, Sakai Y. Enhanced maintenance and functions of rat hepatocytes induced by combination of on-site oxygenation and coculture with fibroblasts. Journal of Biotechnology. 2008;133:253-60.

[27] Jodon de Villeroche V, Brouty-Boye D. Establishment and characterization of atypical fibroblasts from human adult liver contributing to hepatocyte cord-like arrangement. Cell Biology International. 2008;32:605-14.

[28] Leite SB, Teixeira AP, Miranda JP, Tostoes RM, Clemente JJ, Sousa MF, et al. Merging bioreactor technology with 3D hepatocyte-fibroblast culturing approaches: Improved in vitro models for toxicological applications. Toxicology In Vitro. 2011;25:825-32.

[29] Kalluri R, Zeisberg M. Fibroblasts in cancer. Nature Reviews Cancer. 2006;6:392-401.

[30] Tyan SW, Kuo WH, Huang CK, Pan CC, Shew JY, Chang KJ, et al. Breast cancer cells induce cancer-associated fibroblasts to secrete hepatocyte growth factor to enhance breast tumorigenesis. PloS One. 2011;6:e15313.

[31] Paraiso KH, Smalley KS. Fibroblast-mediated drug resistance in cancer. Biochemical Pharmacology. 2013;85:1033-41.

[32] Shiga K, Hara M, Nagasaki T, Sato T, Takahashi H, Takeyama H. Cancer-Associated Fibroblasts: Their Characteristics and Their Roles in Tumor Growth. Cancers. 2015;7:2443-58.

[33] Kendall RT, Feghali-Bostwick CA. Fibroblasts in fibrosis: novel roles and mediators. Frontiers in Pharmacology. 2014;5:123.

[34] Junttila MR, de Sauvage FJ. Influence of tumour micro-environment heterogeneity on therapeutic response. Nature. 2013;501:346-54.

[35] Dang TT, Prechtl AM, Pearson GW. Breast cancer subtype-specific interactions with the microenvironment dictate mechanisms of invasion. Cancer Research. 2011;71:6857-66.

[36] Olsen CJ, Moreira J, Lukanidin EM, Ambartsumian NS. Human mammary fibroblasts stimulate invasion of breast cancer cells in a three-dimensional culture and increase stroma development in mouse xenografts. BMC Cancer. 2010;10:444.

[37] Adair TH, Montani JP. Angiogenesis. San Rafael, CA Morgan and Claypool Life Sciences; 2010.

[38] Song HH, Park KM, Gerecht S. Hydrogels to model 3D in vitro microenvironment of tumor vascularization. Advanced Drug Delivery Reviews. 2014;79-80:19-29.

[39] Leung M, Kievit FM, Florczyk SJ, Veiseh O, Wu J, Park JO, et al. Chitosan-alginate scaffold culture system for hepatocellular carcinoma increases malignancy and drug resistance. Pharmaceutical Research. 2010;27:1939-48.

[40] Lan SF, Safiejko-Mroczka B, Starly B. Long-term cultivation of HepG2 liver cells encapsulated in alginate hydrogels: a study of cell viability, morphology and drug metabolism. Toxicology in Vitro. 2010;24:1314-23.

[41] Hou YT, Ijima H, Matsumoto S, Kubo T, Takei T, Sakai S, et al. Effect of a hepatocyte growth factor/heparin-immobilized collagen system on albumin synthesis and spheroid formation by hepatocytes. Journal of Bioscience and Bioengineering. 2010;110:208-16.

[42] Charoen KM, Fallica B, Colson YL, Zaman MH, Grinstaff MW. Embedded multicellular spheroids as a biomimetic 3D cancer model for evaluating drug and drug-device combinations. Biomaterials. 2014;35:2264-71.

[43] Liang Y, Jeong J, DeVolder RJ, Cha C, Wang F, Tong YW, et al. A cell-instructive hydrogel to regulate malignancy of 3D tumor spheroids with matrix rigidity. Biomaterials. 2011;32:9308-15.

[44] Schrader J, Gordon-Walker TT, Aucott RL, van Deemter M, Quaas A, Walsh S, et al. Matrix stiffness modulates proliferation, chemotherapeutic response, and dormancy in hepatocellular carcinoma cells. Hepatology. 2011;53:1192-205.

[45] Tong WH, Fang Y, Yan J, Hong X, Hari Singh N, Wang SR, et al. Constrained spheroids for prolonged hepatocyte culture. Biomaterials. 2016;80:106-20.

[46] Nakamura K, Mizutani R, Sanbe A, Enosawa S, Kasahara M, Nakagawa A, et al. Evaluation of drug toxicity with hepatocytes cultured in a micro-space cell culture system. Journal of Bioscience and Bioengineering. 2011;111:78-84.

[47] Yip D, Cho CH. A multicellular 3D heterospheroid model of liver tumor and stromal cells in collagen gel for anti-cancer drug testing. Biochemical and Biophysical Research Communications. 2013;433:327-32.

[48] Cao L, Zhou Y, Zhai B, Liao J, Xu W, Zhang R, et al. Sphere-forming cell subpopulations with cancer stem cell properties in human hepatoma cell lines. BMC Gastroenterology. 2011;11:71.

[49] Uchida Y, Tanaka S, Aihara A, Adikrisna R, Yoshitake K, Matsumura S, et al. Analogy between sphere forming ability and stemness of human hepatoma cells. Oncology Reports. 2010;24:1147-51.

[50] Zhang L, Jiao M, Li L, Wu D, Wu K, Li X, et al. Tumorspheres derived from prostate cancer cells possess chemoresistant and cancer stem cell properties. Journal of Cancer Research and Clinical Oncology. 2012;138:675-86.

[51] Elliott NT, Yuan F. A review of three-dimensional in vitro tissue models for drug discovery and transport studies. Journal of Pharmaceutical Sciences. 2011;100:59-74.

[52] Materne EM, Ramme AP, Terrasso AP, Serra M, Alves PM, Brito C, et al. A multi-organ chip co-culture of neurospheres and liver equivalents for long-term substance testing. Journal of Biotechnology. 2015;205:36-46.

[53] Leite SB, Roosens T, El Taghdouini A, Mannaerts I, Smout AJ, Najimi M, et al. Novel human hepatic organoid model enables testing of drug-induced liver fibrosis in vitro. Biomaterials. 2016;78:1-10.

[54] Weiswald LB, Bellet D, Dangles-Marie V. Spherical cancer models in tumor biology. Neoplasia. 2015;17:1-15.

[55] Aboussekhra A. Role of cancer-associated fibroblasts in breast cancer development and prognosis. The International Journal of Developmental Biology. 2011;55:841-9.

[56] Bhowmick NA, Neilson EG, Moses HL. Stromal fibroblasts in cancer initiation and progression. Nature. 2004;432:332-7.

[57] Shimoda M, Mellody KT, Orimo A. Carcinoma-associated fibroblasts are a rate-limiting determinant for tumour progression. Seminars in Cell and Developmental Biology. 2010;21:19-25.

[58] Miszczuk GS, Barosso IR, Zucchetti AE, Boaglio AC, Pellegrino JM, Sanchez Pozzi EJ, et al. Sandwich-cultured rat hepatocytes as an in vitro model to study canalicular transport alterations in cholestasis. Archives of Toxicology. 2015;89:979-90.

[59] Ramaiahgari SC, den Braver MW, Herpers B, Terpstra V, Commandeur JN, van de Water B, et al. A 3D in vitro model of differentiated HepG2 cell spheroids with improved liver-like properties for repeated dose high-throughput toxicity studies. Archives of Toxicology. 2014;88:1083-95.

[60] Reif R, Karlsson J, Gunther G, Beattie L, Wrangborg D, Hammad S, et al. Bile canalicular dynamics in hepatocyte sandwich cultures. Archives of Toxicology. 2015;89:1861-70.

[61] Swift B, Pfeifer ND, Brouwer KL. Sandwich-cultured hepatocytes: an in vitro model to evaluate hepatobiliary transporter-based drug interactions and hepatotoxicity. Drug Metabolism Reviews. 2010;42:446-71.

[62] Sun HC, Tang ZY. Angiogenesis in hepatocellular carcinoma: the retrospectives and perspectives. Journal of Cancer Research and Clinical Oncology. 2004;130:307-19.

[63] Semela D, Dufour JF. Angiogenesis and hepatocellular carcinoma. Journal of Hepatology. 2004;41:864-80.

[64] Goel S, Wong AH, Jain RK. Vascular normalization as a therapeutic strategy for malignant and nonmalignant disease. Cold Spring Harbor Perspectives in Medicine. 2012;2:a006486.

[65] Lee JS, Semela D, Iredale J, Shah VH. Sinusoidal remodeling and angiogenesis: a new function for the liver-specific pericyte? Hepatology. 2007;45:817-25.

[66] Morikawa S, Baluk P, Kaidoh T, Haskell A, Jain RK, McDonald DM. Abnormalities in pericytes on blood vessels and endothelial sprouts in tumors. The American Journal of Pathology. 2002;160:985-1000.

[67] Nakatsu MN, Sainson RC, Aoto JN, Taylor KL, Aitkenhead M, Perez-del-Pulgar S, et al. Angiogenic sprouting and capillary lumen formation modeled by human umbilical vein endothelial cells (HUVEC) in fibrin gels: the role of fibroblasts and Angiopoietin-1. Microvascular Research. 2003;66:102-12.

[68] Newman AC, Nakatsu MN, Chou W, Gershon PD, Hughes CC. The requirement for fibroblasts in angiogenesis: fibroblast-derived matrix proteins are essential for endothelial cell lumen formation. Molecular Biology of the Cell. 2011;22:3791-800.

[69] He Q, Ao Q, Gong Y, Zhang X. Preparation of chitosan films using different neutralizing solutions to improve endothelial cell compatibility. Journal of Materials Science: Materials in Medicine. 2011;22:2791-802.

[70] Chen L, He Z, Chen B, Yang M, Zhao Y, Sun W, et al. Loading of VEGF to the heparin cross-linked demineralized bone matrix improves vascularization of the scaffold. Journal of Materials Science: Materials in Medicine. 2010;21:309-17.

[71] Singh S, Wu BM, Dunn JC. The enhancement of VEGF-mediated angiogenesis by polycaprolactone scaffolds with surface cross-linked heparin. Biomaterials. 2011;32:2059-69.

[72] Wu JM, Xu YY, Li ZH, Yuan XY, Wang PF, Zhang XZ, et al. Heparin-functionalized collagen matrices with controlled release of basic fibroblast growth factor. Journal of Materials Science: Materials in Medicine. 2011;22:107-14.

[73] Zhou M, Liu Z, Wei Z, Liu C, Qiao T, Ran F, et al. Development and validation of small-diameter vascular tissue from a decellularized scaffold coated with heparin and vascular endothelial growth factor. Artificial Organs. 2009;33:230-9.

[74] Cabric S, Sanchez J, Johansson U, Larsson R, Nilsson B, Korsgren O, et al. Anchoring of vascular endothelial growth factor to surface-immobilized heparin on pancreatic islets: implications for stimulating islet angiogenesis. Tissue Engineering Part A. 2010;16:961-70.

[75] Hu X, Neoh KG, Zhang J, Kang ET, Wang W. Immobilization strategy for optimizing VEGF's concurrent bioactivity towards endothelial cells and osteoblasts on implant surfaces. Biomaterials. 2012;33:8082-93.

[76] Lin S. Low molecular weight chitosan prepared with the aid of celllulase, lysozyme, and chitinase: Characterisation and anti-bacterial activity. Food Chemistry. 2009;116:47-53.

[77] Yang ZF, Poon RT. Vascular changes in hepatocellular carcinoma. Anatomical Record. 2008;291:721-34.

[78] Zhu AX, Duda DG, Sahani DV, Jain RK. HCC and angiogenesis: possible targets and future directions. Nature Reviews Clinical Oncology. 2011;8:292-301.

[79] Ribatti D, Vacca A, Nico B, Sansonno D, Dammacco F. Angiogenesis and anti-angiogenesis in hepatocellular carcinoma. Cancer Treatment Reviews. 2006;32:437-44.

[80] Wang J, Wan Y, Huang Y. Immobilisation of heparin on bacterial cellulose-chitosan nano-fibres surfaces via the cross-linking technique. IET Nanobiotechnology. 2012;6:52-7.

[81] Chupa JM, Foster AM, Sumner SR, Madihally SV, Matthew HW. Vascular cell responses to polysaccharide materials: in vitro and in vivo evaluations. Biomaterials. 2000;21:2315-22.

[82] Kean T, Thanou M. Biodegradation, biodistribution and toxicity of chitosan. Advanced Drug Delivery Reviews. 2010;62:3-11.

[83] Aranaz I. Functionalization of Chitin and Chitosan. Current Chemical Biology. 2010;3:203-30.

[84] Chen L, Li B, Xiao X, Meng Q, Li W, Yu Q, et al. Preparation and evaluation of an Arg-Gly-Asp-modified chitosan/hydroxyapatite scaffold for application in bone tissue engineering. Molecular Medicine Reports. 2015;12:7263-70.

[85] Hansson A, Hashom N, Falson F, Rousselle P, Jordan O, Borchard G. In vitro evaluation of an RGD-functionalized chitosan derivative for enhanced cell adhesion. Carbohydrate Polymers. 2012;90:1494-500.

[86] Ho MH, Wang DM, Hsieh HJ, Liu HC, Hsien TY, Lai JY, et al. Preparation and characterization of RGD-immobilized chitosan scaffolds. Biomaterials. 2005;26:3197-206.

[87] Kuwabara F, Narita Y, Yamawaki-Ogata A, Kanie K, Kato R, Satake M, et al. Novel small-caliber vascular grafts with trimeric Peptide for acceleration of endothelialization. The Annals of Thoracic Surgery. 2012;93:156-63.

[88] Astrof S, Hynes RO. Fibronectins in vascular morphogenesis. Angiogenesis. 2009;12:165-75.

[89] Han H, Ao Q, Chen G, Wang S, Zuo H. A novel basic fibroblast growth factor delivery system fabricated with heparin-incorporated fibrin-fibronectin matrices for repairing rat sciatic nerve disruptions. Biotechnology Letters. 2010;32:585-91.

[90] Hussain A, Collins G, Yip D, Cho CH. Functional 3-D cardiac co-culture model using bioactive chitosan nanofiber scaffolds. Biotechnology and Bioengineering. 2013;110:637-47.

[91] Yang Z, Tu Q, Wang J, Huang N. The role of heparin binding surfaces in the direction of endothelial and smooth muscle cell fate and re-endothelialization. Biomaterials. 2012;33:6615-25.

[92] Cozzolino AM, Noce V, Battistelli C, Marchetti A, Grassi G, Cicchini C, et al. Modulating the Substrate Stiffness to Manipulate Differentiation of Resident Liver Stem Cells and to Improve the Differentiation State of Hepatocytes. Stem Cells International. 2016;2016:5481493.

[93] Canver AC, Ngo O, Urbano RL, Clyne AM. Endothelial directed collective migration depends on substrate stiffness via localized myosin contractility and cell-matrix interactions. Journal of Biomechanics. 2015.

[94] Santos L, Fuhrmann G, Juenet M, Amdursky N, Horejs CM, Campagnolo P, et al. Extracellular Stiffness Modulates the Expression of Functional Proteins and Growth Factors in Endothelial Cells. Advanced Healthcare Materials. 2015.

[95] Birukova AA, Tian X, Cokic I, Beckham Y, Gardel ML, Birukov KG. Endothelial barrier disruption and recovery is controlled by substrate stiffness. Microvascular Research. 2013;87:50-7.

[96] Huveneers S, Daemen MJ, Hordijk PL. Between Rho(k) and a hard place: the relation between vessel wall stiffness, endothelial contractility, and cardiovascular disease. Circulation Research. 2015;116:895-908.

[97] Lesman A, Rosenfeld D, Landau S, Levenberg S. Mechanical regulation of vascular network formation in engineered matrices. Advanced Drug Delivery Reviews. 2016;96:176-82.

[98] Mazzone M, Dettori D, Leite de Oliveira R, Loges S, Schmidt T, Jonckx B, et al. Heterozygous deficiency of PHD2 restores tumor oxygenation and inhibits metastasis via endothelial normalization. Cell. 2009;136:839-51.

[99] Xia W, Liu P, Liu J. Advance in chitosan hydrolysis by non-specific cellulases. Bioresource Technology. 2008;99:6751-62.

[100] Hsiao AY, Okitsu T, Onoe H, Kiyosawa M, Teramae H, Iwanaga S, et al. Smooth muscle-like tissue constructs with circumferentially oriented cells formed by the cell fiber technology. PloS One. 2015;10:e0119010.

[101] Kim J, Chung M, Kim S, Jo DH, Kim JH, Jeon NL. Engineering of a Biomimetic Pericyte-Covered 3D Microvascular Network. PloS One. 2015;10:e0133880.

[102] Lee VK, Kim DY, Ngo H, Lee Y, Seo L, Yoo SS, et al. Creating perfused functional vascular channels using 3D bio-printing technology. Biomaterials. 2014;35:8092-102.
[103] Lee VK, Lanzi AM, Haygan N, Yoo SS, Vincent PA, Dai G. Generation of Multi-Scale Vascular Network System within 3D Hydrogel using 3D Bio-Printing Technology. Cellular and Molecular Bioengineering. 2014;7:460-72.

[104] Price GM, Wong KH, Truslow JG, Leung AD, Acharya C, Tien J. Effect of mechanical factors on the function of engineered human blood microvessels in microfluidic collagen gels. Biomaterials. 2010;31:6182-9.

[105] Eckermann CW, Lehle K, Schmid SA, Wheatley DN, Kunz-Schughart LA. Characterization and modulation of fibroblast/endothelial cell co-cultures for the in vitro preformation of three-dimensional tubular networks. Cell Biology International. 2011;35:1097-110.

[106] Hughes CC. Endothelial-stromal interactions in angiogenesis. Current Opinion in Hematology. 2008;15:204-9.

[107] Xie B, Wang DH, Spechler SJ. Sorafenib for treatment of hepatocellular carcinoma: a systematic review. Digestive Diseases and Sciences. 2012;57:1122-9.

[108] Zhai B, Sun XY. Mechanisms of resistance to sorafenib and the corresponding strategies in hepatocellular carcinoma. World Journal of Hepatology. 2013;5:345-52.

[109] Abou-Alfa GK, Johnson P, Knox JJ, Capanu M, Davidenko I, Lacava J, et al. Doxorubicin plus sorafenib vs doxorubicin alone in patients with advanced hepatocellular carcinoma: a randomized trial. JAMA. 2010;304:2154-60.

[110] Manov I, Pollak Y, Broneshter R, Iancu TC. Inhibition of doxorubicin-induced autophagy in hepatocellular carcinoma Hep3B cells by sorafenib--the role of extracellular signal-regulated kinase counteraction. FEBS J. 2011;278:3494-507.

[111] Lee ER, Kim JY, Kang YJ, Ahn JY, Kim JH, Kim BW, et al. Interplay between PI3K/Akt and MAPK signaling pathways in DNA-damaging drug-induced apoptosis. Biochimica et Biophysica Acta. 2006;1763:958-68.

[112] Liu L, Cao Y, Chen C, Zhang X, McNabola A, Wilkie D, et al. Sorafenib blocks the RAF/MEK/ERK pathway, inhibits tumor angiogenesis, and induces tumor cell apoptosis in hepatocellular carcinoma model PLC/PRF/5. Cancer Research. 2006;66:11851-8.

[113] Severi T, van Malenstein H, Verslype C, van Pelt JF. Tumor initiation and progression in hepatocellular carcinoma: risk factors, classification, and therapeutic targets. Acta Pharmacologica Sinica. 2010;31:1409-20.

[114] Sullivan R, Graham CH. Hypoxia-driven selection of the metastatic phenotype. Cancer Metastasis Reviews. 2007;26:319-31.

[115] Harris AL. Hypoxia--a key regulatory factor in tumour growth. Nature Reviews Cancer. 2002;2:38-47.

[116] Kim KR, Moon HE, Kim KW. Hypoxia-induced angiogenesis in human hepatocellular carcinoma. Journal of Molecular Medicine. 2002;80:703-14.

[117] Semenza GL. HIF-1 and tumor progression: pathophysiology and therapeutics. Trends in Molecular Medicine. 2002;8:S62-7.

[118] Semenza GL. The hypoxic tumor microenvironment: A driving force for breast cancer progression. Biochimica et Biophysica Acta. 2016;1863:382-91.

[119] Murakami M, Zhao S, Zhao Y, Chowdhury NF, Yu W, Nishijima K, et al. Evaluation of changes in the tumor microenvironment after sorafenib therapy by sequential histology and 18F-fluoromisonidazole hypoxia imaging in renal cell carcinoma. International Journal of Oncology. 2012;41:1593-600.

[120] Bellou S, Pentheroudakis G, Murphy C, Fotsis T. Anti-angiogenesis in cancer therapy: Hercules and hydra. Cancer Letters. 2013;338:219-28.

[121] Chappell JC, Wiley DM, Bautch VL. Regulation of blood vessel sprouting. Seminars in Cell and Developmental Biology. 2011;22:1005-11.

[122] Herbert SP, Stainier DY. Molecular control of endothelial cell behaviour during blood vessel morphogenesis. Nature Reviews Molecular Cell Biology. 2011;12:551-64.

[123] Enzerink A, Rantanen V, Vaheri A. Fibroblast nemosis induces angiogenic responses of endothelial cells. Experimental Cell Research. 2010;316:826-35.

[124] Sasagawa T, Shimizu T, Yamato M, Okano T. Endothelial colony-forming cells for preparing prevascular three-dimensional cell-dense tissues using cell-sheet engineering. Journal of Tissue Engineering and Regenerative Medicine. 2013.

[125] Sorrell JM, Baber MA, Caplan AI. A self-assembled fibroblast-endothelial cell co-culture system that supports in vitro vasculogenesis by both human umbilical vein endothelial cells and human dermal microvascular endothelial cells. Cells, Tissues, Organs. 2007;186:157-68.

[126] Sukmana I, Vermette P. The effects of co-culture with fibroblasts and angiogenic growth factors on microvascular maturation and multi-cellular lumen formation in HUVEC-oriented polymer fibre constructs. Biomaterials. 2010;31:5091-9.

[127] Wenger A, Kowalewski N, Stahl A, Mehlhorn AT, Schmal H, Stark GB, et al. Development and characterization of a spheroidal coculture model of endothelial cells and fibroblasts for improving angiogenesis in tissue engineering. Cells, Tissues, Organs. 2005;181:80-8.

[128] Kim K, Ohashi K, Utoh R, Kano K, Okano T. Preserved liver-specific functions of hepatocytes in 3D co-culture with endothelial cell sheets. Biomaterials. 2012;33:1406-13.

[129] Kim Y, Rajagopalan P. 3D hepatic cultures simultaneously maintain primary hepatocyte and liver sinusoidal endothelial cell phenotypes. PloS One. 2010;5:e15456.

[130] Liu Y, Li H, Yan S, Wei J, Li X. Hepatocyte cocultures with endothelial cells and fibroblasts on micropatterned fibrous mats to promote liver-specific functions and capillary formation capabilities. Biomacromolecules. 2014;15:1044-54.

[131] Ho CT, Lin RZ, Chen RJ, Chin CK, Gong SE, Chang HY, et al. Liver-cell patterning lab chip: mimicking the morphology of liver lobule tissue. Lab on a Chip. 2013;13:3578-87.

[132] Lee D-H. Enhanced liver specific functions of endothelial cell covered hepatocyte hetero-spheroids. Biochemical Engineering Journal. 2004;20:181-7.

[133] Liu LP, Ho RL, Chen GG, Lai PB. Sorafenib inhibits hypoxia-inducible factor-1alpha synthesis: implications for antiangiogenic activity in hepatocellular carcinoma. Clinical Cancer Research. 2012;18:5662-71.

[134] Xu M, Zheng YL, Xie XY, Liang JY, Pan FS, Zheng SG, et al. Sorafenib blocks the HIF-1alpha/VEGFA pathway, inhibits tumor invasion, and induces apoptosis in hepatoma cells. DNA Cell Biology. 2014;33:275-81.

[135] Hurley JR, Balaji S, Narmoneva DA. Complex temporal regulation of capillary morphogenesis by fibroblasts. American Journal of Physiology: Cell Physiology. 2010;299:C444-53.

[136] Korn C, Augustin HG. Mechanisms of Vessel Pruning and Regression. Developmental Cell. 2015;34:5-17.

[137] Nicosia RF. The aortic ring model of angiogenesis: a quarter century of search and discovery. Journal of Cellular and Molecular Medicine. 2009;13:4113-36.

[138] Chiew GG, Fu A, Low KP, Luo KQ. Physical supports from liver cancer cells are essential for differentiation and remodeling of endothelial cells in a HepG2-HUVEC co-culture model. Scientific Reports. 2015;5:10801.

[139] Correa de Sampaio P, Auslaender D, Krubasik D, Failla AV, Skepper JN, Murphy G, et al. A heterogeneous in vitro three dimensional model of tumour-stroma interactions regulating sprouting angiogenesis. PloS One. 2012;7:e30753.

[140] Verbridge SS, Chandler EM, Fischbach C. Tissue-engineered three-dimensional tumor models to study tumor angiogenesis. Tissue Engineering Part A. 2010;16:2147-52.
[141] Lee W, Park J. The design of a heterocellular 3D architecture and its application to monitoring the behavior of cancer cells in response to the spatial distribution of endothelial cells. Advanced Materials. 2012;24:5339-44.

[142] Fung AS, Lee C, Yu M, Tannock IF. The effect of chemotherapeutic agents on tumor vasculature in subcutaneous and orthotopic human tumor xenografts. BMC Cancer. 2015;15:112.

[143] Ghanekar A, Ahmed S, Chen K, Adeyi O. Endothelial cells do not arise from tumor-initiating cells in human hepatocellular carcinoma. BMC Cancer. 2013;13:485.

[144] Bussolati B, Grange C, Camussi G. Tumor exploits alternative strategies to achieve vascularization. FASEB Journal. 2011;25:2874-82.

[145] Ricci-Vitiani L, Pallini R, Biffoni M, Todaro M, Invernici G, Cenci T, et al. Tumour vascularization via endothelial differentiation of glioblastoma stem-like cells. Nature. 2010;468:824-8.

[146] Monzani E, La Porta CA. Targeting cancer stem cells to modulate alternative vascularization mechanisms. Stem Cell Reviews. 2008;4:51-6.

[147] Watt SM, Gullo F, van der Garde M, Markeson D, Camicia R, Khoo CP, et al. The angiogenic properties of mesenchymal stem/stromal cells and their therapeutic potential. British Medical Bulletin. 2013;108:25-53.

[148] Skiles ML, Hanna B, Rucker L, Tipton A, Brougham-Cook A, Jabbarzadeh E, et al. ASC spheroid geometry and culture oxygenation differentially impact induction of preangiogenic behaviors in endothelial cells. Cell Transplantation. 2015;24:2323-35.

[149] Lam CR, Wong HK, Nai S, Chua CK, Tan NS, Tan LP. A 3D biomimetic model of tissue stiffness interface for cancer drug testing. Molecular Pharmaceutics. 2014;11:2016-21.

[150] Fukumura D, Jain RK. Tumor microvasculature and microenvironment: targets for anti-angiogenesis and normalization. Microvascular Research. 2007;74:72-84.

[151] Liu H, Yin Y, Yao K, Ma D, Cui L, Cao Y. Influence of the concentrations of hyaluronic acid on the properties and biocompatibility of Cs-Gel-HA membranes. Biomaterials. 2004; 25:3523-3530.